MEASUREMENT OF SOIL MOISTURE TRENDS WITH AIRBORNE SCATTEROMETERS

Principal Investigator
Bruce J. Blanchard

Remote Sensing Center
Texas A&M University
College Station, Texas 77843

Progress Report for Period
April 1, 1977 to June 1, 1978

Prepared for

Goddard Space Flight Center
Greenbelt, Maryland 20771

Grant No. NSG 5134

TEXAS A&M UNIVERSITY
REMOTE SENSING CENTER
COLLEGE STATION, TEXAS

MEASUREMENT OF SOIL MOISTURE TRENDS WITH AIRBORNE SCATTEROMETERS

Principal Investigator
Bruce J. Blanchard

Remote Sensing Center
Texas A&M University
College Station, Texas 77843

Progress Report for Period
April 1, 1977 to June 1, 1978

Prepared for

Goddard Space Flight Center
Greenbelt, Maryland 20771

Grant No. NSG 5134

TABLE OF CONTENTS

List of Figures

(Appendix)

Figures

List of Tables

(Appendix)

List of Figures - Text

MEASUREMENT OF SOIL MOISTURE TRENDS WITH AIRBORNE SCATTEROMETERS

BACKGROUND AND OBJECTIVES

Background

Truck mounted active microwave systems operated by the University of Kansas have successfully demonstrated a potential for measurement of volumetric soil moisture with airborne active microwave systems. The truck experiment results also show the angular effects on the active microwave return and the effects of roughness experienced over agricultural land.

The differences in active microwave return due to changes in look angle are more significant at near nadir look angles. Differences due to roughness become more significant as the look angle, with respect to nadir, increases. The change in return, due to look angle and roughness, can be relatively large in magnitude in comparison to the differences produced by changing soil moisture. At some look angle for each wave length there is a point where effect of roughness on the microwave is a minimum. This point occurs at relatively near angles where angular effects on return are significant. If we are to minimize the influence of roughness, then a constant angle imager would be required to eliminate the influence of angular differences. Hardware of this nature is conceptually

feasable but is not now available.

Another approach to the measurement of soil moisture with active microwave systems can be made if we concern ourselves with targets where roughness remains constant. It is in this context that this study was undertaken. By repeated observation of fields where roughness remains constant, the roughness variable should be normalized and the active microwave return would then be dependent on soil moisture, look angle and wavelength of the sensor.

At the time this study was initiated three active microwave scatterometers were mounted on the NASA-C130 aircraft. It was proposed that these sensors would be operated over fields in the Brazos river alluvial plain where tillage was restricted to prevent changes in roughness.

Objectives

The objectives of this effort were first to demonstrate the feasability of obtaining an estimate of volumetric soil moisture by use of an airborne active microwave systems. Secondly, we planned to determine if a time series of active microwave return could be related to changes in soil moisture if roughness was held constant.

DATA SOURCES AND PROCESSING

Site Selection and Preparation

A general area for the collection of field data

for this experiment was selected by observing drying conditions on bare fields from a low flying aircraft. After selection of two possible locations where the soils were relatively uniform, owners were contacted to determine if the sites could be left untilled for a two month period and if permission would be granted to collect soil samples.

The final site selected represents two types of soil profiles representative of the Brazos River bottomlands. One flight line has three fields with heavy clay soils throughout the profile. The second flight line is near the river bank and has a topsoil of sandy clay loam to a depth of approximately 18 cm. Soils below that depth along this flight line are heavy clay.

Selected fields (three on each line) were marked and sample points were flagged in each field. Plastic point markers were annotated with the field and point number to avoid error in marking samples. Samples were collected according to the experiment plan (Figure 1) with one exception on a day when the fields were near saturation. The sample network was reduced by excluding alternate points where deep samples (below 15 cm.) were being collected.

Soil Moisture Sample and Data Processing

Gravimetric and bulk density samples were collected in hot drink cups, sealed with plastic, and covered with snap-on lids. Samples were transported to the laboratory

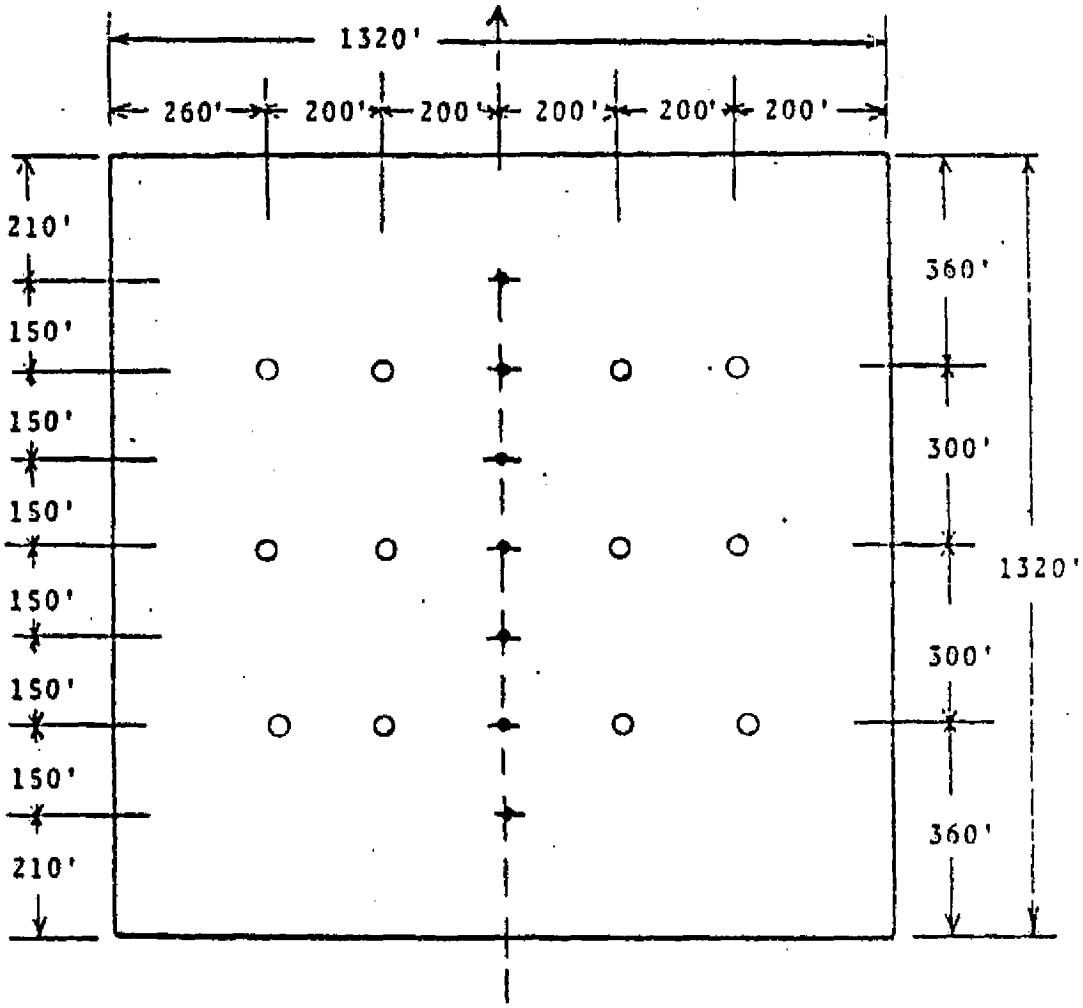

Seven soil moisture sample locations; five samples each (0-1 cm, 1-2 cm, 2-5 cm, 5-9 cm, 9-15 cm).

O Twelve soil moisture sample locations; eight samples each (0-1 cm, 1-2 cm, 2-5 cm, 5-9 cm, 9-15 cm, 0-15 cm, 15-30 cm, 30-45 cm).

— — — Aircraft ground track

Figure 1

and immediately weighed. Drying was accomplished by use of microwave ovens to speed processing.

The sampling was generally of good quality. However, when a sample was suspect, the data were deleted or flagged. All weights were punched on card decks and soil moisture content by volume was calculated for each sample. A card deck was then produced where the samples in each profile were recorded on a single card. Data were then examined for erratic values and high standard deviations. Standard deviation of soil moisture on field five for the fourth flight was high at all depths. The soil moisture averages for individual fields represented a relatively broad range when considering the surface layers. Deeper layers below 5 cm. did not vary significantly during the period of measurement. These data, therefore, do not provide a reliable basis for testing the sensitivity of longer wavelength microwave response to moisture at the lower depths. The soil moisture data used for correlation to the 13.3 GHz scatterometer (Appendix Table 1) come entirely from the top 1 cm. soil samples. Soil moisture data used for correlation with the 1.6 scatterometer returns (Appendix Tables 2 and 3) are averages of the values measured in the top 2 cm. of the soil surface.

Scatterometer Data Processing

A total of seven individual aircraft missions were flown over the selected fields. In all instances

the 13.3 GHz and 1.6 GHz scatterometers appeared to be operating properly. There was some question as to the validity of the .4 GHz scatterometer operation. However, the data were recorded on all flights.

In mid-February 1977, check-out of the software systems required to digitize data from aircraft PCM tapes onto 9-track computer compatible magnetic tapes was completed and installed on the Remote Sensing Center library disk at the TAMU Data Processing Center. The first data set was processed for use in determining scale factors required to overlay the data on photo-mosaics of fields where soil moisture experiments were being conducted.

By studying the correlation of 56 combinations of plotted data with the photographic mosaics of the flight line, best frequency and look angles to use for registering data to the flight line (and thus time) were selected. The combined plot of -5° and -15° look angles of the 13.3 GHz vertically polarized data was considered most useful for registration with known ground features such as water bodies, railroads and forested areas.

Each of the seven sets of scatterometer data was processed and matched such that an average return for each field on each set was calculated. The resulting returns for eight look angles on both the 13.3 GHz and 1.6 GHz systems are both listed in Tables 1, 2, and 3 of the Appendix. Considerable averaging of both the soil moisture and the scattering coefficient has been done to

arrive at these values. The processing of both types of data used relatively independent samples to acquire the averages, therefore less samples were averaged for the 1.6 GHz system.

ANALYSIS AND DISCUSSION

Assessment of Data Quality

Gravimetric sampling of soil moisture is the most reliable technique for determining soil moisture at shallow depths for a specific point. The normal collection and processing of these samples along with the uncertainties concerning the spatial variations of surface moisture can produce large variance in the samples used to calculate field averages. For this experiment, even though some samples had been eliminated due to obvious sample collection error, a further effort was made tc improve the estimate of field averages by eliminating points that fell more than one standard deviation from the mean calculated for all points in a field. This technique assumes outliers are truly an error, which may not always be the case. In all instances more points were used for field averages than have been available in prior aircraft experiments.

The aircraft scatterometer data available for this study was the first extensive set of data available for digital processing to σ_0 values. Therefore, an extensive effort was made to insure that the digital values did

represent a reasonable return that would be expected from the scatterometer systems. A first step in processing these data is visual inspection of the spectrum of the raw data. None of the flights produced data that was judged as reliable from the .4 GHz system. More recent investigation of the system disclosed a malfunction in one portion of the hardware. In this study only the 13.3 GHz and 1.6 GHz data were used in the final analysis. A summary of all basic data used is presented in Tables 1, 2, and 3 of the appendix.

All scatterometer average returns for each field were plotted versus the look angle to verify that return decreased with increasing angles from nadir. There is no reliable way at the present to indicate whether or not the magnitude is correct, thus we cannot say the overall systems are calibrated. Figures 2, 3, and 4 illustrate the returns received on seven flights over field Number 6. Figures of this nature are presented for all six fields in the appendix.

During the fall of 1976 arrangements had been made with the farm owner to leave the fields disked and bare as they were on November 18th. On the last date the fields were flown, in June of the following summer, fields 1, 2 and 3 were planted to skip row cotton, i.e. two rows of cotton and two rows of fallow ground, while fields 4, 5, and 6 were planted to maize. All fields had rows parallel to the flight line.

Figures 2, 3, and 4 indicate that there was

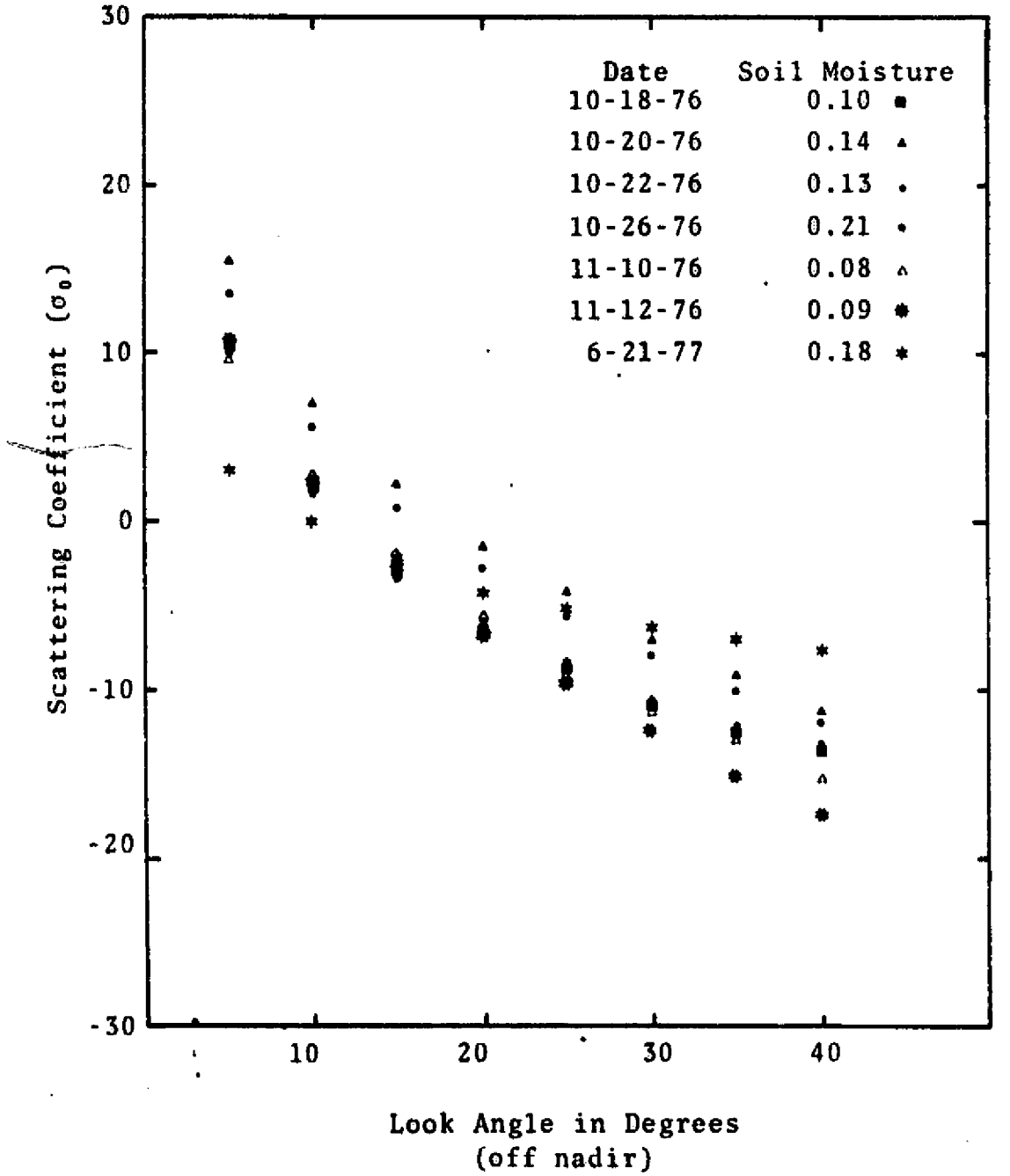

Figure 2. Comparison of σ_0 Values for Each Look Angle on All Missions over Field 6 Using 13.3 GHz-VV

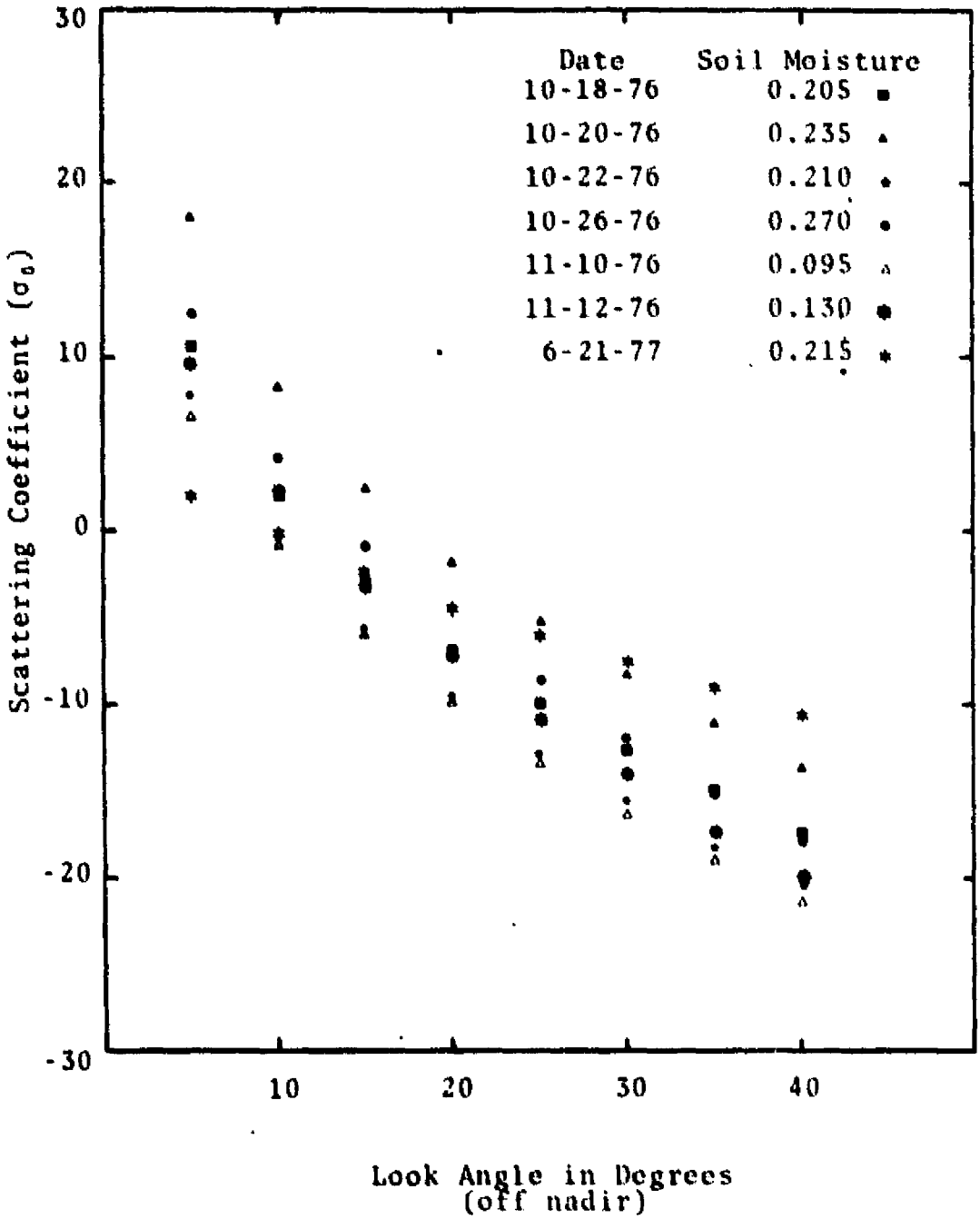

Figure 3. Comparison of σ_0 Values for Each Look Angle on All Missions Over Field 6 Using 1.6 GHz-HH

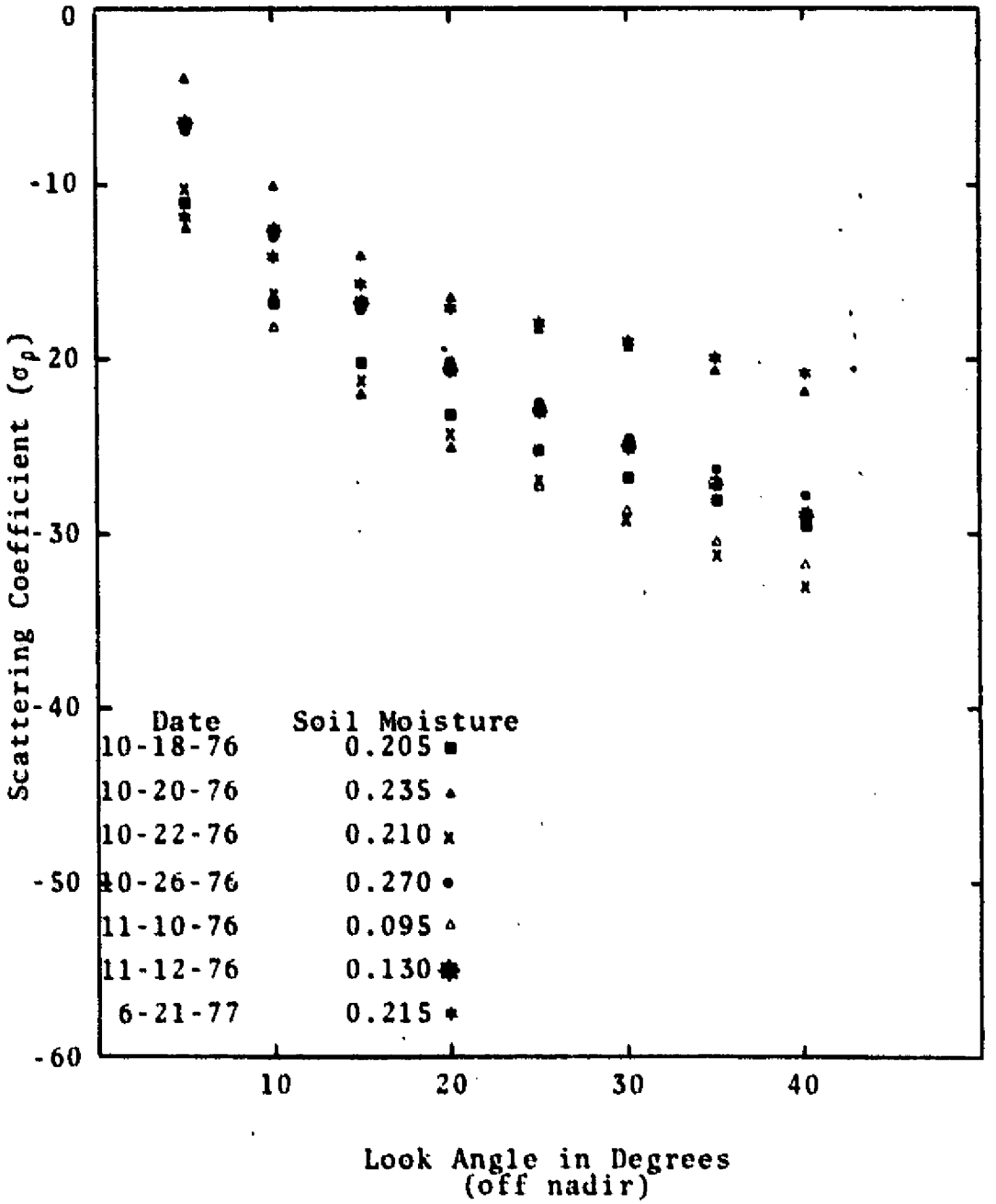

Figure 4. Comparison of σ_0 Values for Each Look Angle on All Missions Over Field 6 Using 1.6 GHz-HV

considerable influence from the vegetation at angles near nadir and at angles beyond 25 degrees. Vertical distribution of the data points at each look angle represents the range of influence on the scattering coefficient σ, produced by differences in soil moisture. A cursory examination of these figures indicates the 1.6 GHz system had a greater range of returns than the 13.3 GHz system. They also indicate that the range was greater for the like polarized (HH) 1.6 GHz than for the cross polarized (HV) 1.6 GHz when looking near nadir, while this relation reversed when looking at angles greater than 20° from nadir.

Time Series Plots

Sequential flights over each field were examined by plotting the data in the form shown in Figures 5, 6, 7 and 8. In general the response over bare ground follows the trends of the soil moisture at all angles. When all fields are considered it becomes obvious that the vegetation on the fields at the time of the last flight causes a reversal in the trend when looking in the near nadir angle. Note in Figure 5, for 13.3 GHz at a look angle of 10°, and in Figure 6 for 1.6 GHz at a look angle of 5°, the change from measurement 6 to 7 is inverse to the change in soil moisture. In Figures 6 and 8 both frequencies at a look angle of twenty degrees, produce a response that changes in the same direction as the soil moisture. Prior investigations have indicated that steep angles were best

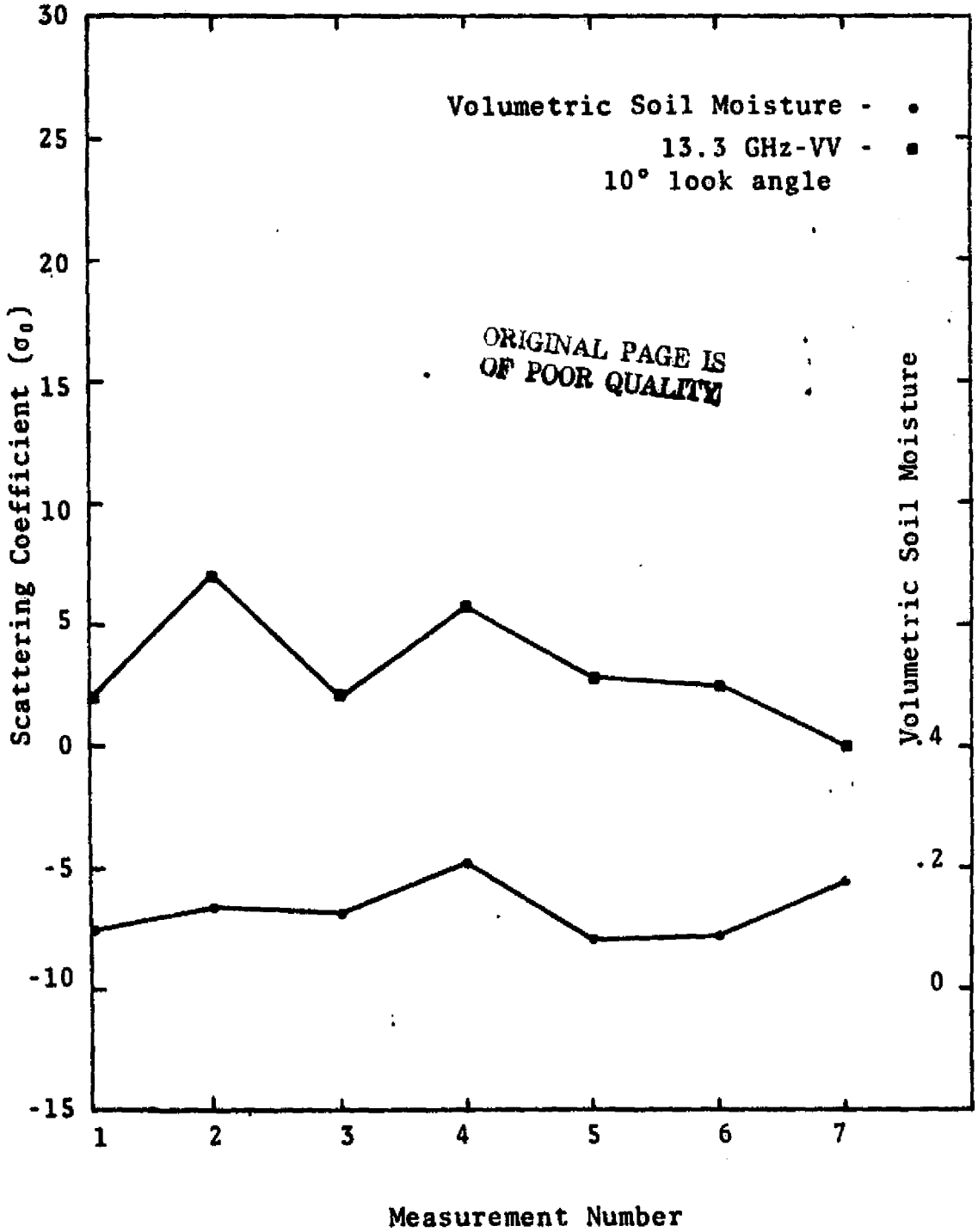

Figure 5. The Relation Between 13.3 GHz-VV Scattering Coefficient (σ_0) and Volumetric Soil Moisture for Field 6 for the Series of Seven Flights (Disked Bare Ground on the First Six Flights and Vegetated on the Final Flight).

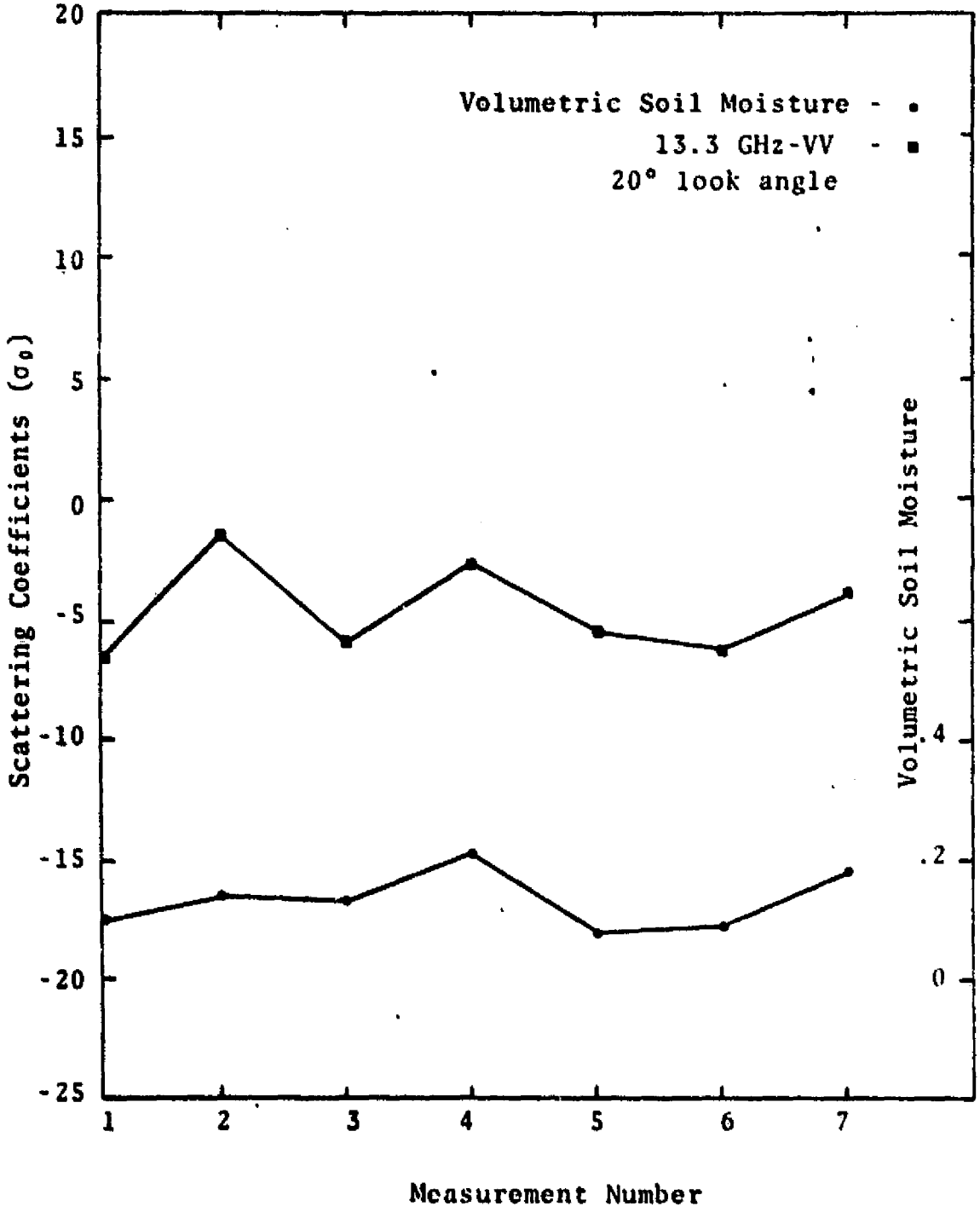

Figure 6. The Relation Between 13.3 GHz-VV Scattering Coefficient (σ_0) and Volumetric Soil Moisture for Field 6 for the Series of Seven Flights (Disked Bare Ground on the First Six Flights and Vegetated on the Final Flight).

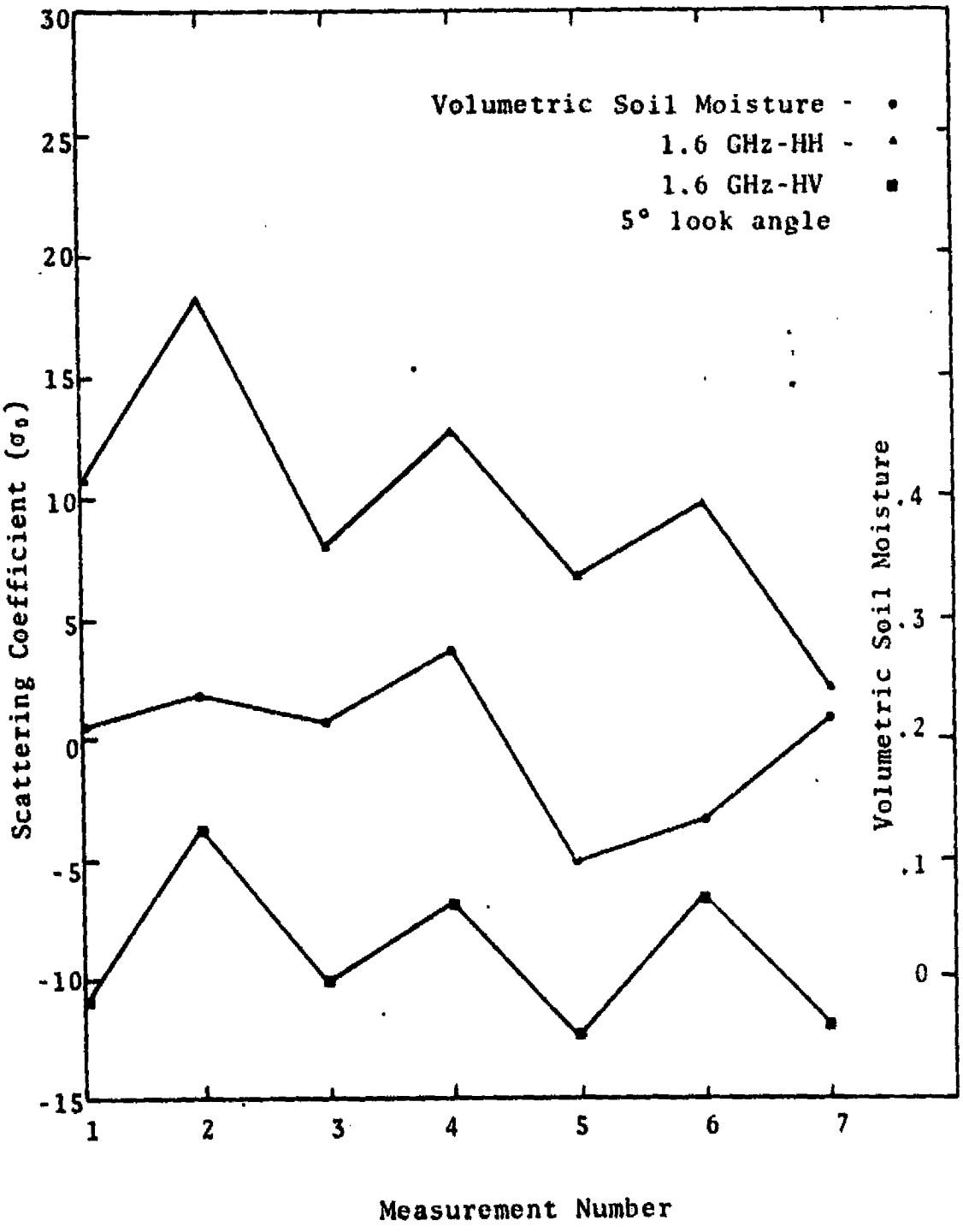

Figure 7. The Relation Between 1.6 GHz-HH and HV Scattering Coefficient (σ_0) and Volumetric Soil Moisture for Field 6 for the Series of Seven Flights (Disked Bare Ground on the First Six Flights and Vegetated on the Final Flight).

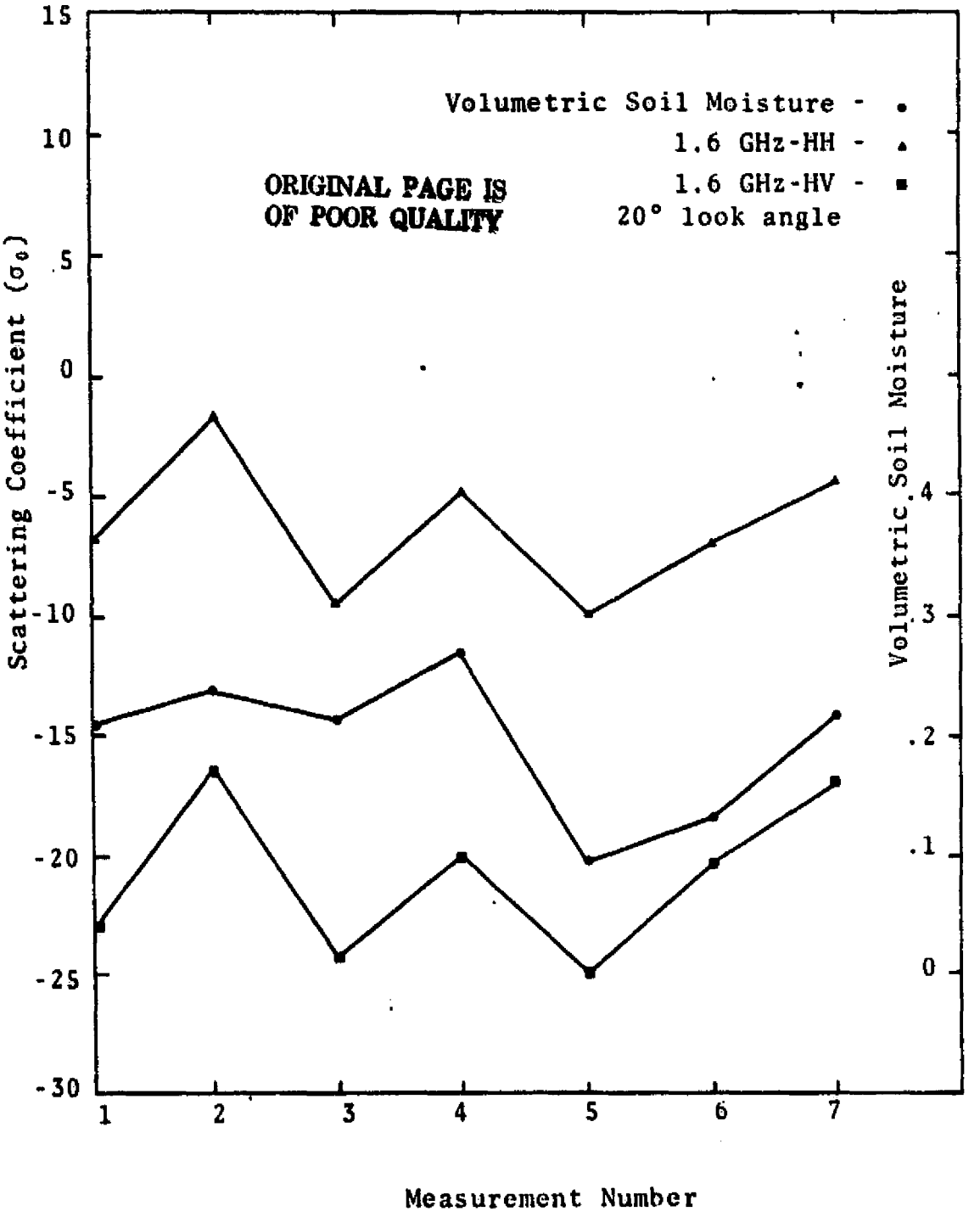

Figure 8. The Relation Between 1.6 GHz-HH and HV Scattering Coefficient (σ_0) and Volumetric Soil Moisture for Field 6 for the Series of Seven Flights (Disked Bare Ground on the First Six Flights and Vegetated on the Final Flight).

for penetration of vegetation contrary to indications in these data. Figures illustrating the remaining data can be found in the appendix.

Simple Correlation of Data

Figure 9 illustrates the simple correlation of all data collected with the 13.3 GHz scatterometer over the six fields at a look angle of twenty degrees. The line on this figure and all similar figures represents a best fit straight line based on bare ground data. Fields 1, 2 and 3 were in cotton on the last flight date, and fields 4, 5 and 6 were in maize. The soil moisture in the skip row cotton was considerable less than the moisture in the maize fields. However, at this look angle little or no effect from the crop is evident.

In Figures 10a, 10b, and 10c, the vegetated fields produce returns that migrate from too low at five degrees look angle to too high for a look angle of forty degrees. Again, the returns at twenty degrees look angle are compatible with data from bare ground. When using the cross polarized (HV) 1.6 GHz data, Figure 11, it appears that a twenty degree look angle is too great. To get good agreement with the bare ground data using the cross polarized return, the data indicates that a look angle near ten degrees would be more useful.

Best fit lines representing all eight look angles for each of the three channels of data are shown in

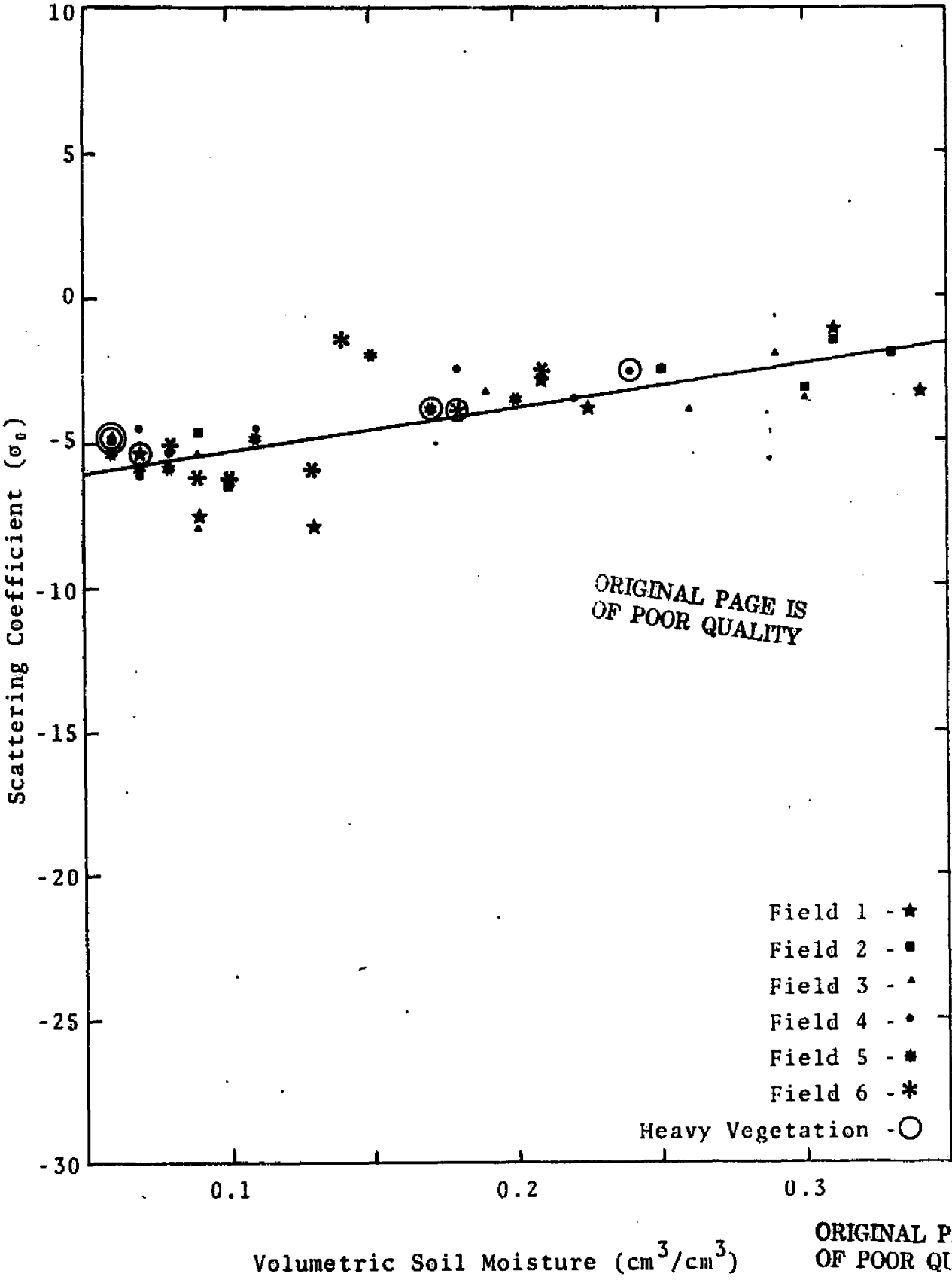

ORIGINAL PAGE IS
OF POOR QUALITY

Figure 9. Relation Between 13.3 GHz-VV Scattering Coefficient and Volumetric Soil Moisture at 20 Degree Look Angle

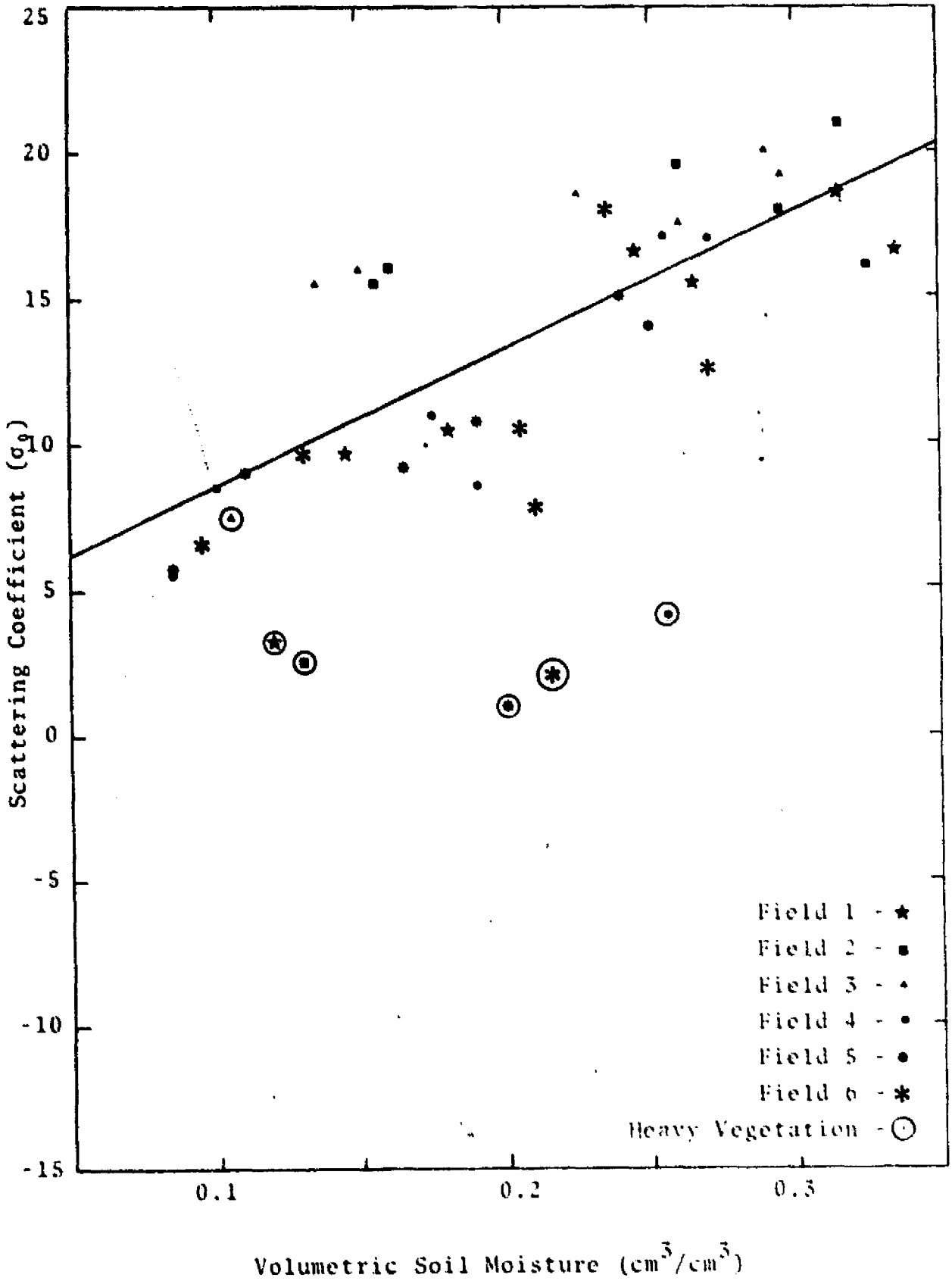

Figure 10A. Relation Between 1.6 GHz-HH Scattering Coefficient and Volumetric Soil Moisture at 5 Degree Angle

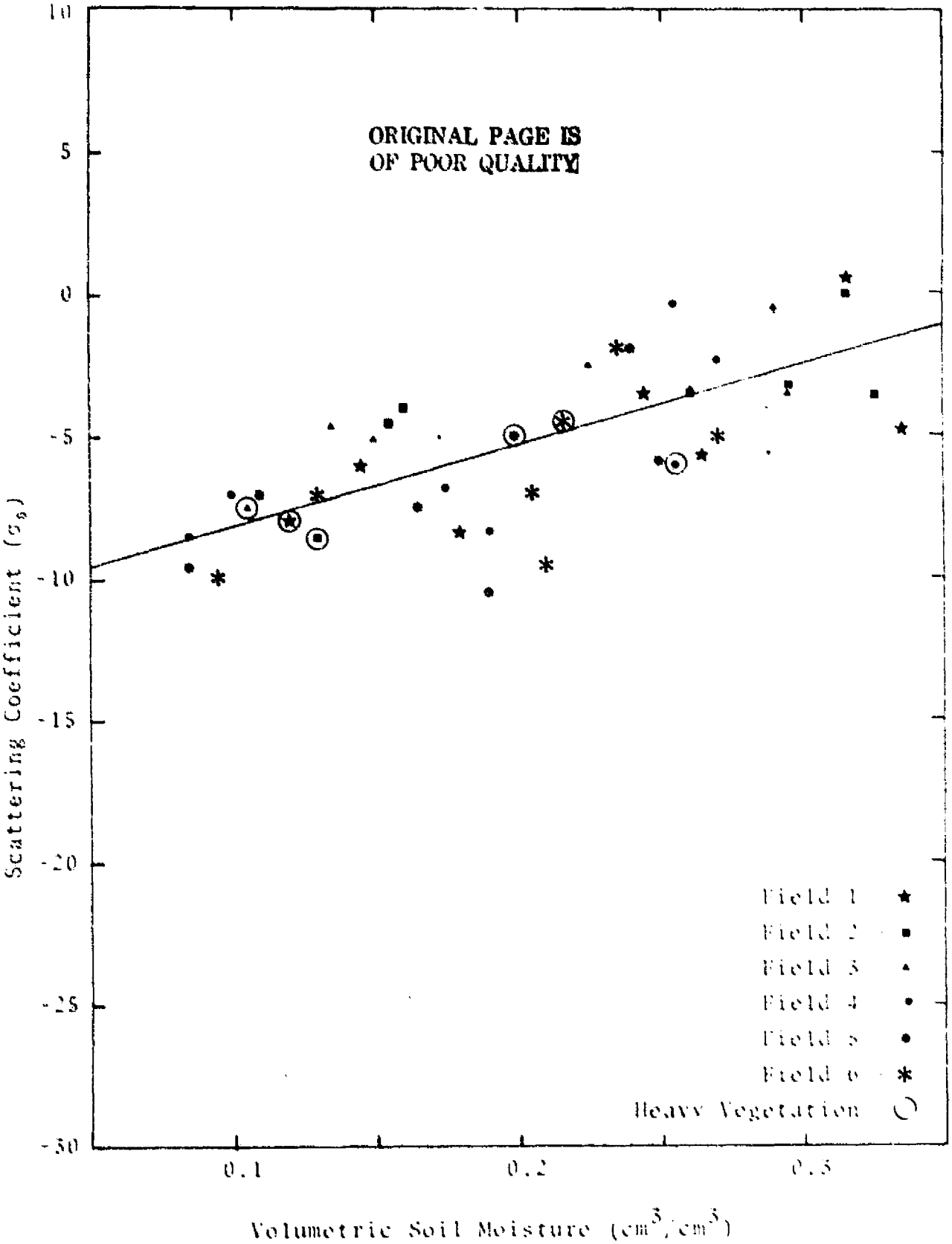

Figure 10B. Relation Between 1.6 GHz-HH Scattering Coefficient and Volumetric Soil Moisture at 20 Degree Look Angle

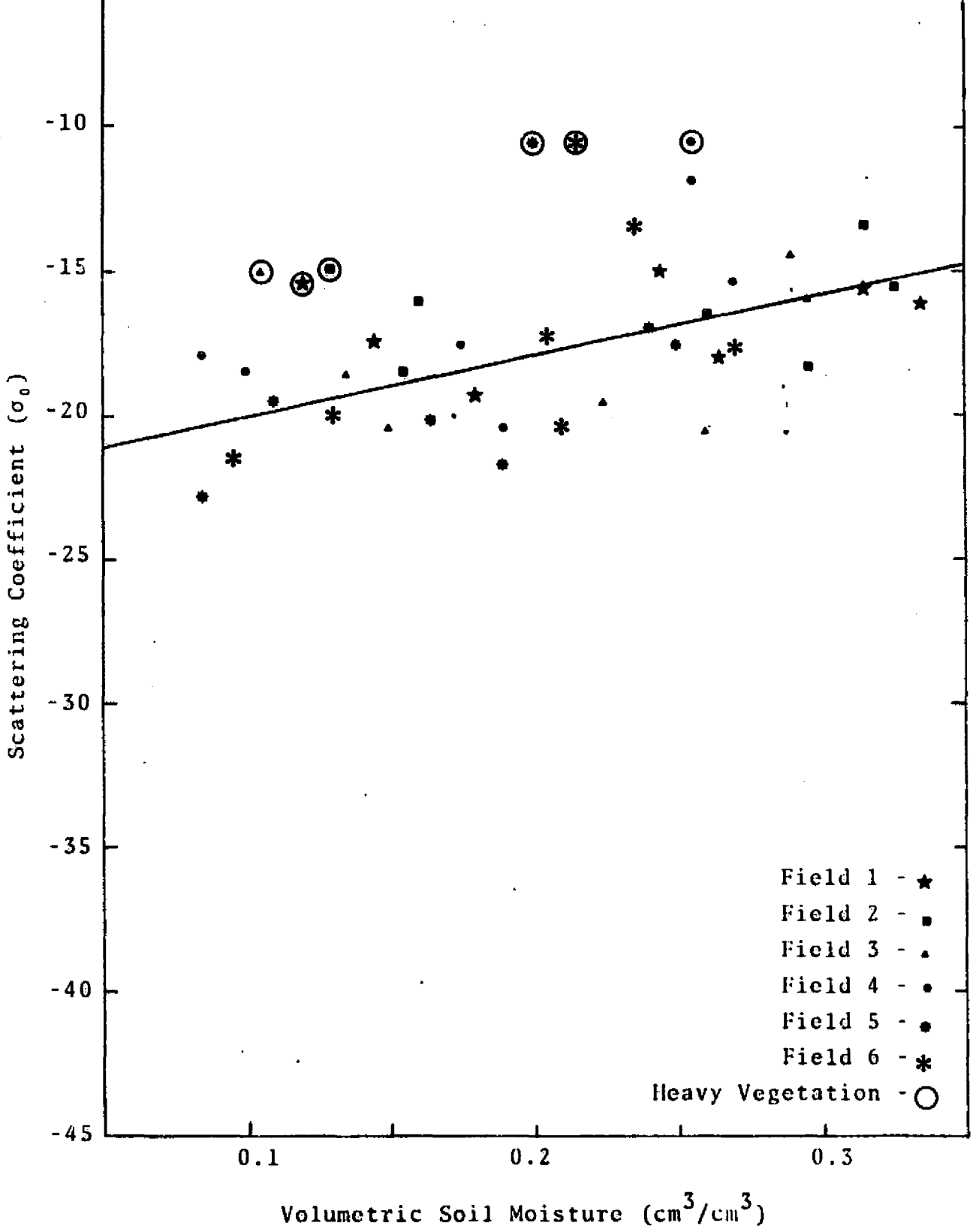

Figure 10C. Relation Between 1.6 GHz-HH Scattering Coefficient and Volumetric Soil Moisture at 40 Degree Look Angle

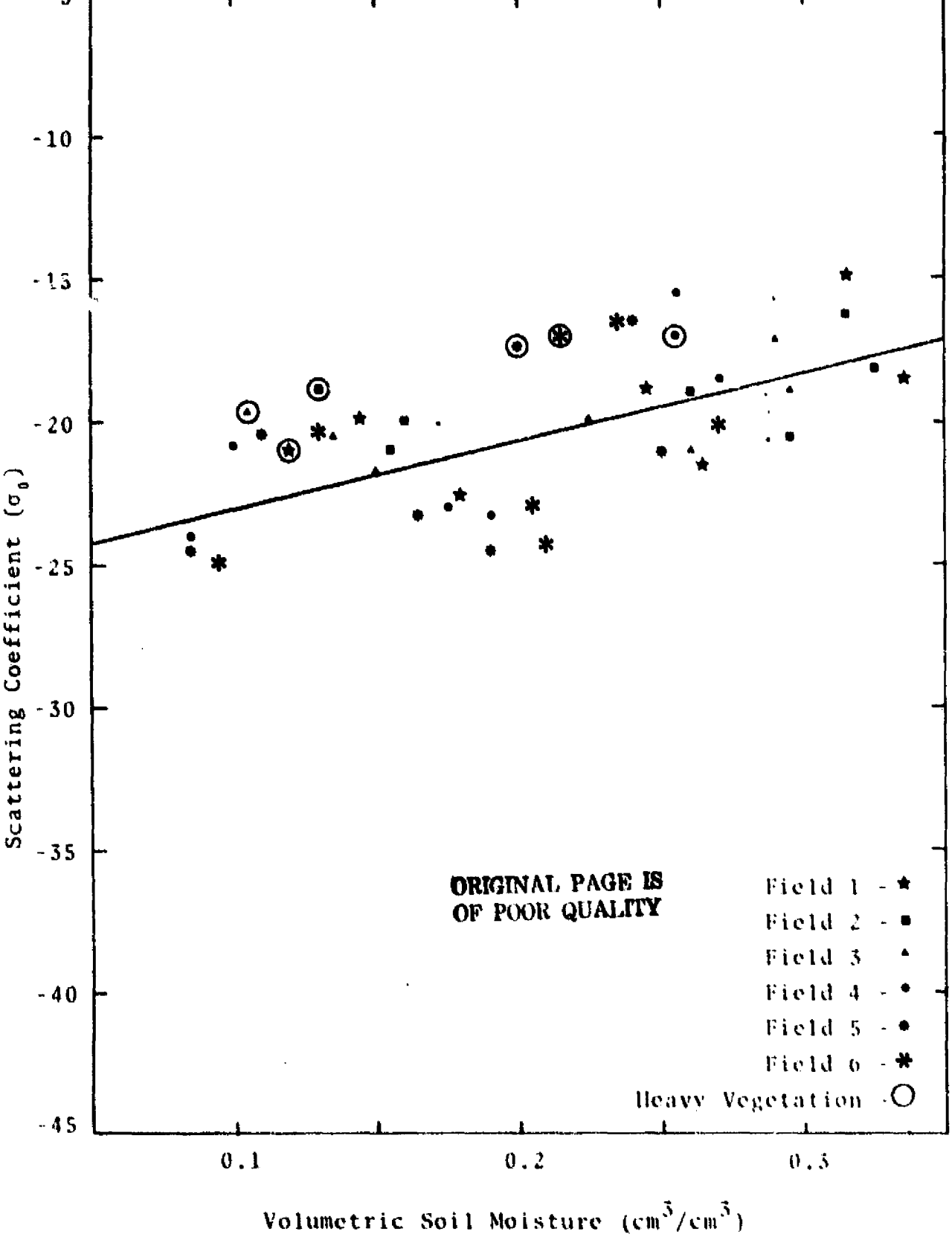

Figure 11. Relation Between 1.6 GHz-HV Scattering Coefficient and Volumetric Soil Moisture at 20 Degree Look Angle

Figures 12, 13, and 14. The slopes of these lines and the coefficient of determination for each line are listed in Tables 4 and 5 of the appendix. The slope is greater for the like polarized 1.6 GHz system than for either the 13.3 GHz system or the cross polarized 1.6 GHz system at each look angle. This would indicate that the Seasat-A imaging radar system should be relatively sensitive to differences in near surface soil moisture. These data indicate that a range of 9db can be expected in Seasat-A data for the full range of soil moisture in the top two centimeters with little influence from crops.

The coefficient of determination, R^2, was calculated for each look angle-frequency combination (Appendix, Table 5). Bare ground values were used to develop this table. Development of a useful application of the measurement will require sensing both bare and vegetated surfaces. Another calculation of R^2 values was made with the vegetated fields included. The results are illustrated in Figure 15, where all three channels of data are represented. It is evident that fifteen degrees look angle appears optimum for the 13.3 GHz frequency when correlated with the top one centimeter of soil. Twenty degrees look angle seems most appropriate for the 1.6 GHz like polarized system when correlated with the top two centimeters of soil.

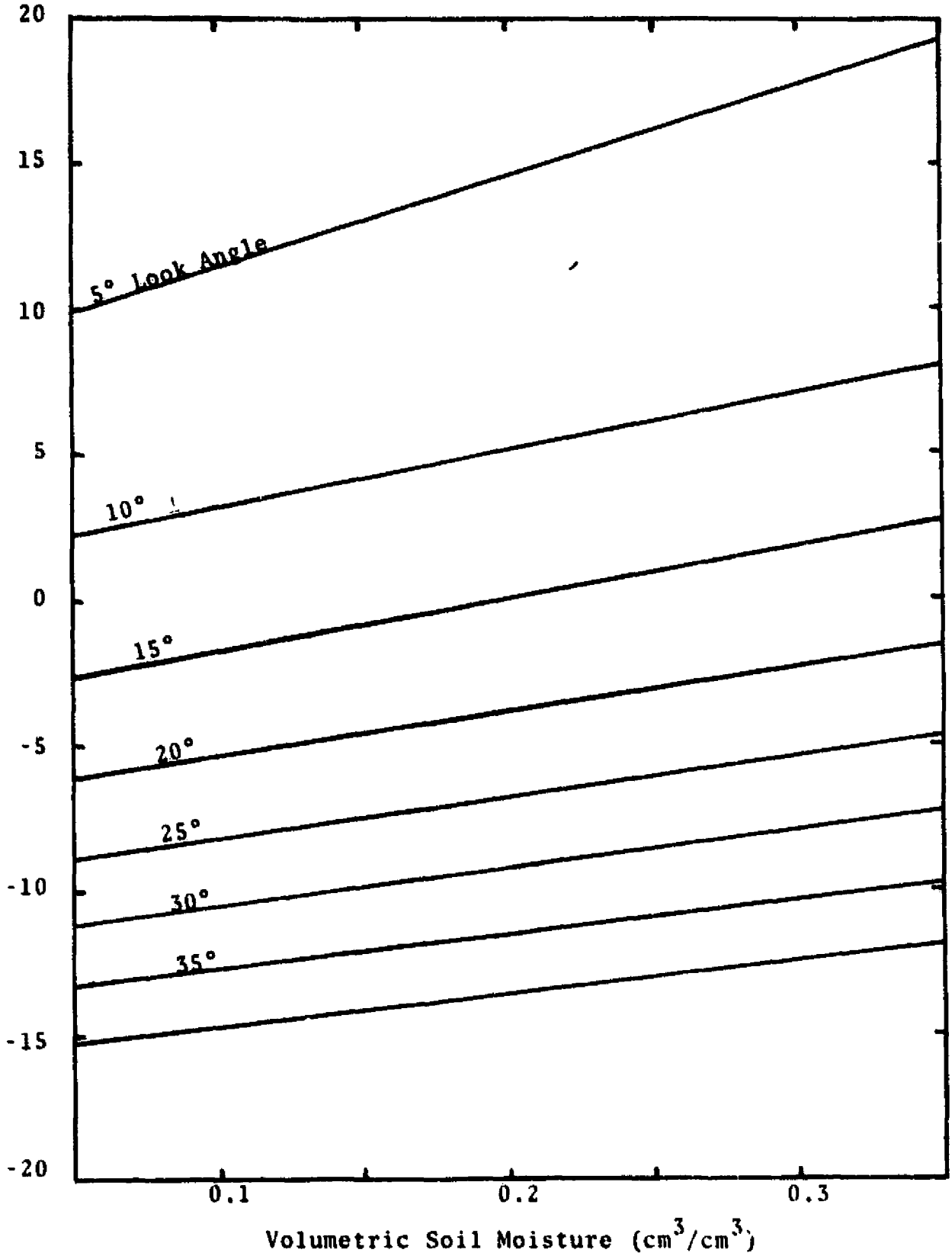

Figure 12. Best Fit Linear Through Data Points For All Look Angles Using 13.3 GHz-VV Polarization and Soil Moisture in the Top One Centimeter of Bare Fields

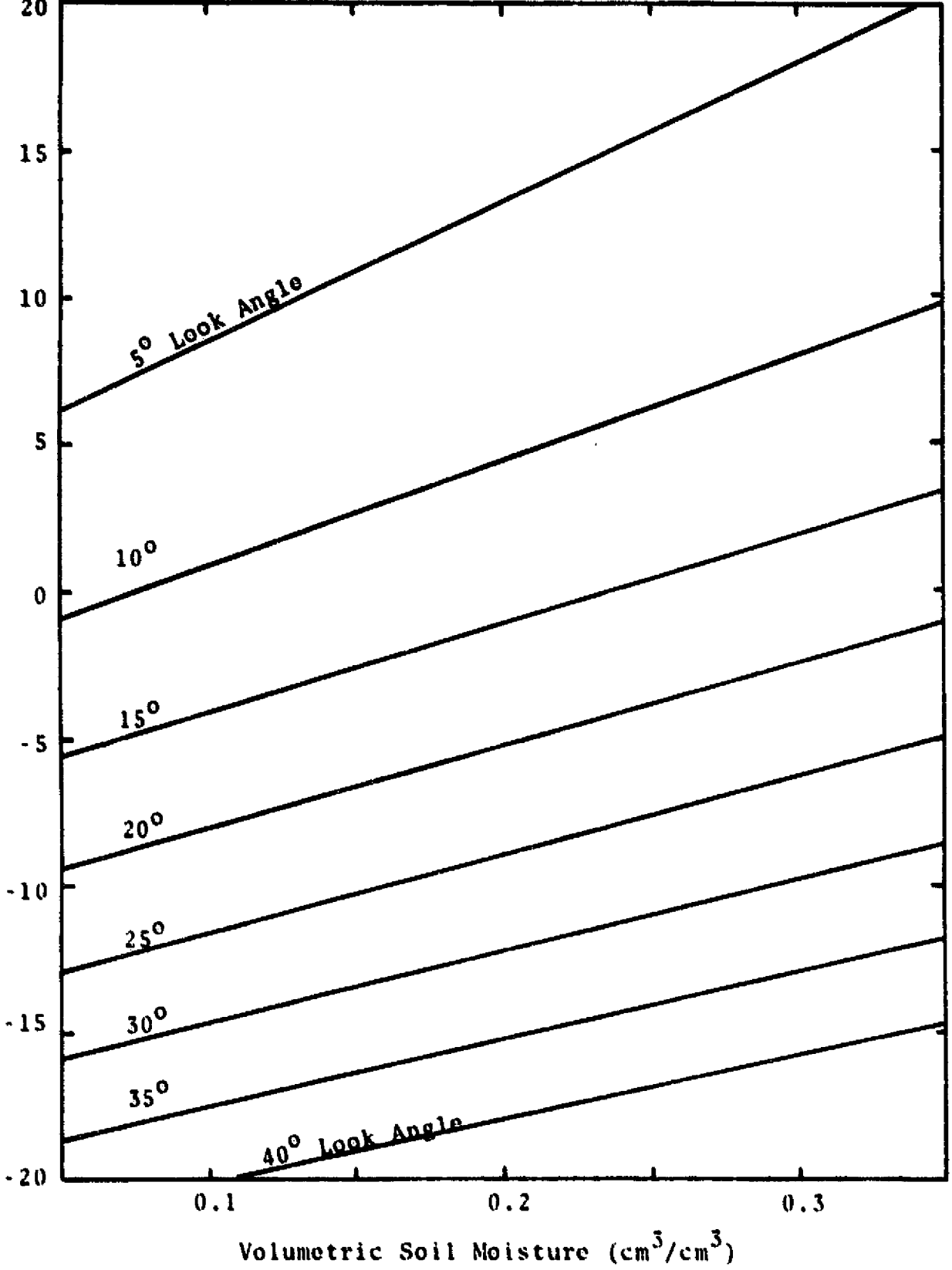

Figure 13. Best Fit Linear Through Data Points For All Look Angles Using 1.6 GHz-HH Polarization and Soil Moisture in the Top Two Centimeter of Bare Fields

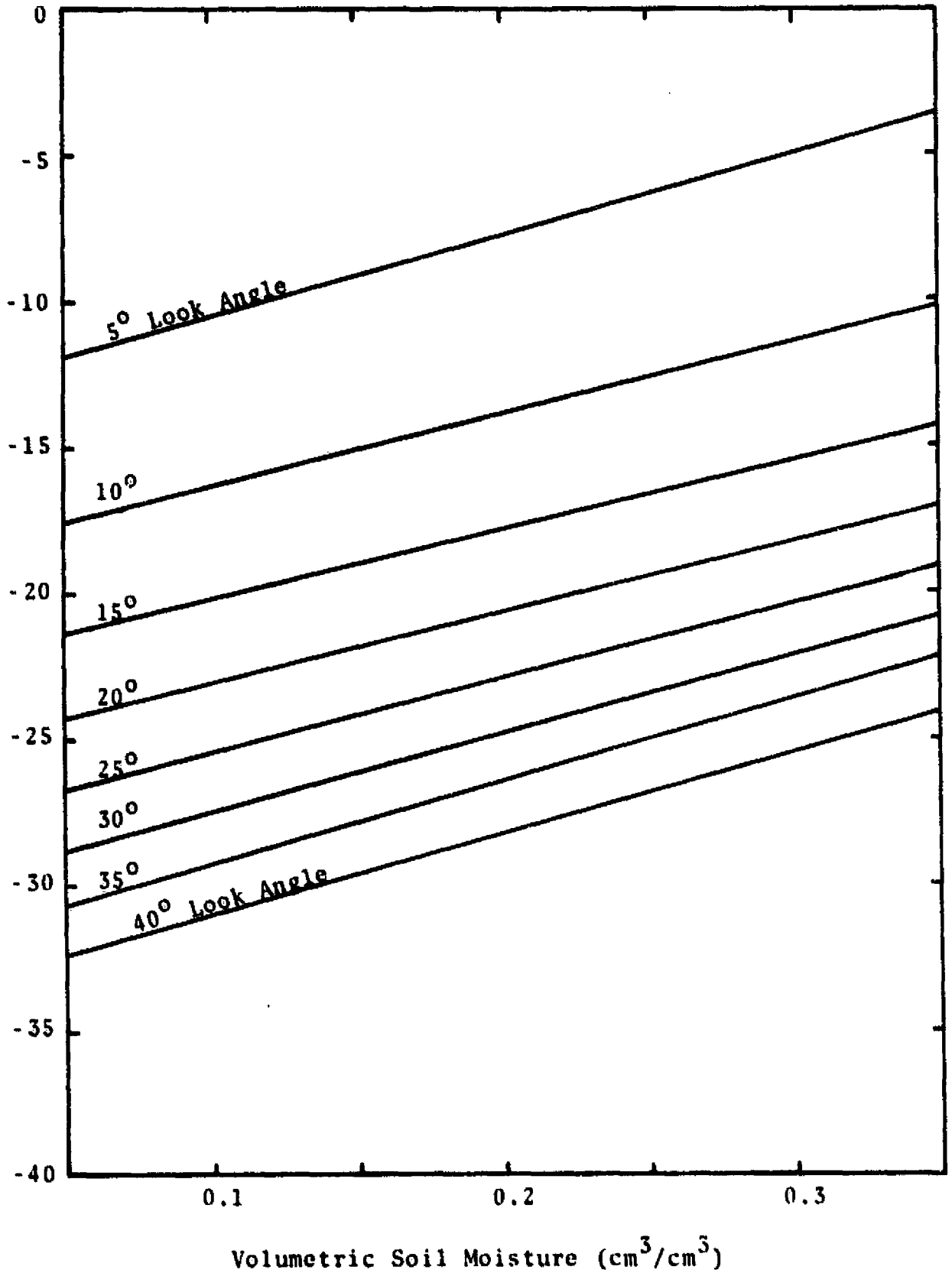

Figure 14. Best Fit Linear Through Data Points For All Look Angles Using 1.6 GHz-HV Polarization and Soil Moisture in the Top Two Centimeter of Bare Fields

CONCLUSIONS

(1) Significant influence due to differences in soil moisture can be detected in the 13.3 GHz and 1.6 GHz scatterometer returns.

(2) Repeated looks at surfaces that maintain constant roughness can provide an estimate of soil moisture in the surface when appropriate radar look angles are used.

(3) Effects of normal crop densities have little influence on the estimate of surface soil moisture when appropriate look angles are used. It appears that different look angles are optimum for different frequencies to avoid effects from vegetation.

(4) Considering the frequency and look angles used on the Seasat-A imaging radar, differences in soil moisture should produce as much as 9db difference in return on that system.

(5) The scatter in data due to both the ground measurement of soil moisture and radar return will make it difficult to determine more than three discrete levels of soil moisture with good reliability even when roughness is held constant.

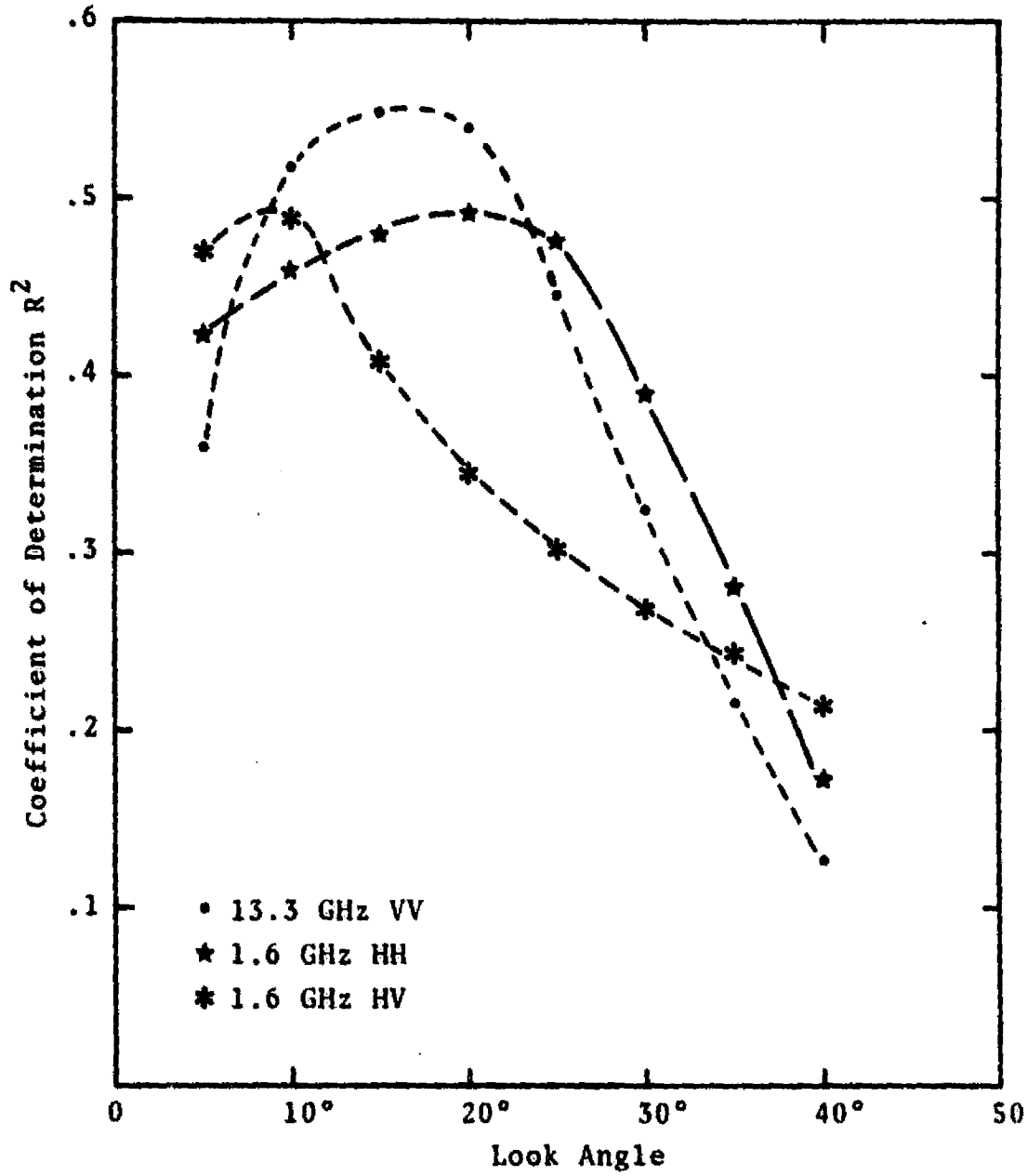

Figure 15. A Comparison of the R^2 Values at Near Nadir Look Angles Between Three Channels of Mcirowave Data and Measured Soil Moisture.

Appendix A

Table A1. 13.3 GHz-VV Scattering Coefficient ($T\sigma$) at Each Look Angle on Each Date for Fields 1-6.

Date	Field No.	Volumetric H_2O Content	5°	10°	15°	20°	25°	30°	35°	40°
10-18-76	4	0.07	13.1	4.0	-1.0	-4.6	-7.5	- 9.9	-11.8	-13.5
10-20-76	4	0.18	13.9	6.0	1.3	-2.5	-5.6	- 8.4	-11.0	-13.2
10-22-76	4	0.11	10.6	3.9	-1.0	-4.6	-7.6	-10.1	-12.1	-14.1
10-26-76	4	0.22	15.3	5.3	0.0	-3.6	-6.4	- 8.0	-10.5	-12.2
11-10-76	4	0.07	10.0	2.3	-2.5	-5.9	-8.5	-10.5	-12.5	-14.1
11-12-76	4	0.08	9.0	2.5	-2.0	-5.4	-8.0	-10.4	-12.5	-14.4
6-21-77	4	0.24	4.6	2.0	-0.5	-2.6	-4.6	- 6.5	- 8.0	- 9.8
10-18-76	5	0.07	12.5	2.5	-2.5	-6.0	-8.4	-10.4	-12.2	-13.9
10-20-76	5	0.15	11.8	6.1	1.8	-2.0	-5.1	- 8.1	-10.9	-13.5
10-22-76	5	0.11	10.7	3.4	-1.2	-4.9	-7.8	-10.3	-12.6	-14.6
10-26-76	5	0.20	13.0	5.0	0.0	-3.6	-6.2	- 8.6	-10.6	-12.5
11-10-76	5	0.06	6.0	1.5	-2.0	-5.4	-8.1	-10.6	-13.0	-15.0
11-12-76	5	0.08	11.0	2.6	-2.5	-6.0	-8.7	-11.1	-13.2	-15.1
6-21-77	5	0.17	2.5	2.4	-1.9	-3.9	-5.6	- 7.4	- 9.0	-10.5
10-18-76	6	0.10	10.5	2.0	-3.0	-6.4	-8.8	-10.9	-12.5	-13.6
10-20-76	6	0.14	15.5	7.0	2.2	-1.5	-4.3	- 6.9	- 9.1	-11.3
10-22-76	6	0.13	10.5	2.0	-2.6	-6.0	-8.5	-10.5	-12.3	-13.7
10-26-76	6	0.21	13.5	5.7	0.9	-2.7	-5.5	- 7.9	-10.0	-11.9
11-10-76	6	0.08	10.0	2.8	-2.0	-5.5	-8.4	-10.9	-12.2	-15.3
11-12-76	6	0.09	10.5	2.5	-2.5	-6.3	-9.5	-12.3	-15.0	-17.2
6-21-77	6	0.18	3.0	0.0	-2.4	-4.0	-5.2	- 6.1	- 7.0	- 7.6

Table A1. 13.3 GHz-VV Scattering Coefficient ($T\sigma$) at Each Look Angle on Each Date for Fields 1-6.

Date	Field No.	Volumetric H_2O Content	5°	10°	15°	20°	25°	30°	35°	40°
10-18-76	1	0.21	16.0	6.5	1.1	-2.7	- 5.9	- 8.4	-10.6	-12.7
10-20-76	1	0.31	15.9	7.9	2.8	-1.2	- 4.5	- 7.6	-10.4	-12.8
10-22-76	1	0.25	15.5	5.4	0.0	-3.9	- 6.9	- 9.4	-11.5	-13.5
10-26-76	1	0.34	18.1	6.0	0.5	-3.3	- 6.5	- 9.0	-11.3	-13.4
11-10-76	1	0.13	7.1	0.0	-4.5	-7.9	-10.4	-12.5	-14.1	-15.8
11-12-76	1	0.09	11.5	1.0	-4.0	-7.6	-10.5	-12.5	-14.5	-16.1
6-21-77	1	0.07	6.0	1.0	-2.6	-5.4	- 7.4	- 8.6	-10.0	-11.0
10-18-76	2	0.25	18.5	7.6	1.4	-2.5	- 5.4	- 8.2	-10.5	-12.5
10-20-76	2	0.31	20.0	8.0	2.5	-1.5	- 4.6	- 7.4	- 9.6	-11.8
10-22-76	2	0.30	18.0	6.0	0.5	-3.2	- 6.2	- 8.7	-10.4	-12.9
10-26-76	2	0.33	17.0	7.5	2.0	-2.0	- 5.4	- 8.4	-11.1	-13.6
11-10-76	2	0.09	11.6	4.0	-1.0	-4.7	- 7.6	-10.1	-12.5	-14.4
11-12-76	2	0.10	13.1	3.0	-2.6	-6.5	- 9.6	-12.4	-14.6	-16.9
6-21-77	2	0.06	6.5	1.5	-2.0	-4.9	- 6.9	- 8.5	-10.0	-11.4
10-18-76	3	0.19	19.2	6.5	0.6	-3.3	- 6.5	- 9.0	-11.3	-13.0
10-20-76	3	0.29	15.5	7.0	1.6	-2.0	- 5.0	- 7.6	-10.1	-12.3
10-22-76	3	0.26	19.5	6.9	0.0	-3.9	- 6.6	- 8.6	-10.5	-12.4
10-26-76	3	0.30	16.5	6.0	0.4	-3.5	- 6.4	- 8.9	-11.1	-13.0
11-10-76	3	0.09	18.0	5.0	-1.0	-5.5	- 8.6	-11.4	-14.0	-16.3
11-12-76	3	0.09	8.4	0.5	-4.4	-8.0	-10.9	-13.5	-16.0	-18.0
6-21-77	3	0.06	7.4	1.5	-2.1	-5.0	- 6.9	- 8.1	- 9.1	-10.0

Table A2.1.6 GHz-HH Scattering Coefficient ($T\sigma$) at Each Look Angle on Each Date for Fields 1-6.

Date	Field No.	Volumetric H_2O Content	5°	10°	15°	20°	25°	30°	35°	40°
10-18-76	1	0.245	16.6	6.5	0.6	-3.5	- 6.7	- 9.9	-12.5	-15.0
10-20-76	1	0.315	18.6	11.4	5.6	0.6	- 3.7	- 7.9	-11.8	-15.6
10-22-76	1	0.265	15.5	4.5	-1.5	-5.7	- 9.3	-12.5	-15.4	-17.9
10-26-76	1	0.335	16.6	5.3	-0.6	-4.8	- 8.1	-11.1	-13.6	-16.1
11-10-76	1	0.180	10.4	1.2	-4.5	-8.4	-11.6	-14.5	-17.0	-19.4
11-12-76	1	0.145	9.6	2.5	-2.1	-6.0	- 9.4	-12.4	-15.0	-17.5
6-21-77	1	0.120	3.1	-1.6	-5.2	-8.0	-10.1	-12.2	-14.0	-15.5
10-18-76	2	0.260	19.5	9.0	0.8	-3.5	- 6.0	- 9.8	-13.1	-16.4
10-20-76	2	0.315	20.9	10.5	4.6	0.0	- 3.8	- 7.4	-10.5	-13.3
10-22-76	2	0.295	18.0	7.9	1.8	-3.2	- 7.5	-11.5	-15.0	-18.3
10-26-76	2	0.325	16.1	6.5	0.6	-3.6	- 7.0	-10.1	-13.0	-15.5
11-10-76	2	0.155	15.5	6.0	0.0	-4.5	- 8.5	-12.2	-15.5	-18.5
11-12-76	2	0.160	16.0	6.0	0.0	-4.0	- 7.6	-10.6	-13.6	-16.1
6-21-77	2	0.130	2.6	-2.4	-6.0	-8.5	-10.5	-12.2	-13.7	-15.0
10-18-76	3	0.225	18.5	9.0	2.6	-2.5	- 6.9	-10.7	-13.8	-19.5
10-20-76	3	0.290	20.0	10.0	4.1	-0.5	- 4.5	- 8.1	-11.4	-14.4
10-22-76	3	0.260	17.6	8.3	1.9	-3.5	- 8.3	-12.6	-16.8	-20.6
10-26-76	3	0.295	19.2	7.3	1.0	-3.5	- 7.0	-10.4	-13.4	-16.0
11-10-76	3	0.150	16.0	6.0	-0.5	-5.1	- 9.5	-13.4	-17.0	-20.5
11-12-76	3	0.135	15.5	5.9	0.0	-4.6	- 8.6	-12.5	-15.6	-18.7
6-21-77	3	0.105	7.4	0.4	-4.0	-7.5	- 9.9	-11.9	-13.6	-15.1

Table A2. 1.6 GHz-HH Scattering Coefficient (Tσ) at Each Look Angle on Each Date for Fields 1-6.

Date	Field No.	Volumetric H_2O Content	5°	10°	15°	20°	25°	30°	35°	40°
10-18-76	4	0.175	10.9	2.5	-2.8	- 6.7	-10.0	-13.0	-15.4	-17.6
10-20-76	4	0.255	17.0	9.0	3.5	- 0.3	- 3.6	- 6.6	- 9.4	-11.8
10-22-76	4	0.190	8.5	0.6	-4.4	- 8.3	-11.8	-15.0	-17.3	-20.4
10-26-76	4	0.270	17.0	7.3	1.5	- 2.3	- 6.4	- 9.6	-12.6	-15.3
11-10-76	4	0.085	5.5	-1.0	-5.3	- 8.5	-11.4	-13.9	-16.0	-18.0
11-12-76	4	0.100	8.5	1.5	-3.1	- 7.0	-10.3	-13.4	-16.1	-18.6
6-21-76	4	0.255	4.1	-0.5	-3.8	- 6.0	- 7.6	- 9.0	-10.0	-10.6
10-18-76	5	0.165	9.2	0.6	-3.6	- 7.4	-10.5	-13.5	-16.6	-20.2
10-20-76	5	0.240	15.0	8.3	2.9	- 1.9	- 6.2	-10.0	-13.5	-17.0
10-22-76	5	0.190	10.7	-0.5	-6.4	-10.5	-13.7	-16.6	-19.4	-21.8
10-26-76	5	0.250	14.0	4.0	-1.8	- 5.9	- 9.3	-12.5	-15.1	-17.6
11-10-76	5	0.085	5.6	-0.8	-5.5	- 9.5	-13.5	-16.8	-19.9	-22.9
11-12-76	5	0.110	9.0	1.7	-3.0	- 7.0	-10.5	-13.8	-16.8	-19.5
6-21-77	5	0.200	1.0	-1.3	-3.4	- 5.0	- 6.5	- 8.0	- 9.4	-10.5
10-18-76	6	0.205	10.5	2.1	-3.0	- 6.9	-10.0	-12.7	-15.0	-17.4
10-20-76	6	0.235	18.0	8.1	2.4	- 1.9	- 5.3	- 8.4	-11.1	-13.6
10-22-76	6	0.210	7.8	-0.5	-5.7	- 9.6	-12.9	-15.6	-18.2	-20.5
10-26-76	6	0.270	12.5	4.1	-1.0	- 5.0	- 8.6	-12.0	-15.0	-17.7
11-10-76	6	0.095	6.5	-1.0	-6.0	-10.0	-13.5	-16.4	-19.0	-21.5
11-12-76	6	0.130	9.6	2.2	-3.0	- 7.1	-11.0	-14.2	-17.4	-20.0
6-21-77	6	0.215	2.0	-0.5	-2.5	- 4.5	- 6.1	- 7.6	- 9.1	-10.6

Table A3. 1.6 GHz-HV Scattering Coefficient ($T\sigma$) at Each Look Angle on Each Date for Fields 1-6.

Date	Field No.	Volumetric H_2O Content	5°	10°	15°	20°	25°	30°	35°	40°
10-18-76	1	0.245	- 5.6	-11.7	-15.7	-18.8	-21.5	-23.7	-25.4	-27.0
10-20-76	1	0.315	- 2.5	- 8.1	-11.9	-14.8	-17.1	-19.1	-20.6	-22.0
10-22-76	1	0.265	- 7.0	-14.1	-18.6	-21.5	-23.5	-25.3	-27.0	-28.6
10-26-76	1	0.335	- 6.2	-12.0	-15.9	-18.5	-20.5	-21.9	-23.1	-24.1
11-10-76	1	0.180	-11.7	-16.4	-19.8	-22.6	-25.3	-27.6	-29.7	-31.6
11-12-76	1	0.145	- 7.5	-13.3	-17.1	-20.0	-22.4	-24.0	-25.7	-27.2
6-21-77	1	0.120	-15.0	-17.7	-19.6	-21.1	-22.5	-23.3	-24.0	-24.5
10-18-76	2	0.260	- 6.0	-12.4	-16.1	-18.9	-21.1	-23.5	-25.2	-27.0
10-20-76	2	0.315	- 3.6	- 9.5	-13.5	-16.2	-18.3	-19.7	-21.0	-22.0
10-22-76	2	0.295	- 5.5	-12.8	-17.3	-20.5	-23.2	-25.4	-27.2	-28.9
10-26-76	2	0.325	- 5.5	-11.1	-15.1	-18.1	-20.5	-22.6	-24.5	-26.1
11-10-76	2	0.155	- 9.6	-14.5	-18.0	-21.0	-23.5	-25.6	-27.5	-29.3
11-12-76	2	0.160	- 7.2	-13.1	-17.1	-20.0	-22.2	-24.0	-25.5	-27.0
6-21-77	2	0.130	-13.0	-15.2	-17.1	-18.9	-20.2	-21.5	-22.5	-23.5
10-18-76	3	0.225	- 6.5	-13.0	-16.9	-19.9	-22.1	-24.0	-25.5	-26.7
10-20-76	3	0.290	- 3.1	-10.4	-14.3	-17.1	-19.8	-19.9	-20.6	-22.0
10-22-76	3	0.260	- 6.0	-13.1	-17.7	-21.0	-23.5	-25.7	-27.7	-29.3
10-26-76	3	0.295	- 6.2	-12.1	-16.0	-18.8	-20.6	-22.3	-23.6	-24.7
11-10-76	3	0.130	- 8.4	-14.4	-18.5	-21.8	-24.5	-26.8	-28.8	-30.8
11-12-76	3	0.135	- 8.0	-13.6	-17.6	-20.6	-22.9	-24.7	-26.4	-27.7
6-21-77	3	0.105	-13.2	-16.0	-18.0	-19.7	-21.3	-22.6	-23.6	-24.6

Table A3. 1.6 GHz-HV Scattering Coefficient (Tσ) at Each Look Angle on Each Date for Fields 1-6.

Date	Field No.	Volumetric H_2O Content	5°	10°	15°	20°	25°	30°	35°	40°
10-18-76	4	0.175	-10.5	-16.5	-20.2	-23.0	-25.1	-26.8	-28.3	-29.4
10-20-76	4	0.255	- 4.5	- 9.5	-13.0	-15.5	-17.5	-19.0	-20.4	-21.5
10-22-76	4	0.190	- 7.1	-15.1	-20.0	-23.3	-26.0	-28.0	-29.9	-31.5
10-26-76	4	0.270	- 5.5	-11.5	-15.6	-18.4	-20.6	-22.2	-23.6	-25.0
11-10-76	4	0.085	-13.0	-18.0	-21.5	-24.1	-26.2	-27.9	-29.4	-30.5
11-12-76	4	0.100	- 7.0	-13.5	-17.7	-20.9	-23.4	-25.5	-27.4	-29.0
6-21-77	4	0.255	-11.0	-13.5	-15.5	-17.0	-18.4	-19.5	-20.4	-20.1
10-18-76	5	0.165	-10.8	-17.9	-21.0	-23.3	-25.2	-27.0	-28.7	-30.7
10-20-76	5	0.240	- 3.2	- 9.9	-13.8	-16.4	-18.0	-19.3	-20.5	-21.6
10-22-76	5	0.190	-11.1	-17.6	-21.6	-24.5	-26.5	-28.0	-29.3	-30.3
10-26-76	5	0.250	- 6.0	-13.7	-18.1	-21.0	-23.1	-25.0	-27.0	-29.0
11-10-76	5	0.085	-14.5	-18.5	-21.9	-24.6	-27.0	-29.5	-31.5	-33.3
11-12-76	5	0.110	- 7.0	-13.3	-17.5	-20.5	-23.0	-25.1	-27.0	-28.6
6-21-77	5	0.200	-12.1	-14.2	-16.0	-17.4	-18.5	-19.5	-20.5	-21.0
10-18-76	6	0.205	-11.0	-16.6	-20.1	-23.0	-25.1	-26.8	-28.0	-29.4
10-20-76	6	0.235	- 3.9	-10.1	-14.0	-16.5	-18.2	-19.4	-20.6	-21.9
10-22-76	6	0.210	-10.2	-16.7	-21.1	-24.3	-26.9	-29.1	-31.2	-33.0
10-26-76	6	0.270	- 7.0	-13.0	-17.1	-20.1	-22.5	-24.4	-26.1	-27.7
11-10-76	6	0.095	-12.5	-18.1	-22.1	-25.0	-27.2	-29.0	-30.5	-31.7
11-12-76	6	0.130	- 6.7	-13.0	-17.1	-20.4	-22.9	-25.0	-27.0	-29.0
6-21-77	6	0.215	-11.9	-14.0	-15.5	-17.0	-18.0	-19.0	-19.9	-20.6

Table A4. Slope of best fit straight lines in scattering coefficient versus volumetric soil moisture plots for each frequency and look angle. (db/gm/cc)

Frequency	Polarization	Look Angle							
		5°	10°	15°	20°	25°	30°	35°	40°
13.3 GHz	VV	31.02	19.96	17.75	15.34	14.01	13.02	12.04	10.99
1.6 GHz	HH	47.40	35.76	30.25	27.48	26.53	24.53	22.84	21.46
1.6 GHz	HV	28.36	25.03	23.84	24.32	25.45	26.79	28.43	29.41

Table A5. R^2 values of scattering coefficient versus volumetric soil moisture plots for each frequency and look angle.

Frequency	Polarization	Look Angle							
		5°	10°	15°	20°	25°	30°	35°	40°
13.3 GHz	VV	0.586	0.637	0.559	0.542	0.512	0.497	0.454	0.388
1.6 GHz	HH	0.603	0.513	0.477	0.471	0.491	0.482	0.451	0.385
1.6 GHz	HV	0.497	0.459	0.433	0.433	0.436	0.427	0.424	0.413

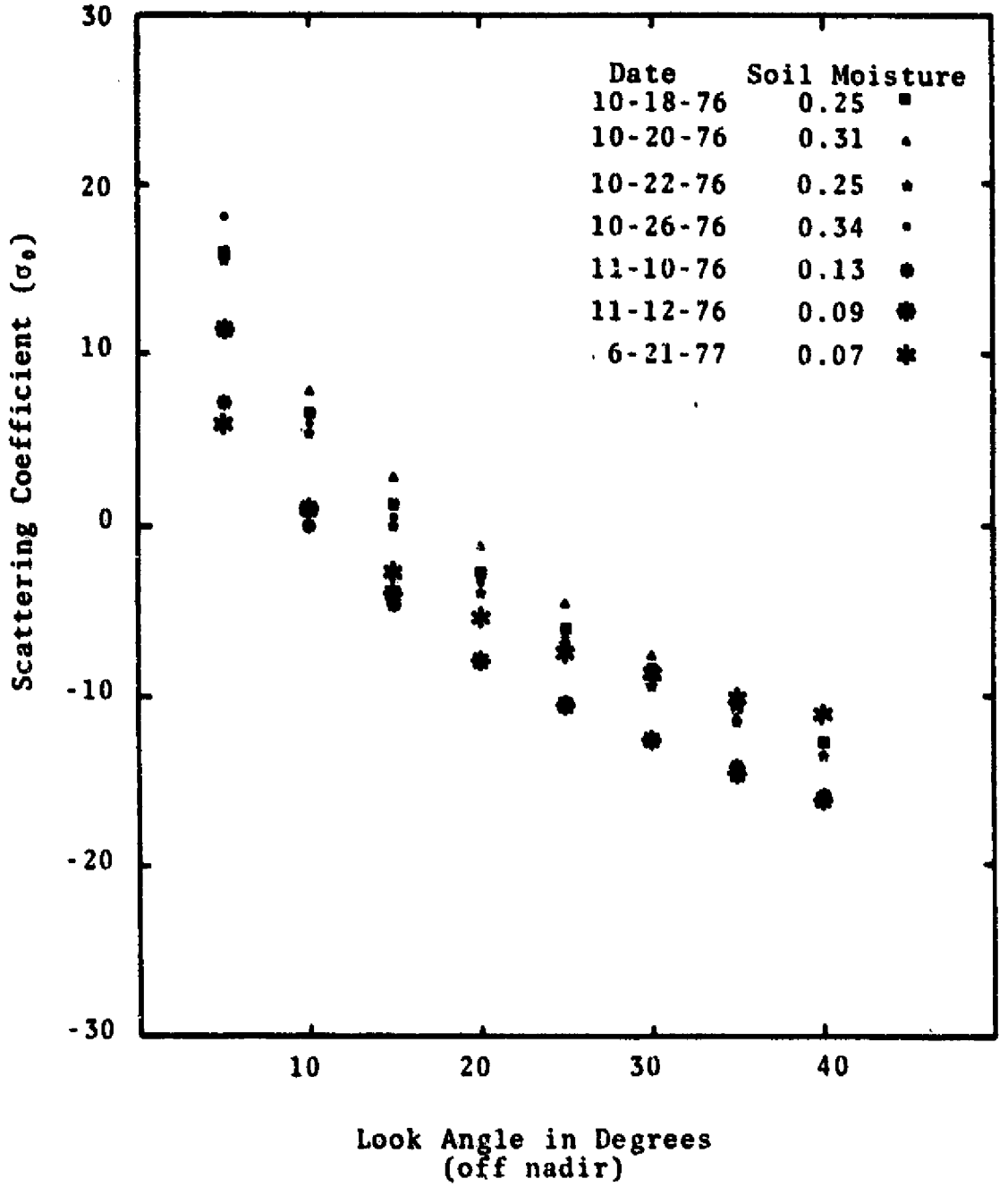

Figure A1. Comparison of σ_0 Values for Each Look Angle on All Missions Over Field 1 Using 13.3 GHz-VV

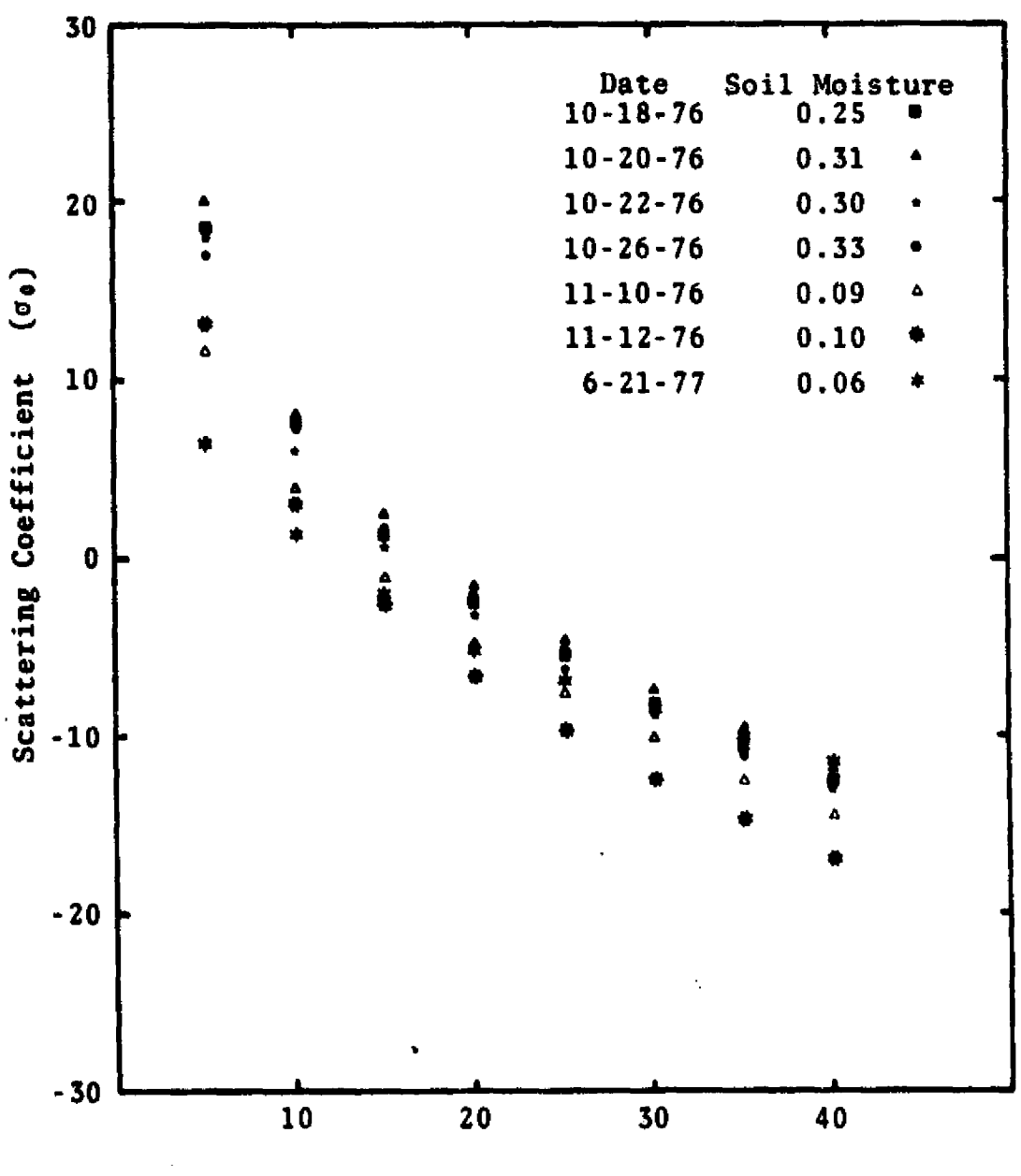

Figure A2. Comparison of σ_0 Values for Each Look Angle on All Missions Over Field 2 Using 13.3 GHz-VV

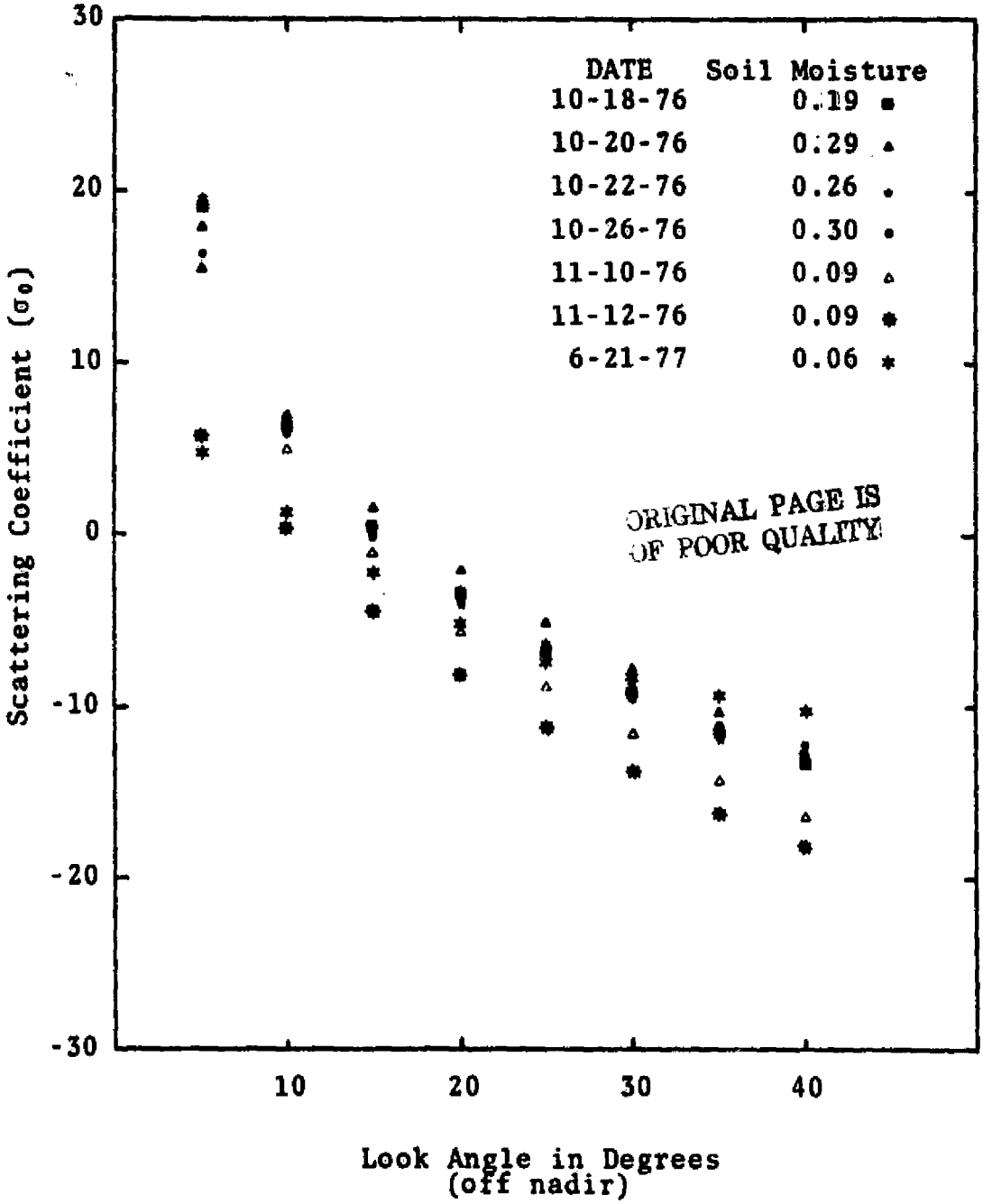

Figure A3. Comparison of σ_0 Values for Each Look Angle on All Missions Over Field 3 Using 13.3 GHz-VV

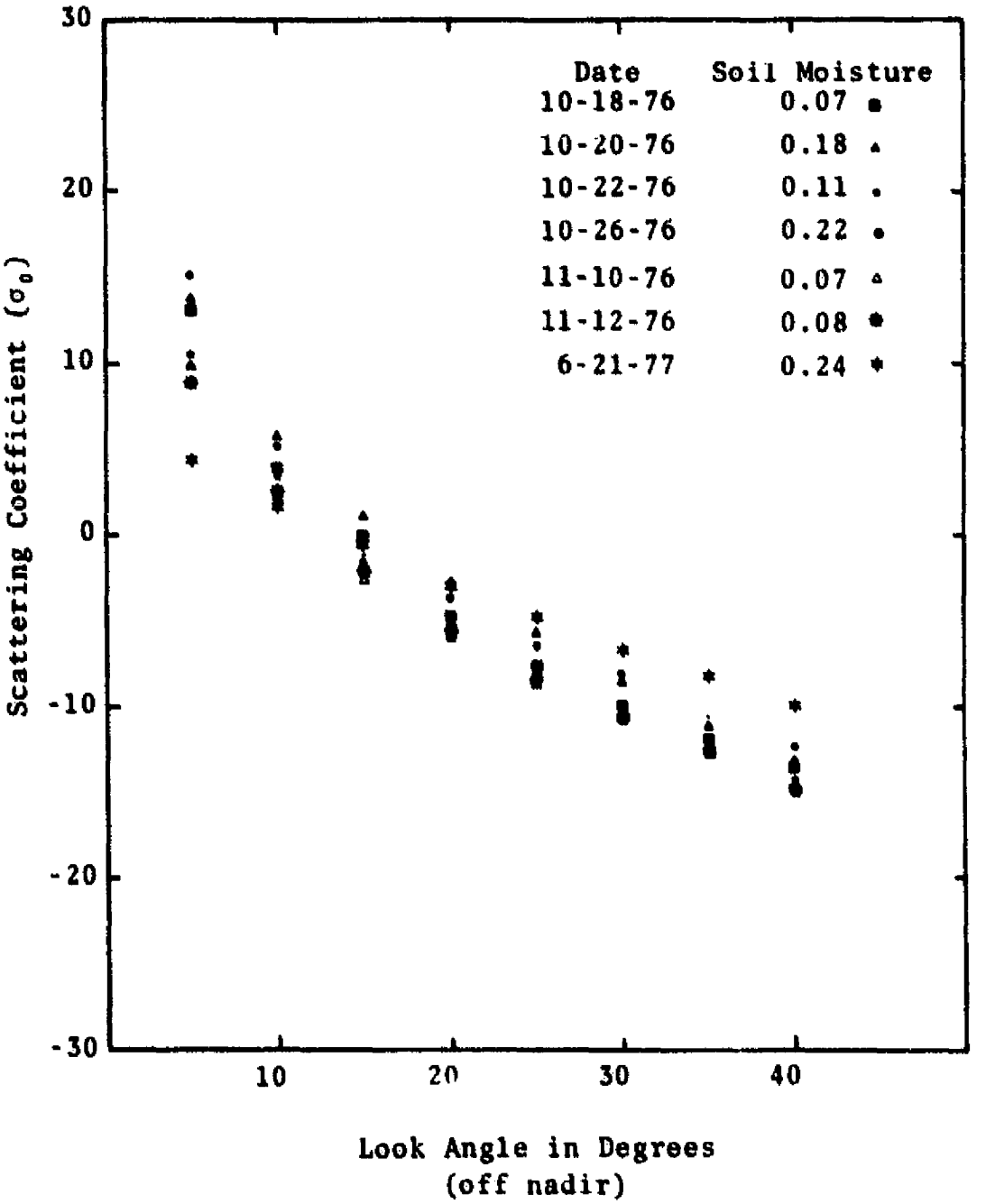

Figure A4. Comparison of σ_0 Values for Each Look Angle on All Missions Over Field 4 Using 13.3 GHz-VV

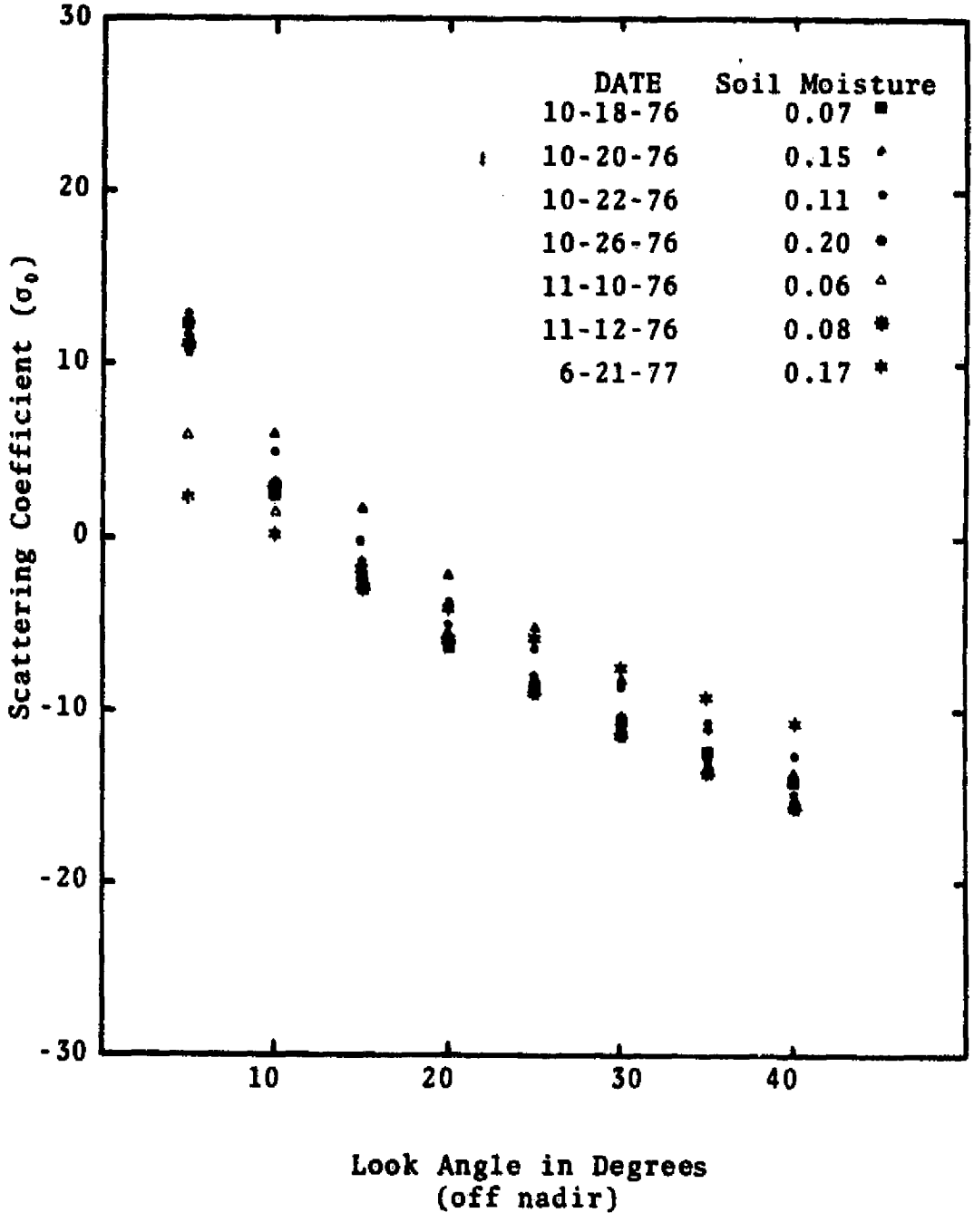

Figure A5. Comparison of σ_0 Values for Each Look Angle on All Missions Over Field 5 Using 13.3 GHz-VV

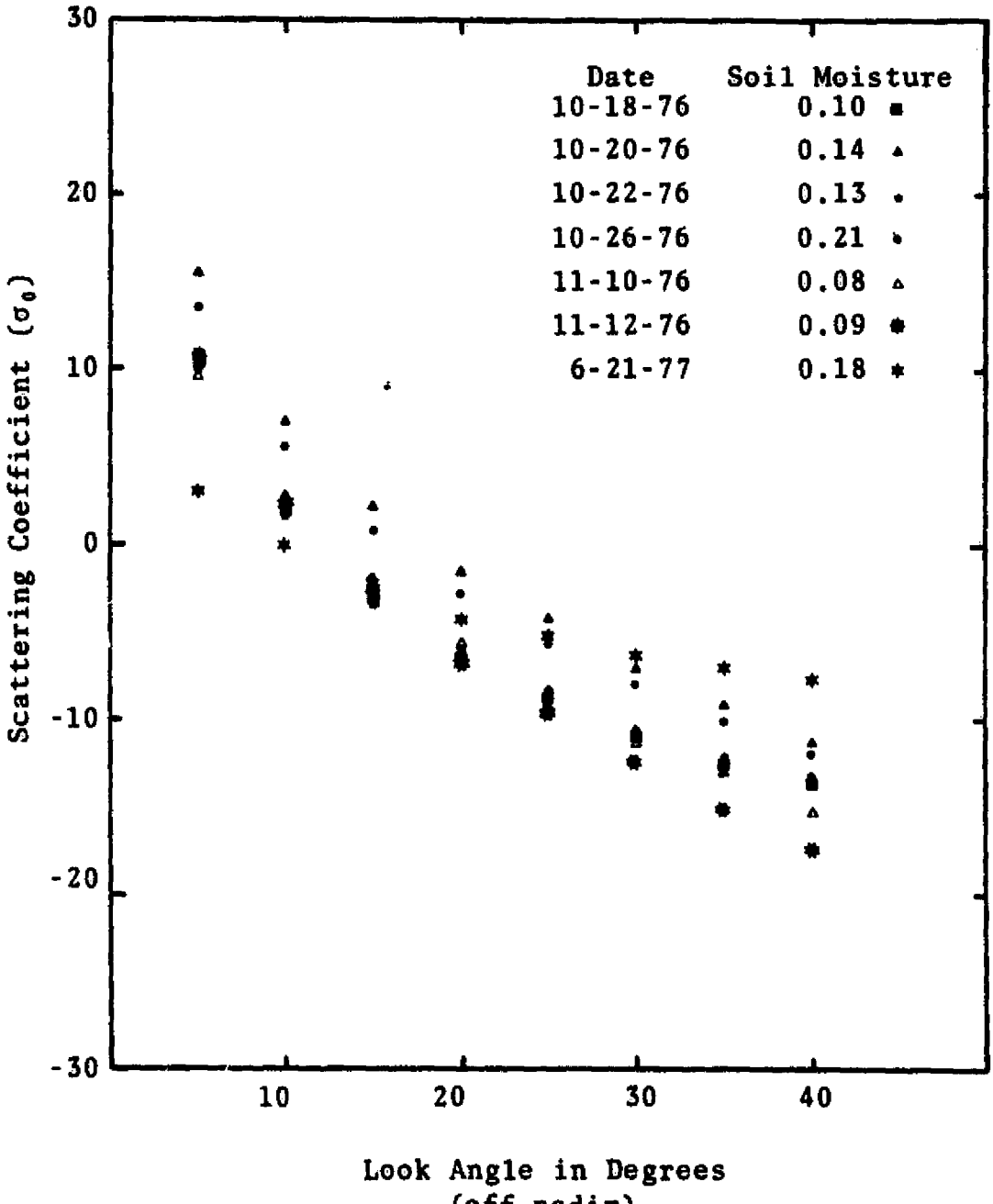

Figure A6. Comparison of σ_0 Values for Each Look Angle on All Missions over Field 6 Using 13.3 GHz-VV

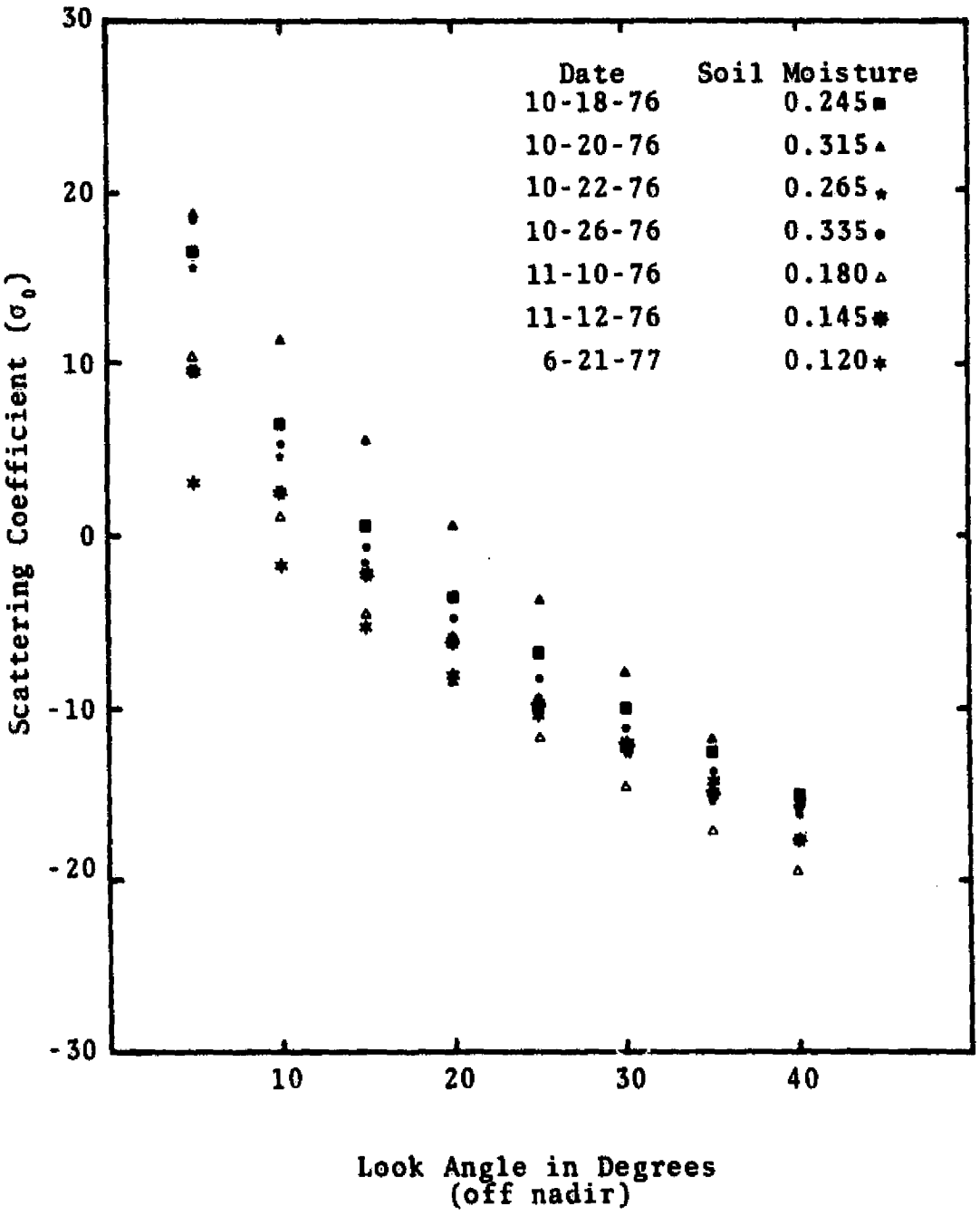

Figure A7. Comparison of σ_0 Values for Each Look Angle on All Missions Over Field 1 Using 1.6 GHz-HH

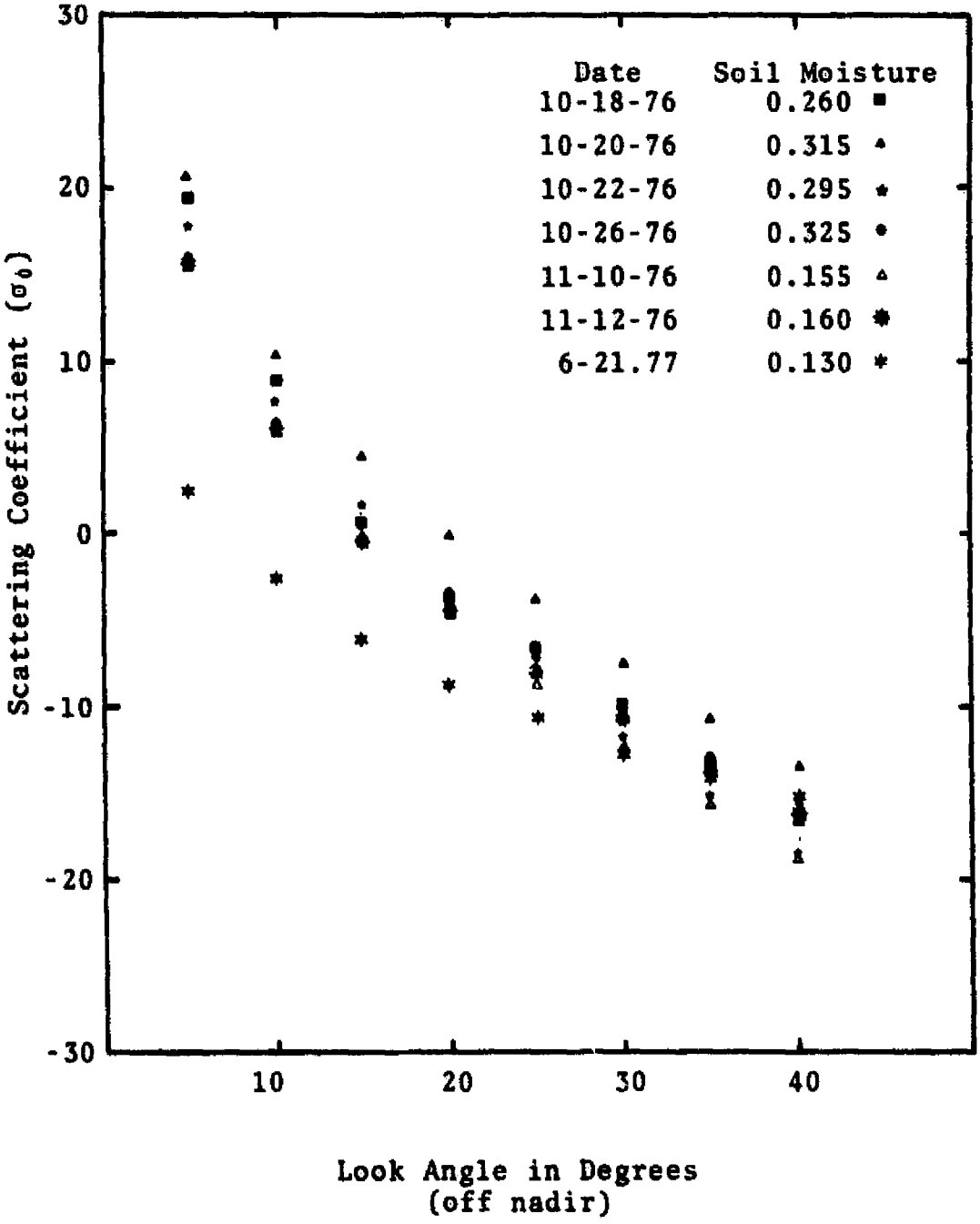

Figure A8. Comparison of σ_0 Values for Each Look Angle on All Missions over Field 2 Using 1.6 GHz-HH

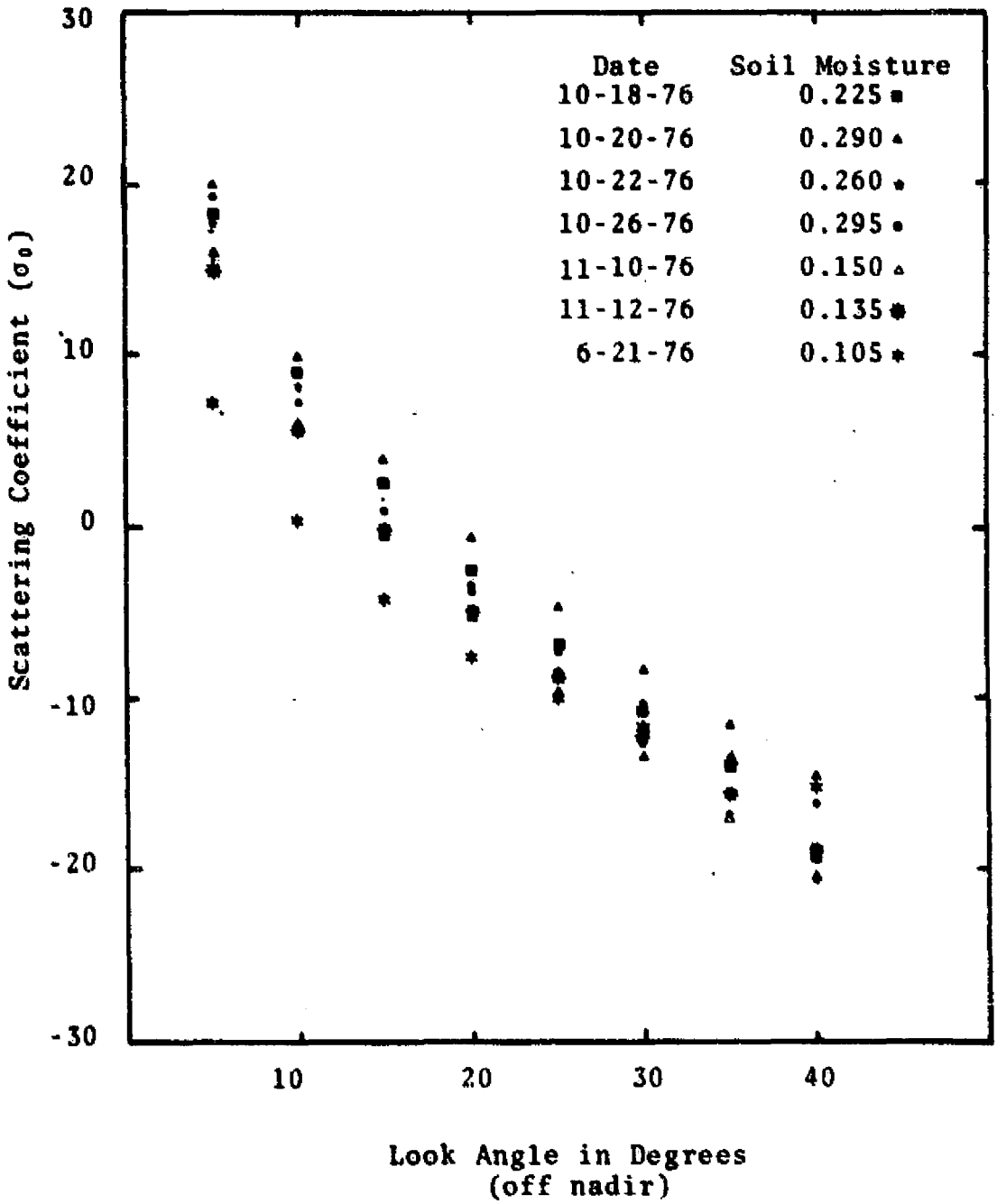

Figure A9. Comparison of σ_0 Values for Each Look Angle on All Missions Over Field 3 Using 1.6GHz-HH

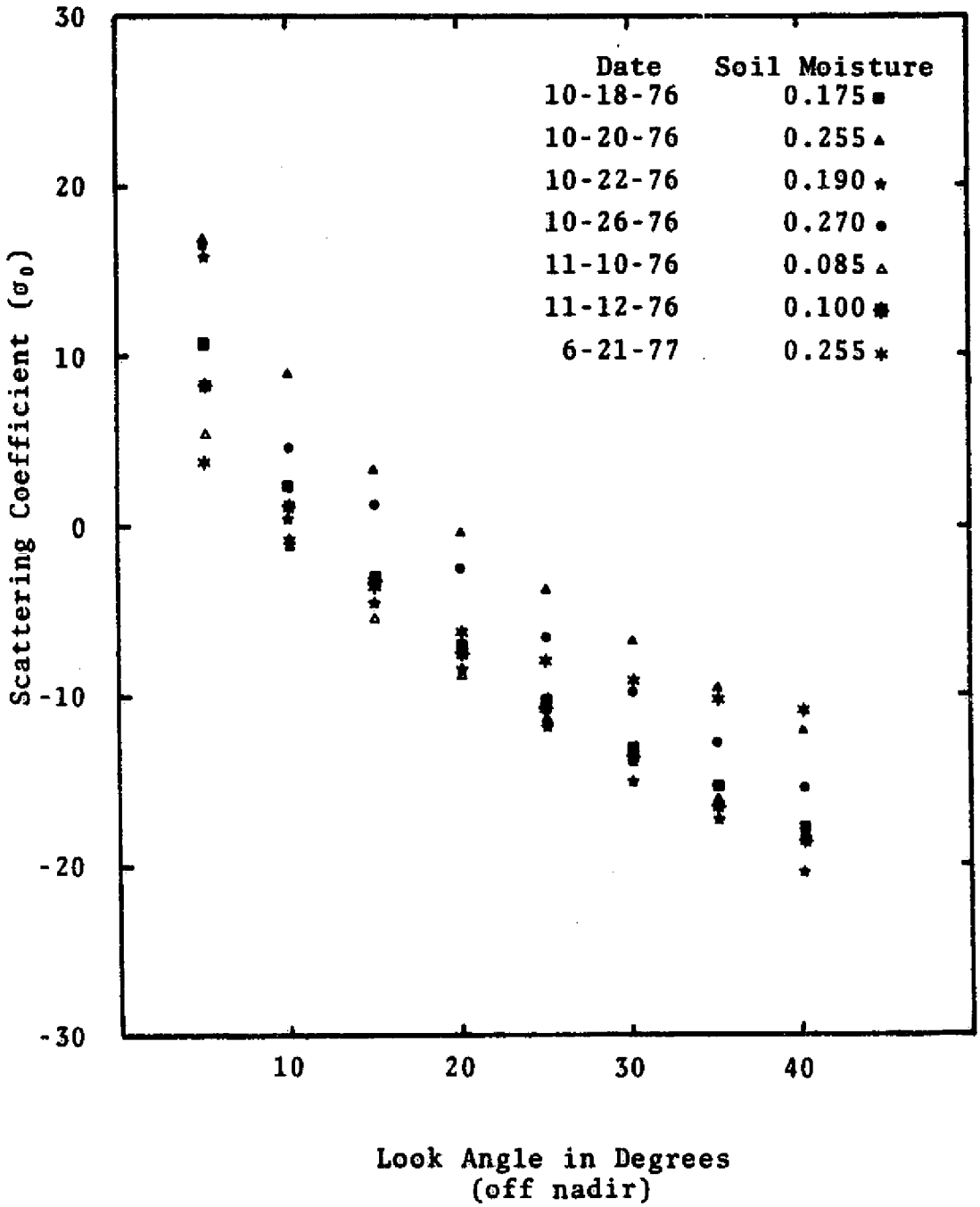

Figure A10. Comparison of σ_0 Values for Each Look Angle on All Missions Over Field 4 Using 1.6 GHz-HH

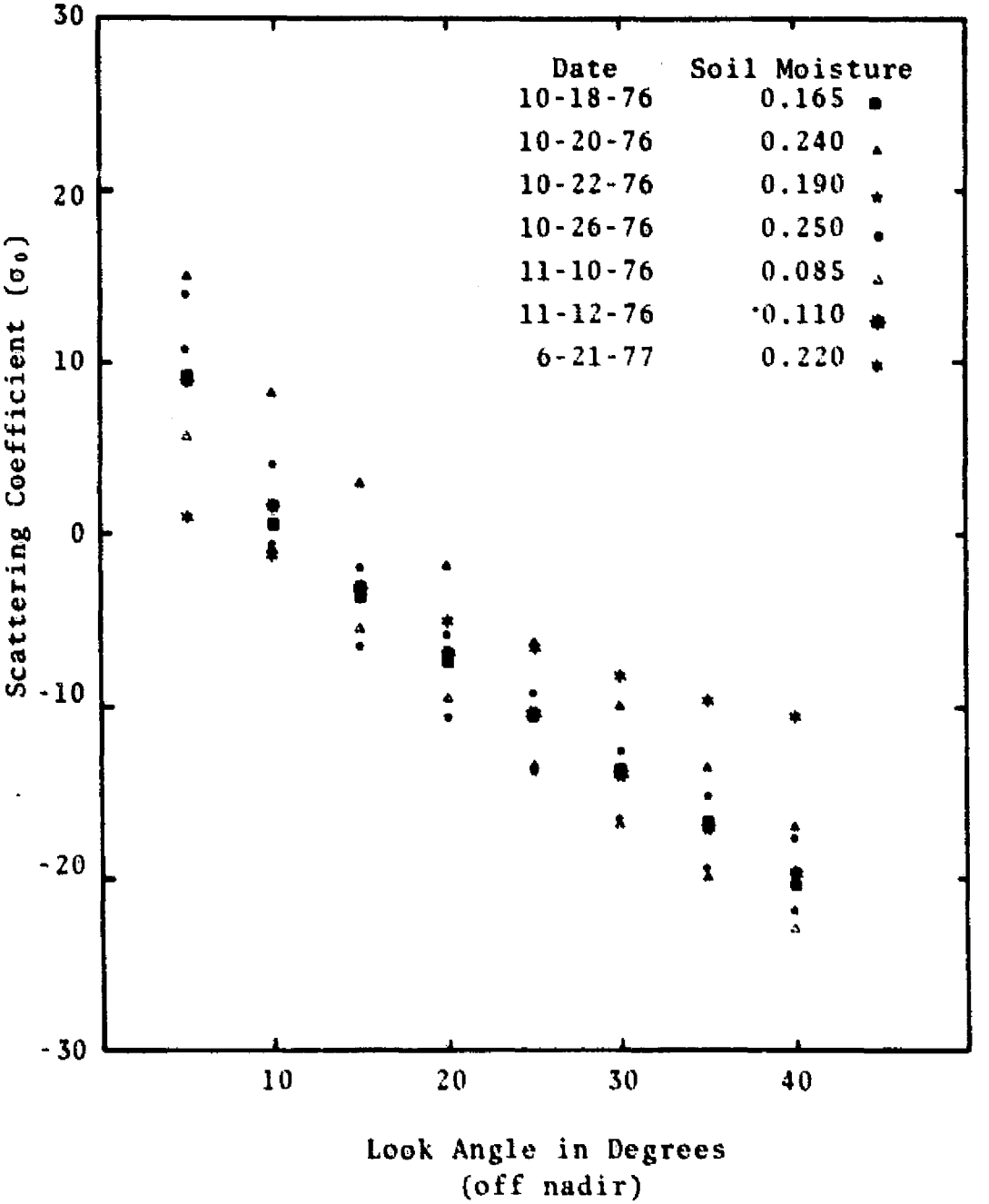

Figure A11. Comparison of σ_0 Values For Each Look Angle on All Missions Over Field 5 Using 1.6 GHz-HH

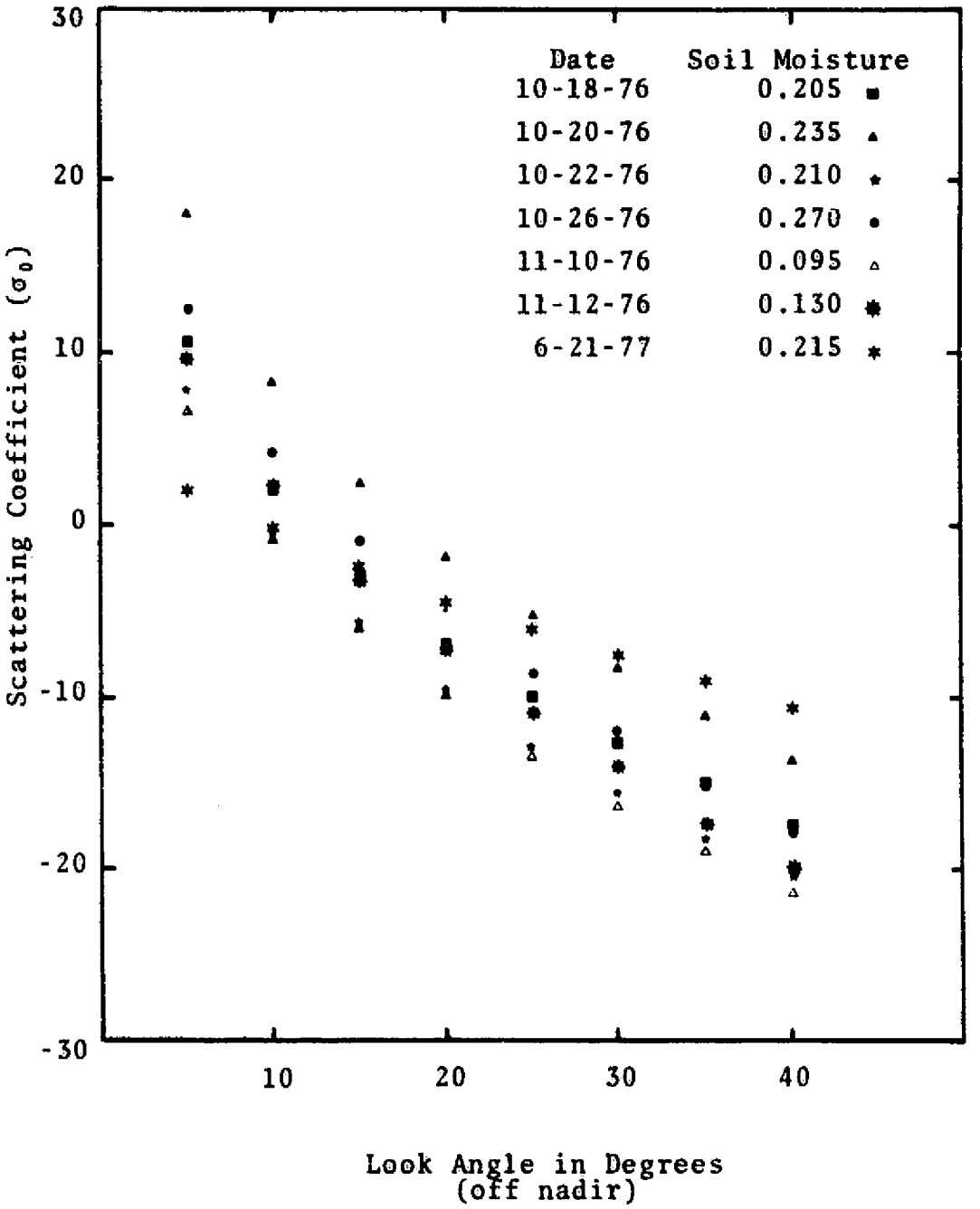

Figure A12. Comparison of σ_0 Values for Each Look Angle on All Missions Over Field 6 Using 1.6 GHz-HH

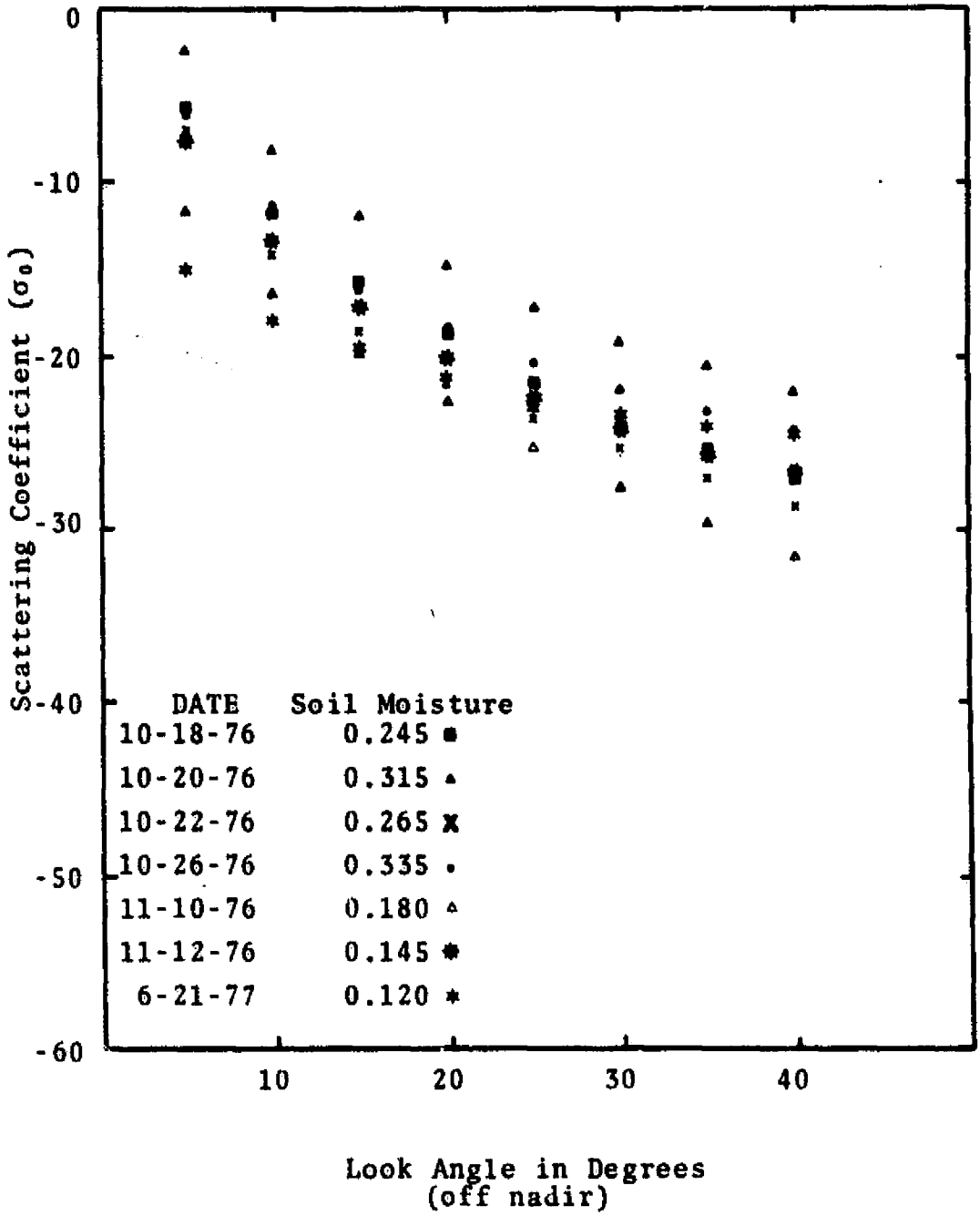

Figure A13. Comparison of σ_0 Values for Each Look Angle on All Missions Over Field 1 Using 1.6 GHz-HV

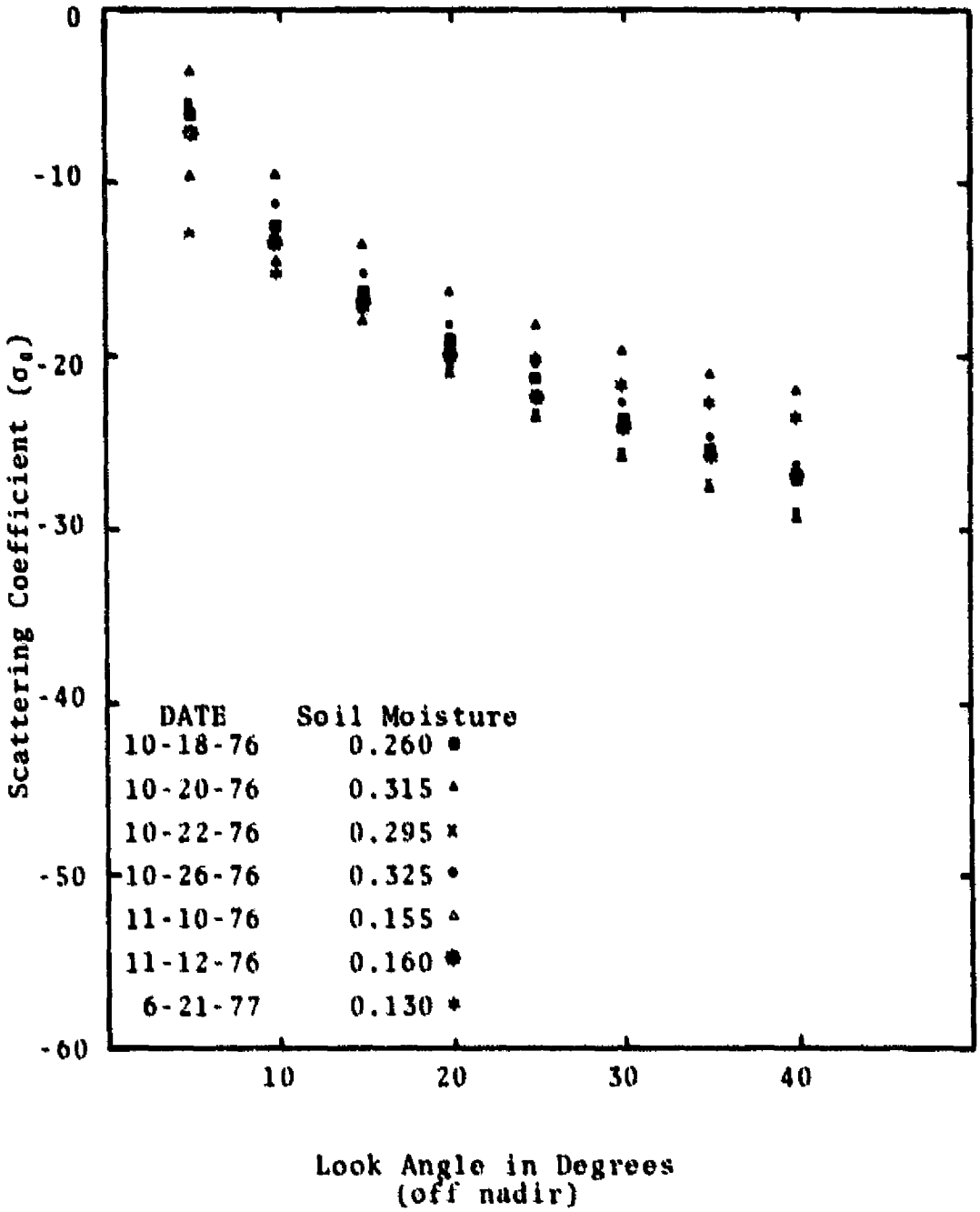

Figure A14. Comparison of σ_0 Values for Each Look Angle on All Missions Over Field 2 Using 1.6 GHz-HV

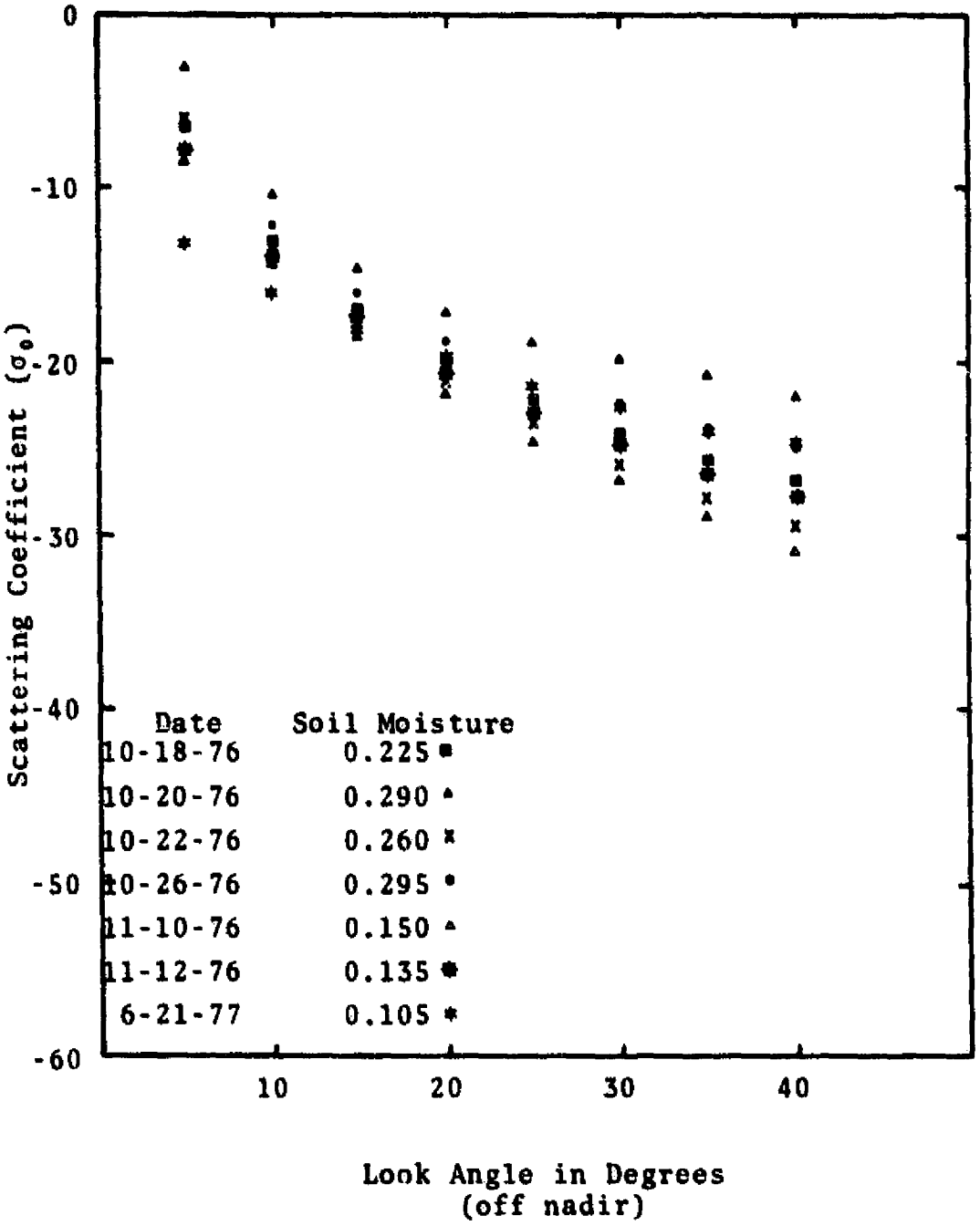

Figure A15. Comparison of σ_0 Values for Each Look Angle on All Missions Over Field 3 Using 1.6 GHz-HV

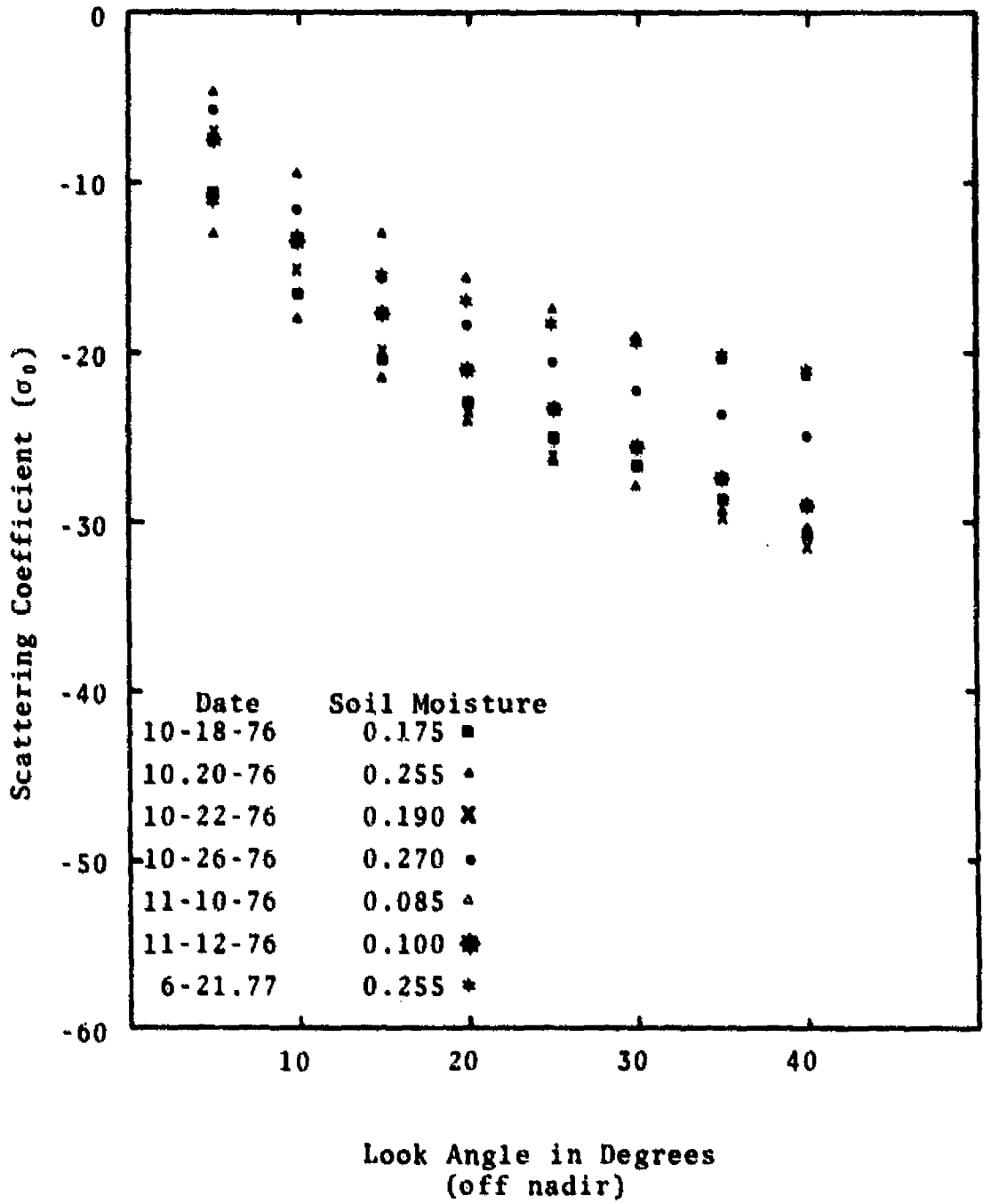

Figure A16. Comparison of σ_0 Values for Each Look Angle on All Missions Over Field 4 Using 1.6 GHz-HV

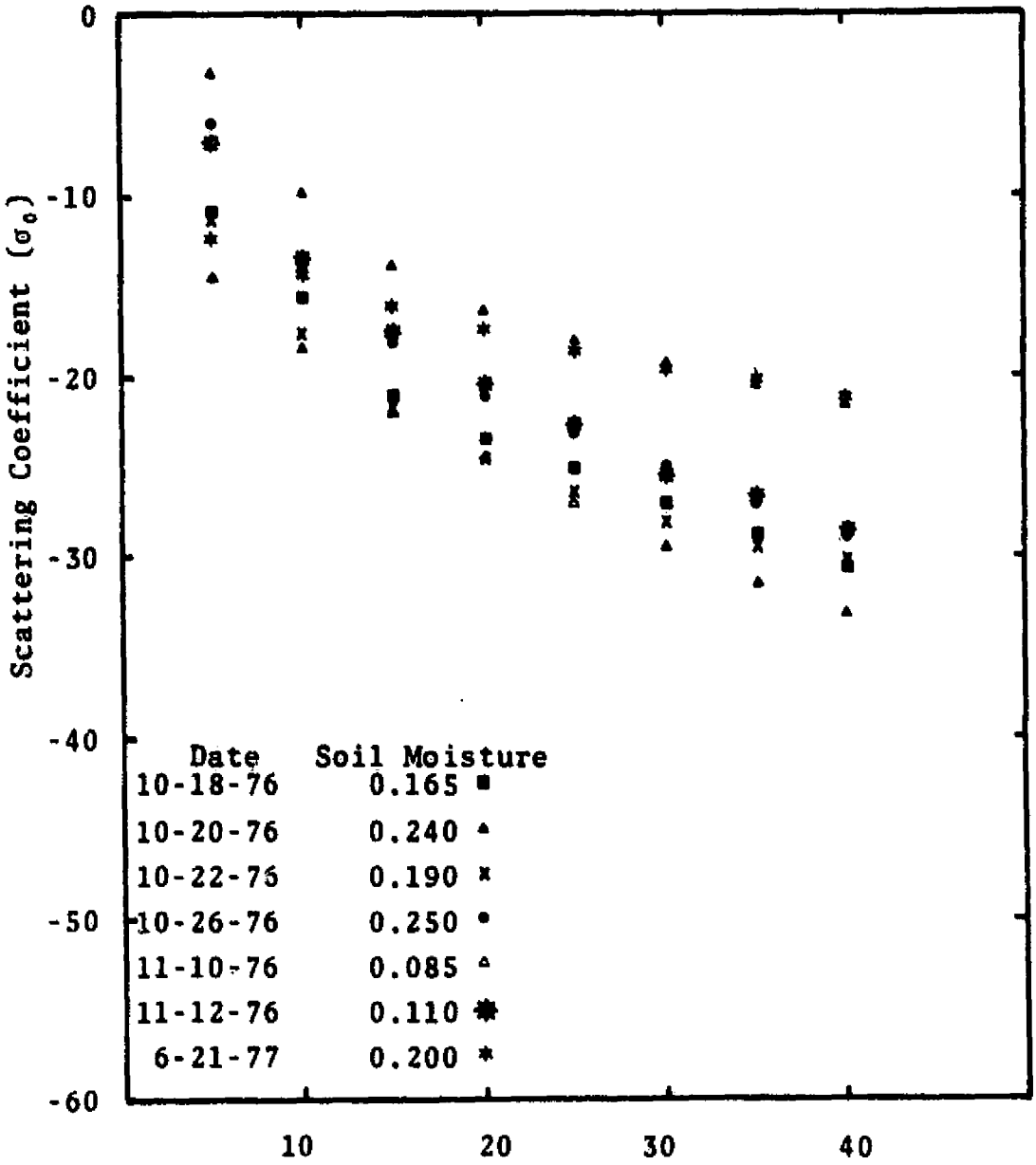

Figure A17. Comparison of σ_0 Values for Each Look Angle on All Missions Over Field 5 Using 1.6 GHz-HV

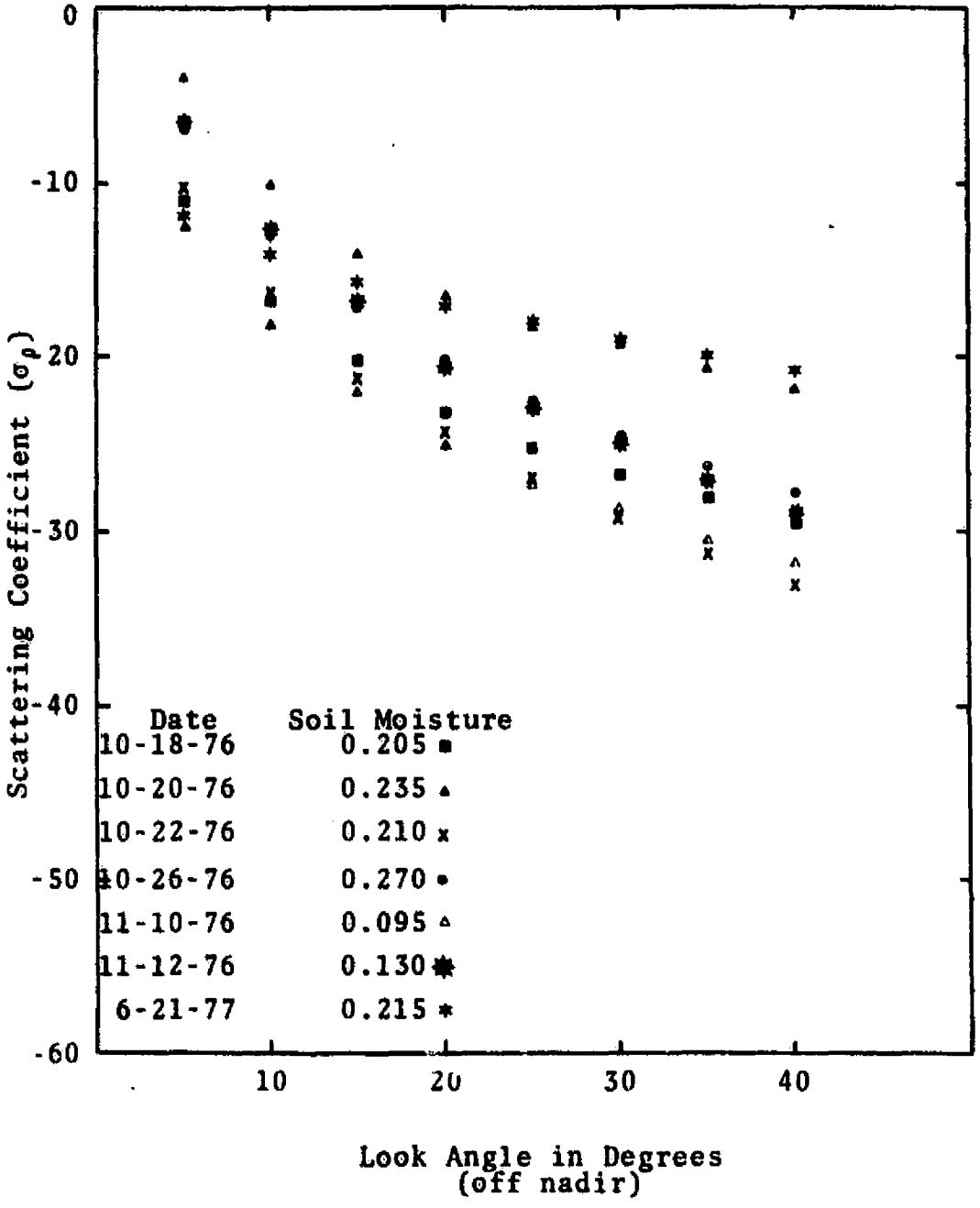

Figure A18. Comparison of σ_0 Values for Each Look Angle on All Missions Over Field 6 Using 1.6 GHz-HV

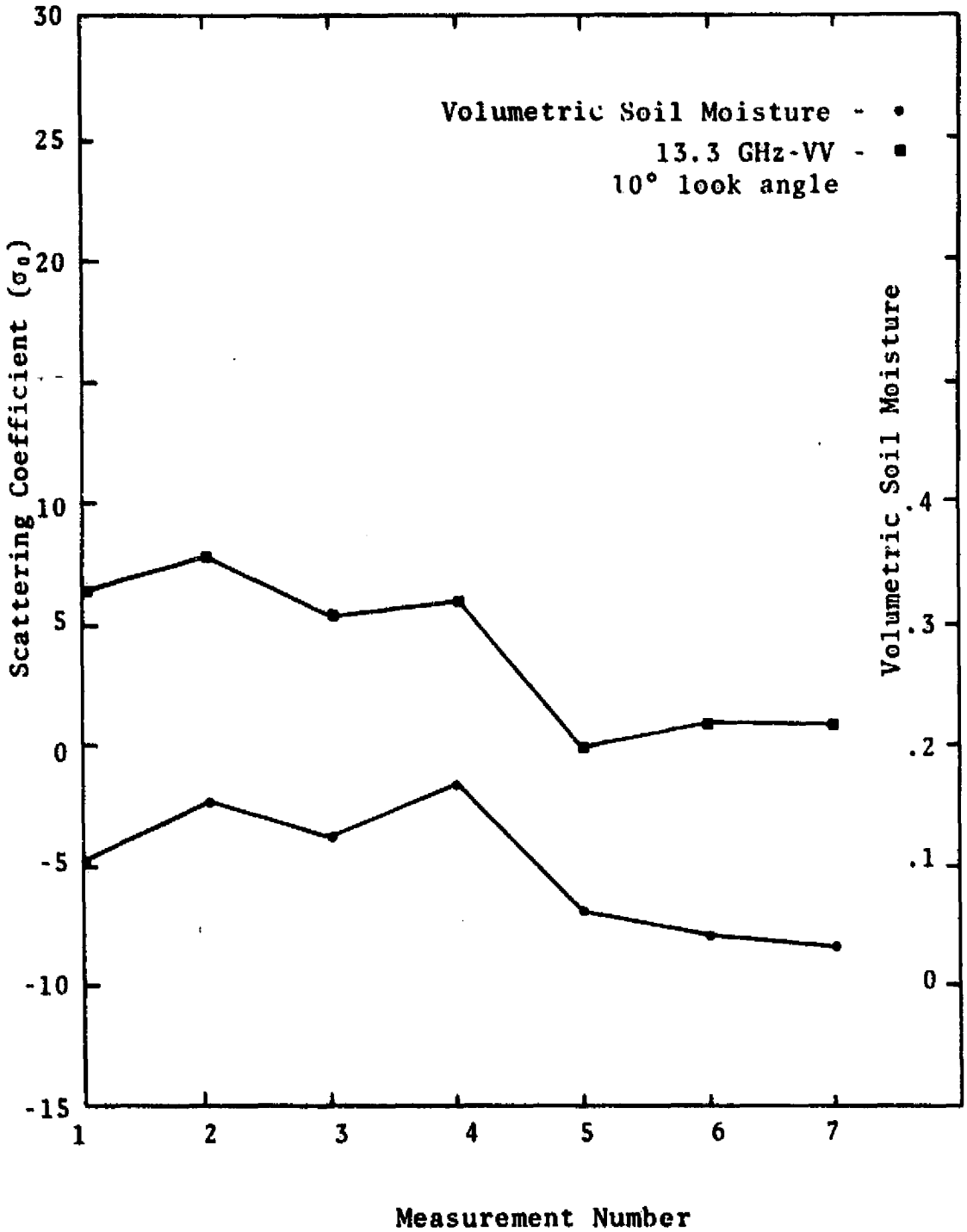

Figure A19. The Relation Between 13.3 GHz-VV Scattering Coefficient (σ_0) and Volumetric Soil Moisture for Field 1 for the Series of Seven Flights (Disked Bare Ground on the First Six Flights and Vegetated on the Final Flight).

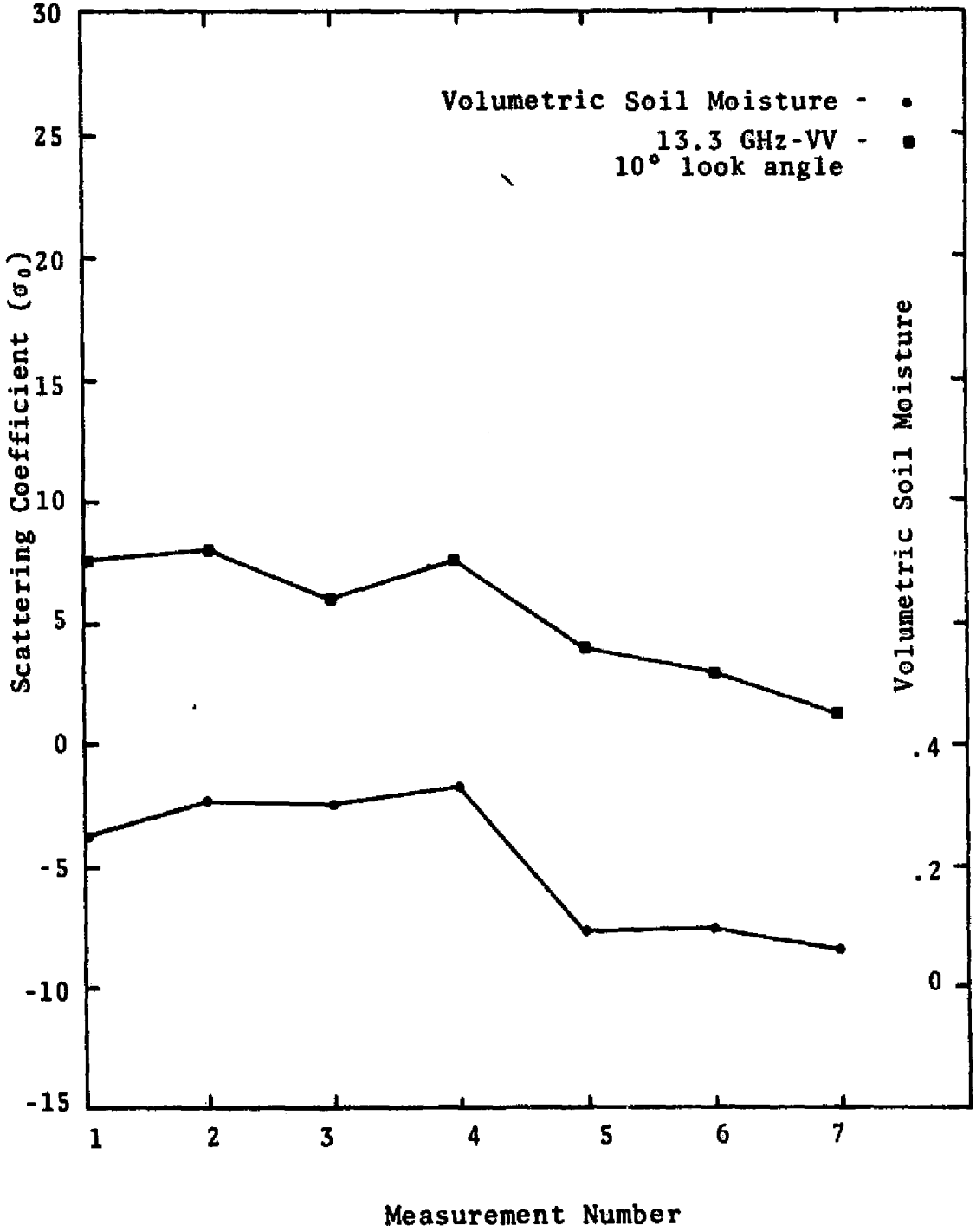

Figure A20. The Relation Between 13.3 GHz-VV Scattering Coefficient (σ_0) and Volumetric Soil Moisture for Field 2 for the Series of Seven Flights (Disked Bare Ground on the First Six Flights and Vegetated on the Final Flight).

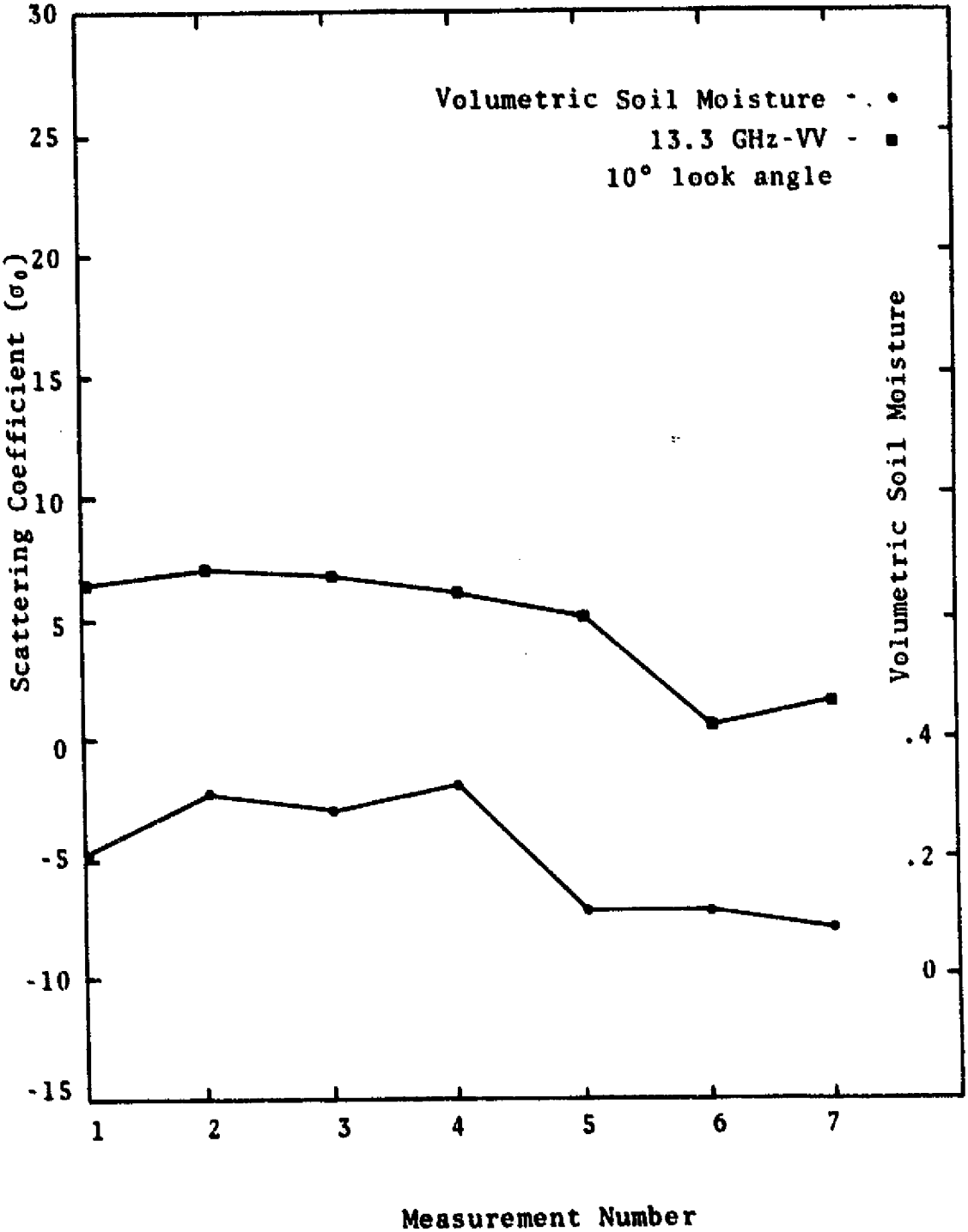

Figure A21. The Relation Between 13.3 GHz-VV Scattering Coefficient (σ_0) and Volumetric Soil Moisture for Field 3 for the Series of Seven Flights (Disked Bare Ground on the First Six Flights and Vegetated on the Final Flight).

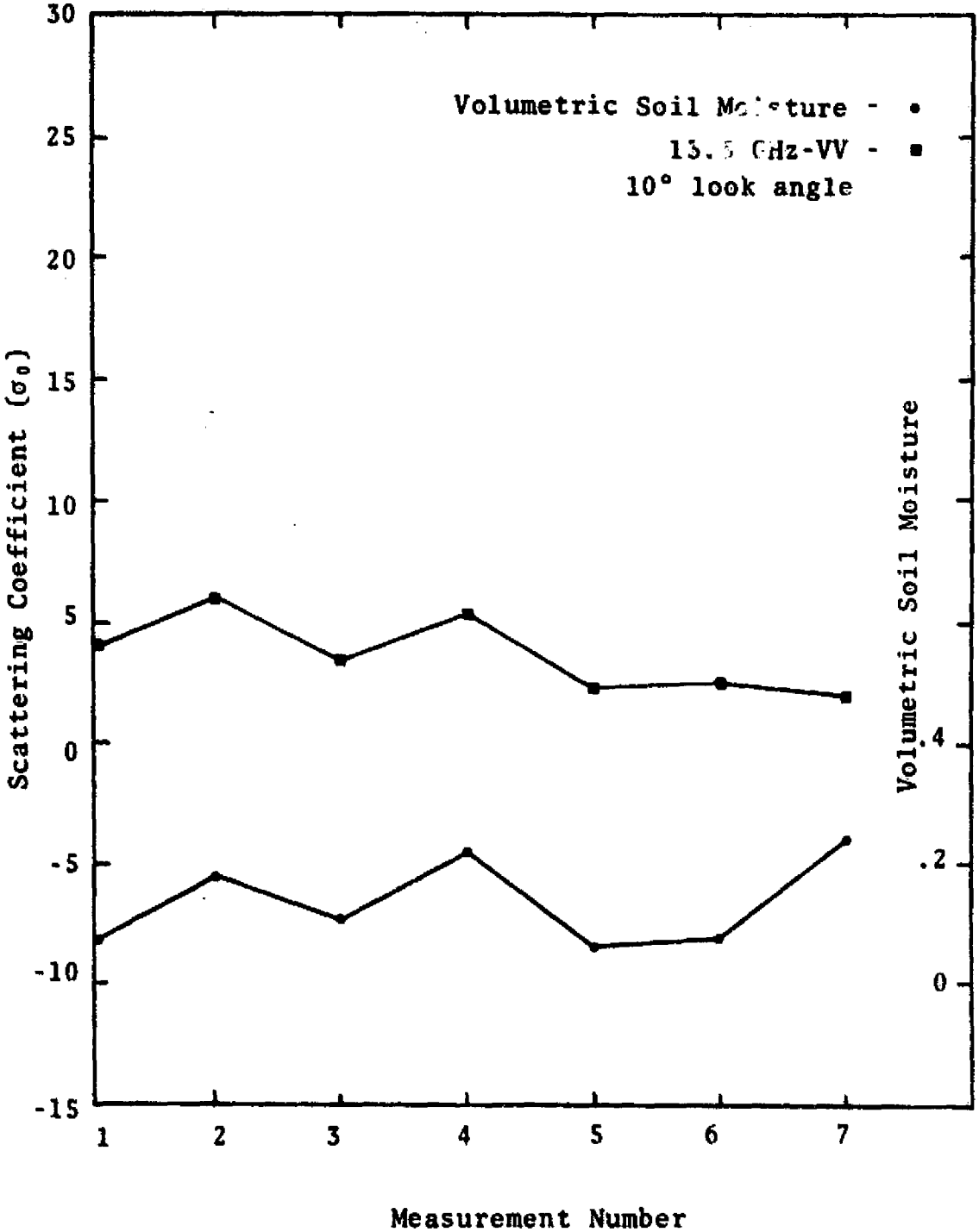

Figure A22. The Relation Between 13.3 GHz-VV Scattering Coefficient (σ_0) and Volumetric Soil Moisture for Field 4 for the Series of Seven Flights (Disked Bare Ground on the First Six Flights and Vegetated on the Final Flight).

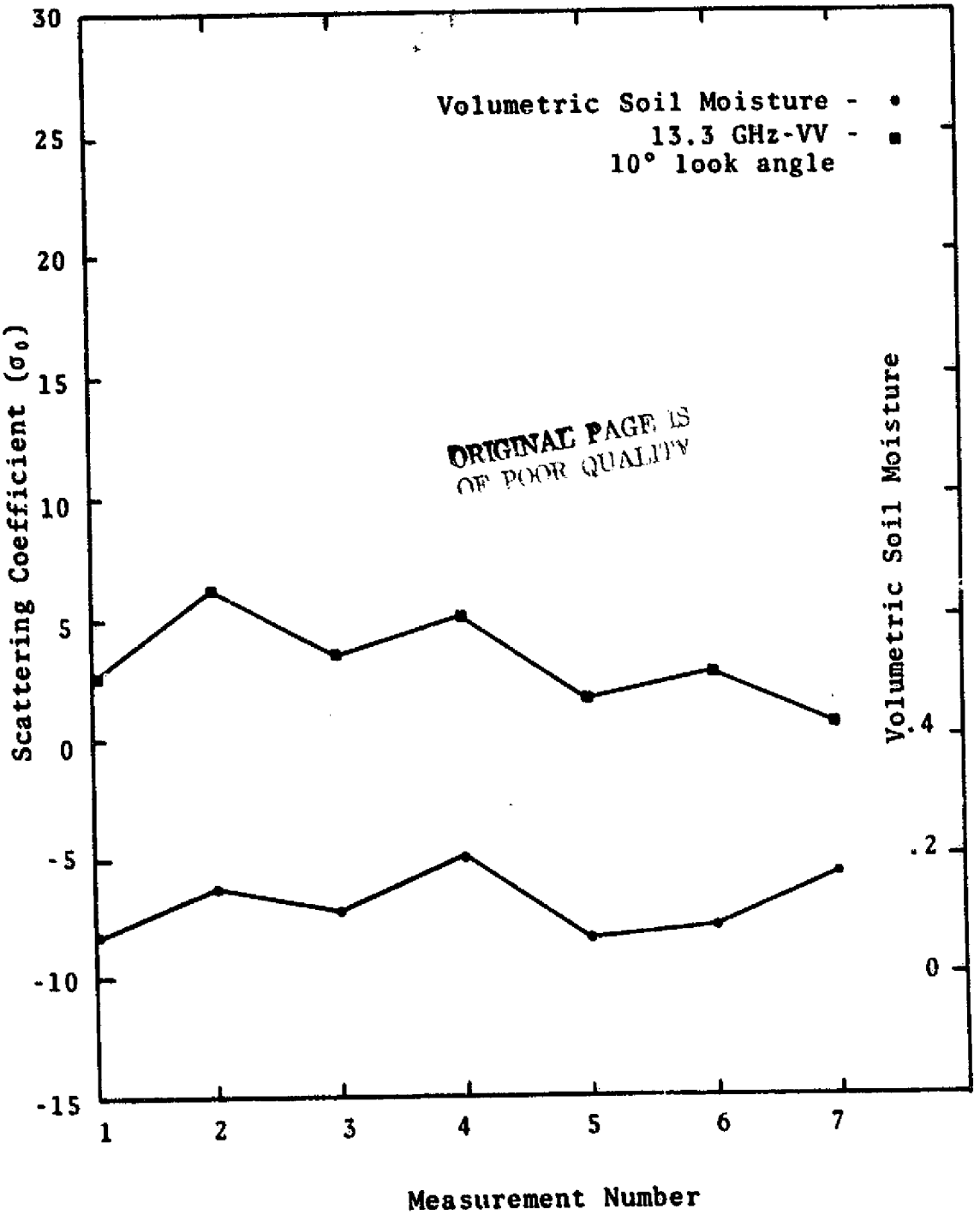

Figure A23. The Relation Between 13.3 GHz-VV Scattering Coefficient (σ_0) and Volumetric Soil Moisture for Field 5 for the Series of Seven Flights (Disked Bare Ground on the First Six Flights and Vegetated on the Final Flight).

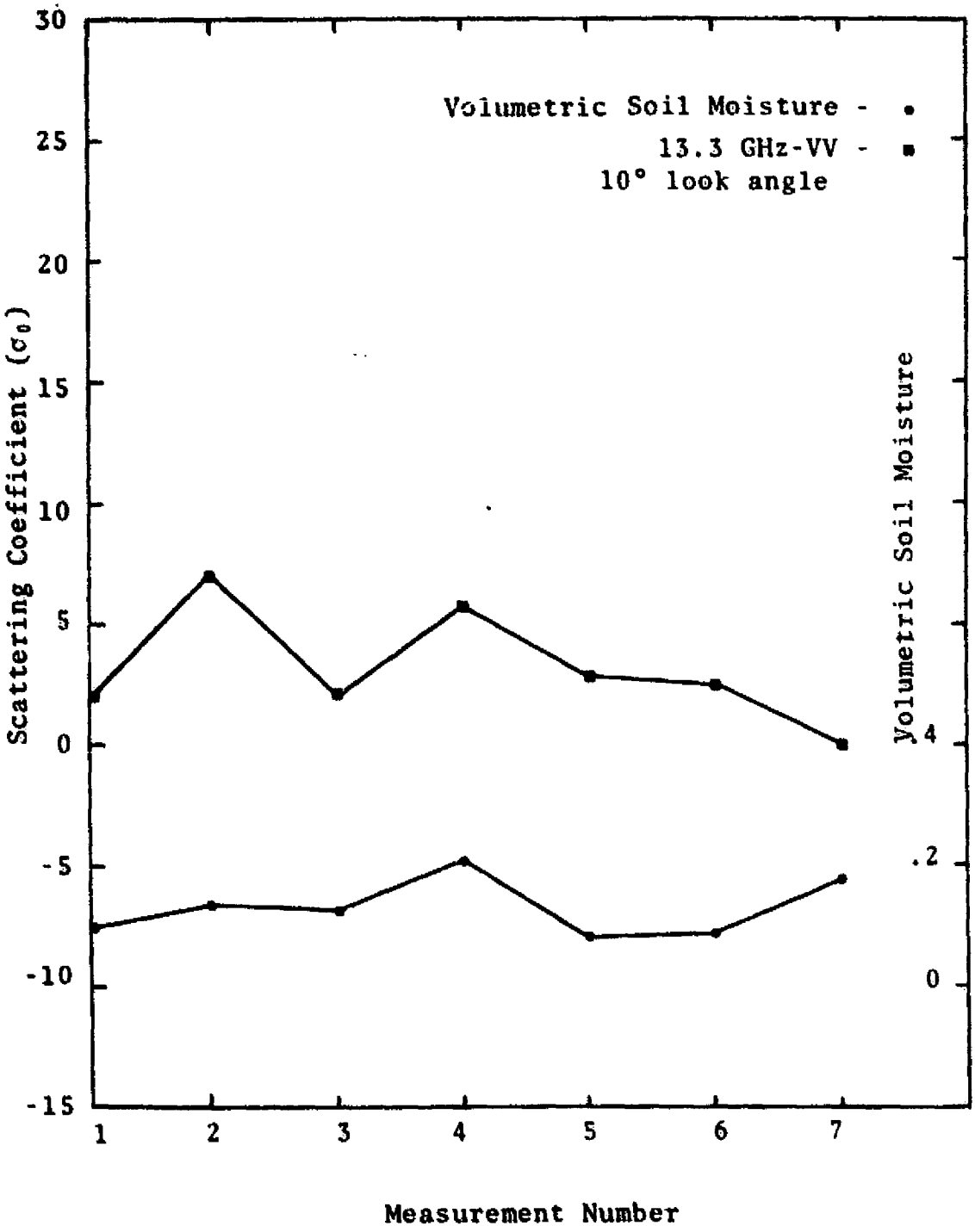

Figure A24. The Relation Between 13.3 GHz-VV Scattering Coefficient (σ_0) and Volumetric Soil Moisture for Field 6 for the Series of Seven Flights (Disked Bare Ground on the First Six Flights and Vegetated on the Final Flight).

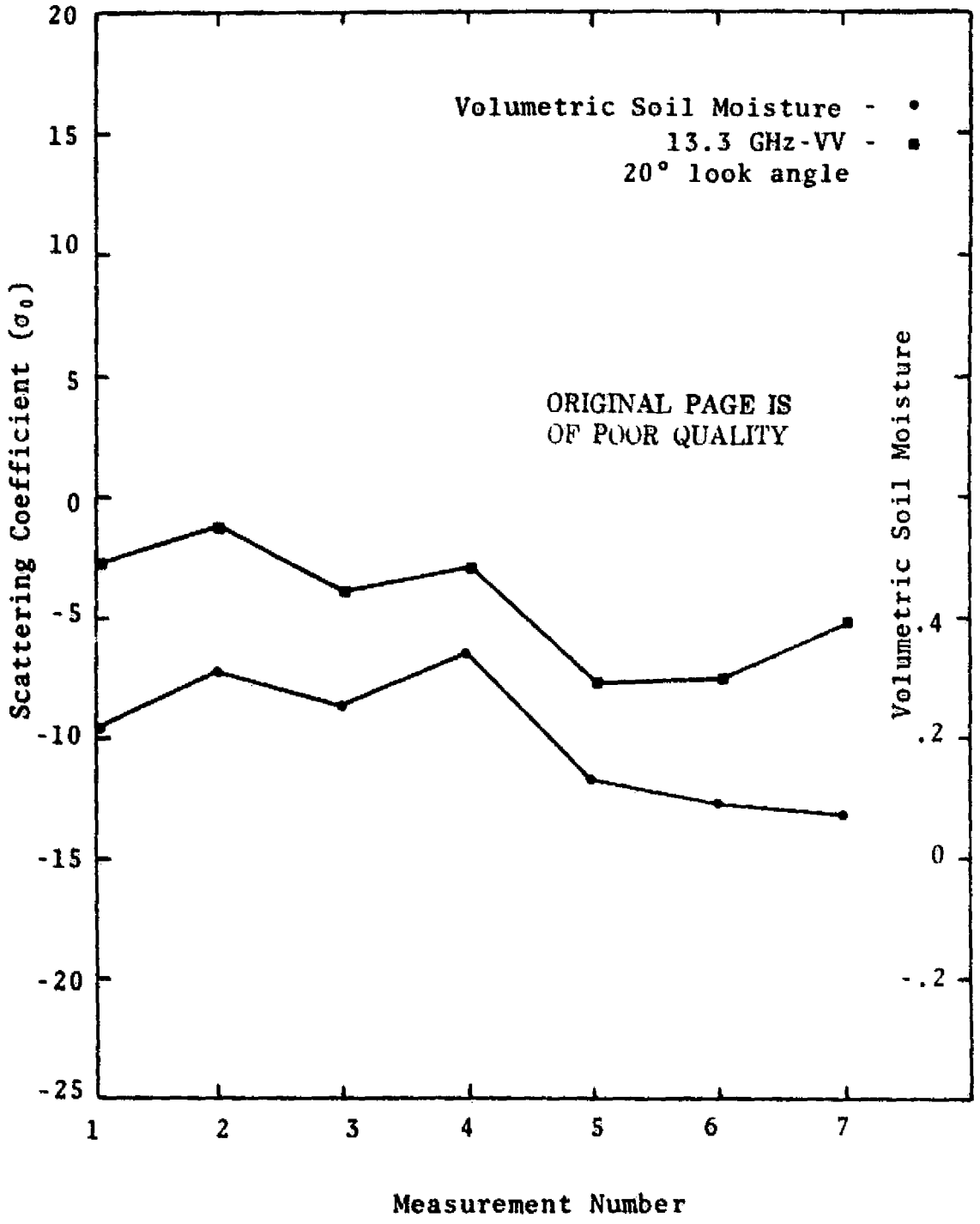

Figure A25. The Relation Between 13.3 GHz-VV Scattering Coefficient (σ_0) and Volumetric Soil Moisture for Field 1 for the Series of Seven Flights (Disked Bare Ground on the First Six Flights and Vegetated on the Final Flight).

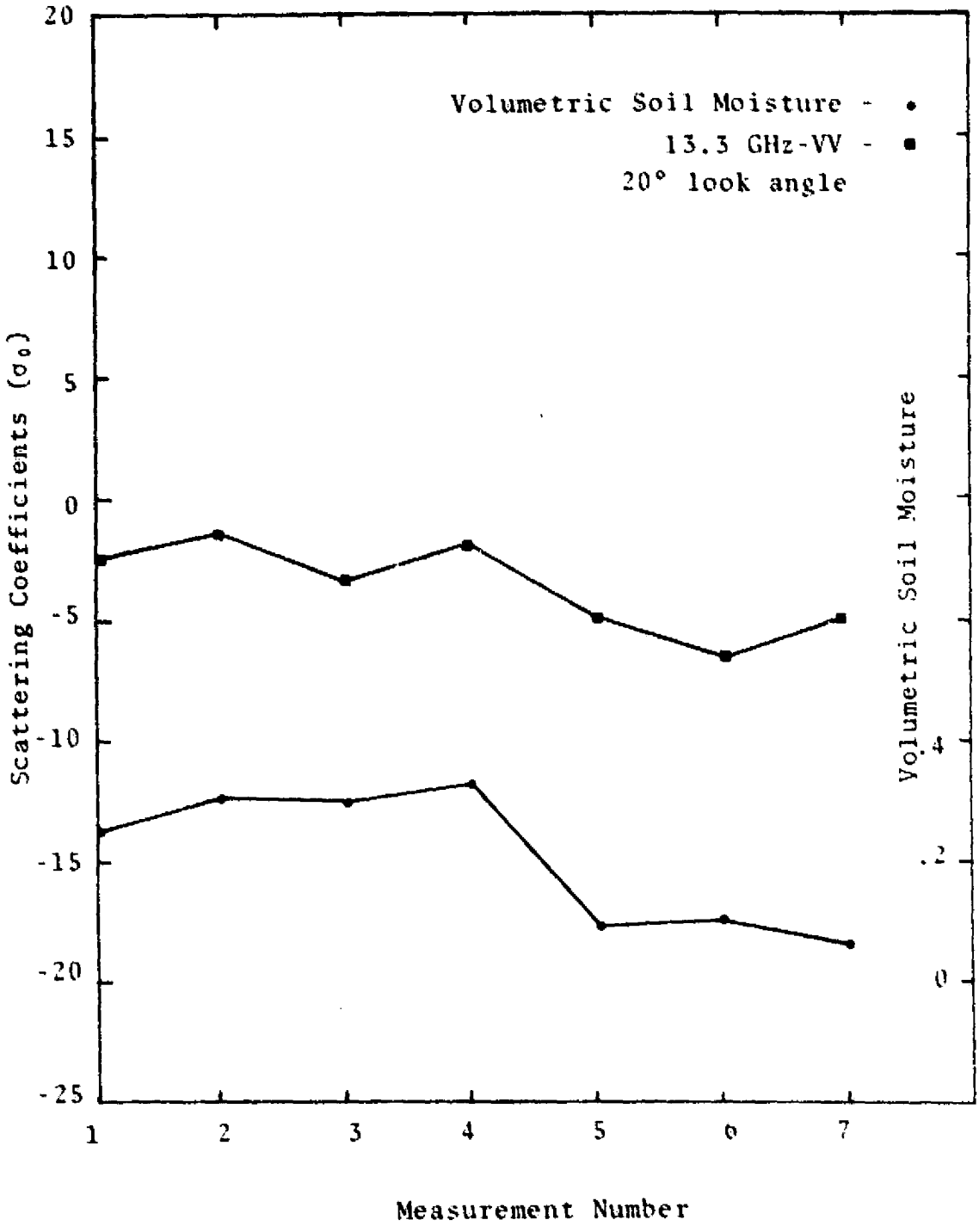

Figure A26. The Relation Between 13.3 GHz-VV Scattering Coefficient (σ_0) and Volumetric Soil Moisture for Field 2 for the Series of Seven Flights (Disked Bare Ground on the First Six Flights and Vegetated on the Final Flight).

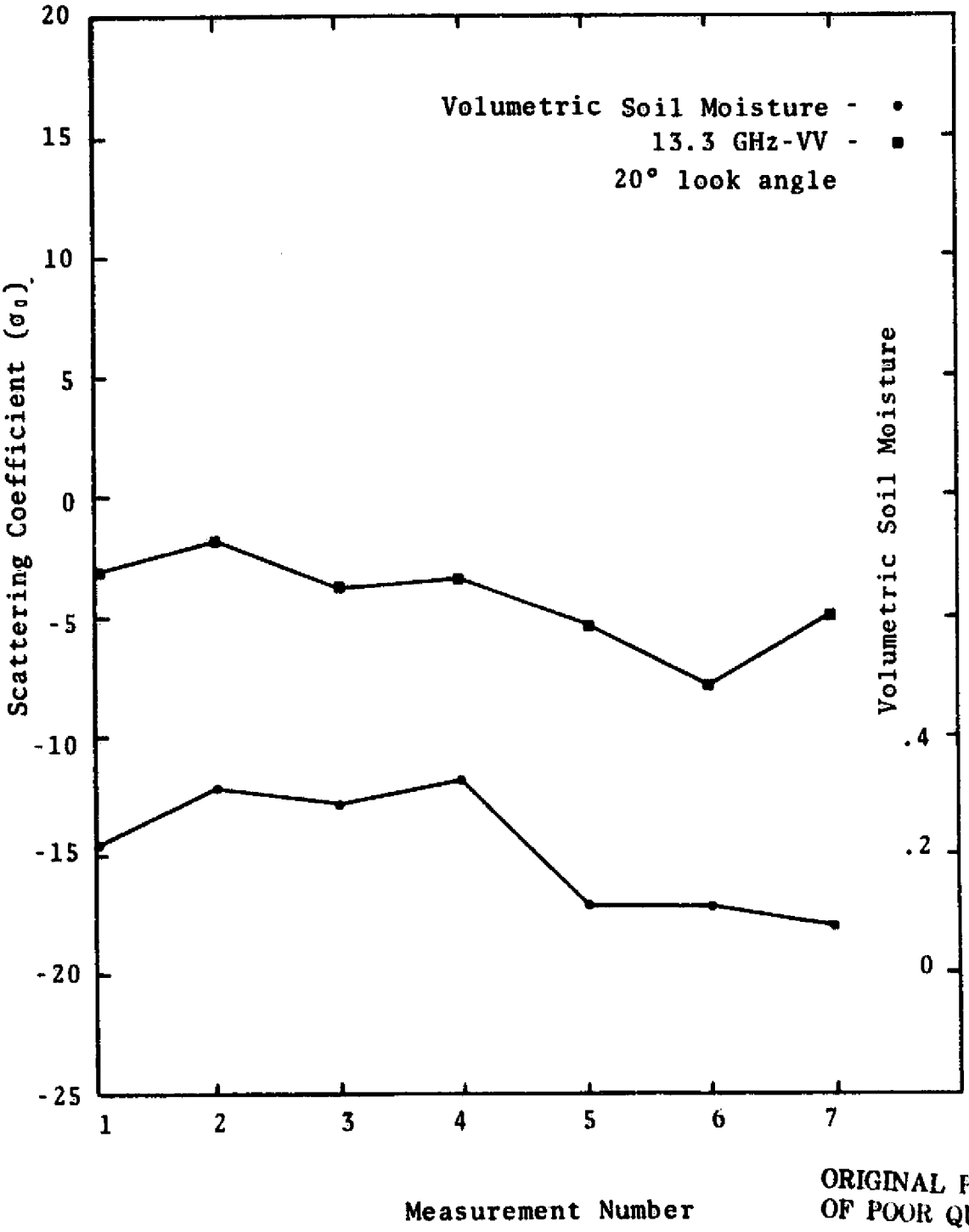

Figure A27. The Relation Between 13.3 GHz-VV Scattering Coefficient (σ_0) and Volumetric Soil Moisture for Field 3 for the Series of Seven Flights (Disked Bare Ground on the First Six Flights and Vegetated on the Final Flight).

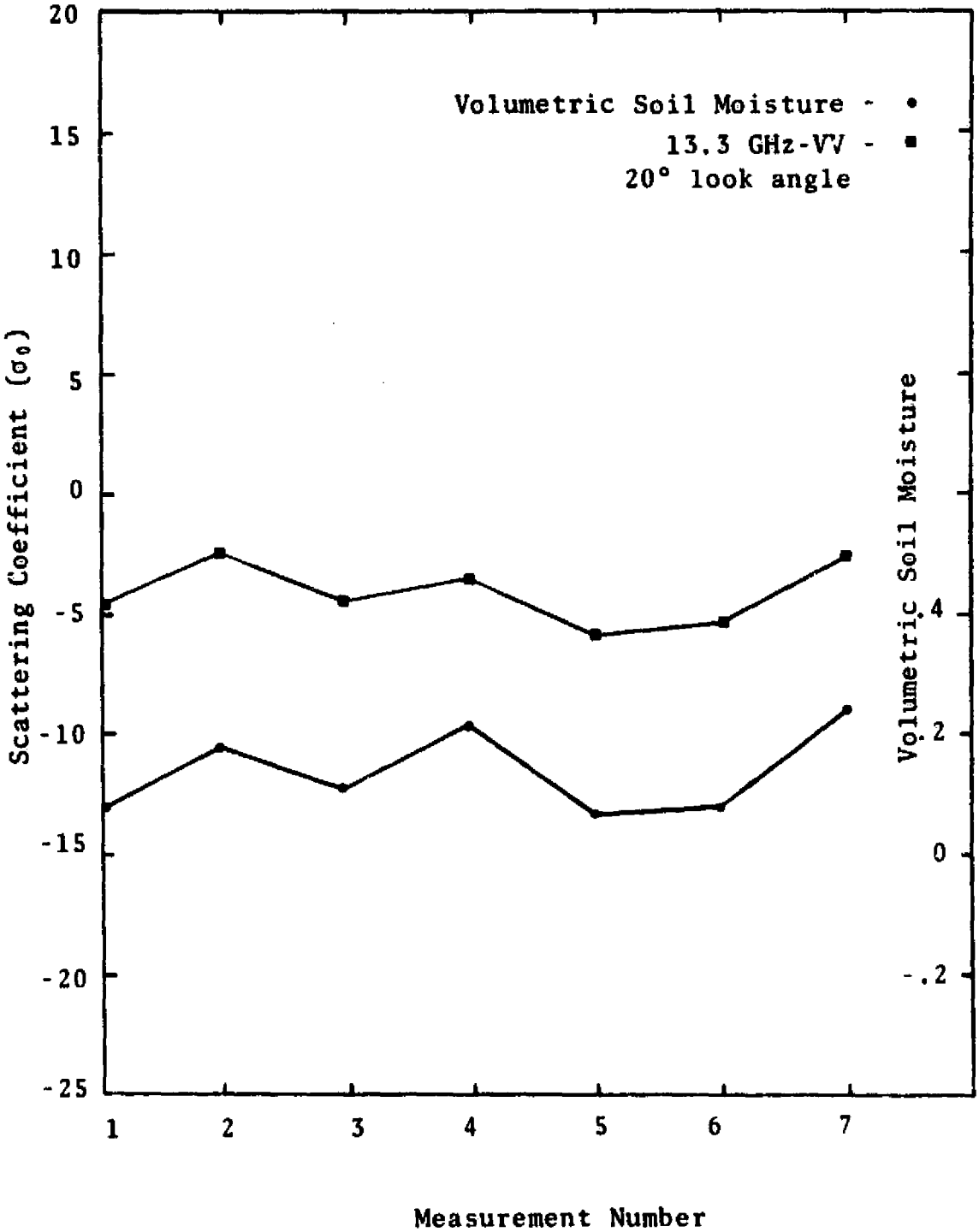

Figure A28. The Relation Between 13.3 GHz-VV Scattering Coefficient (σ_0) and Volumetric Soil Moisture for Field 4 for the Series of Seven Flights (Disked Bare Ground on the First Six Flights and Vegetated on the Final Flight).

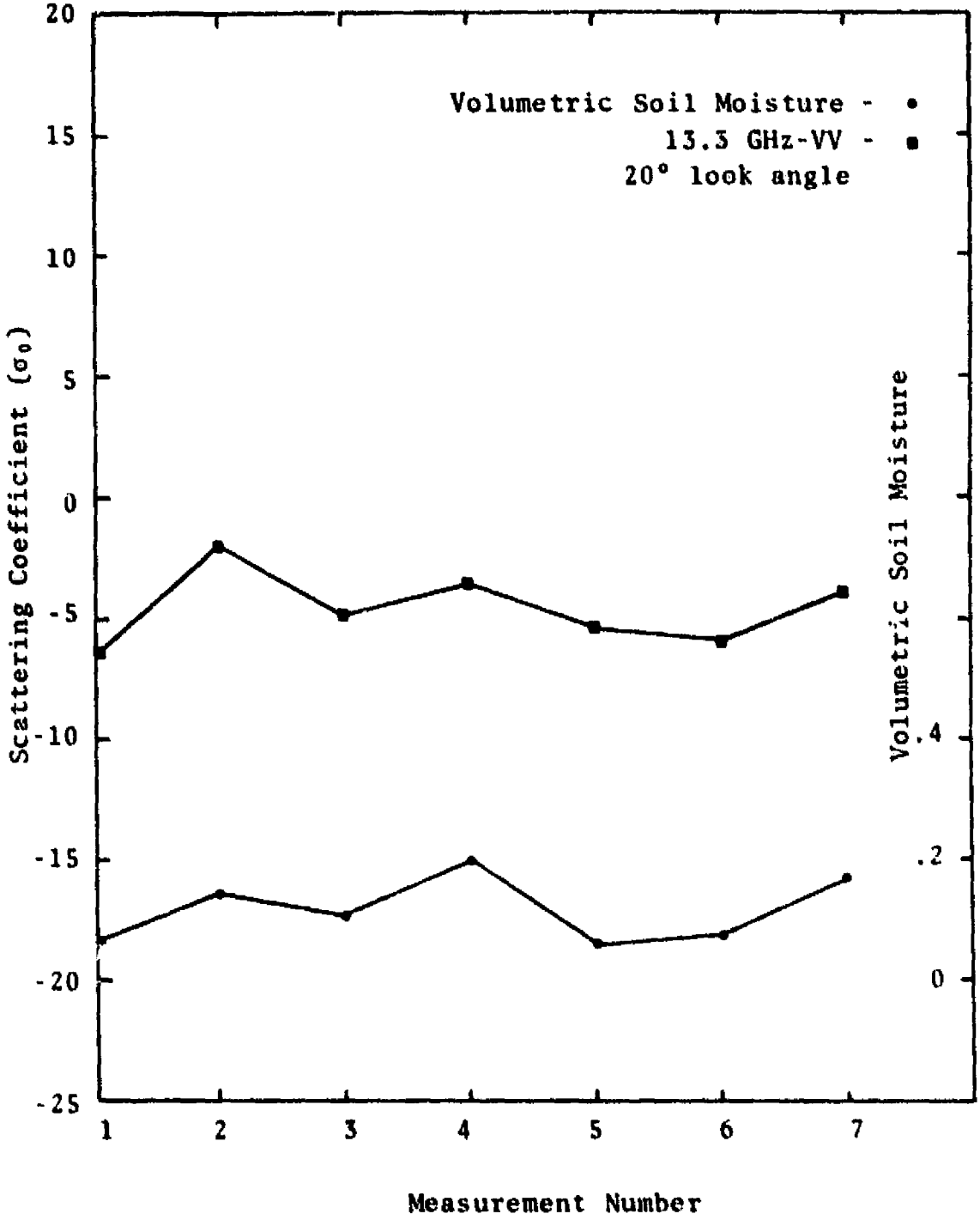

Figure A29. The Relation Between 13.3 GHz-VV Scattering Coefficient (σ_0) and Volumetric Soil Moisture for Field 5 for the Series of Seven Flights (Disked Bare Ground on the First Six Flights and Vegetated on the Final Flight).

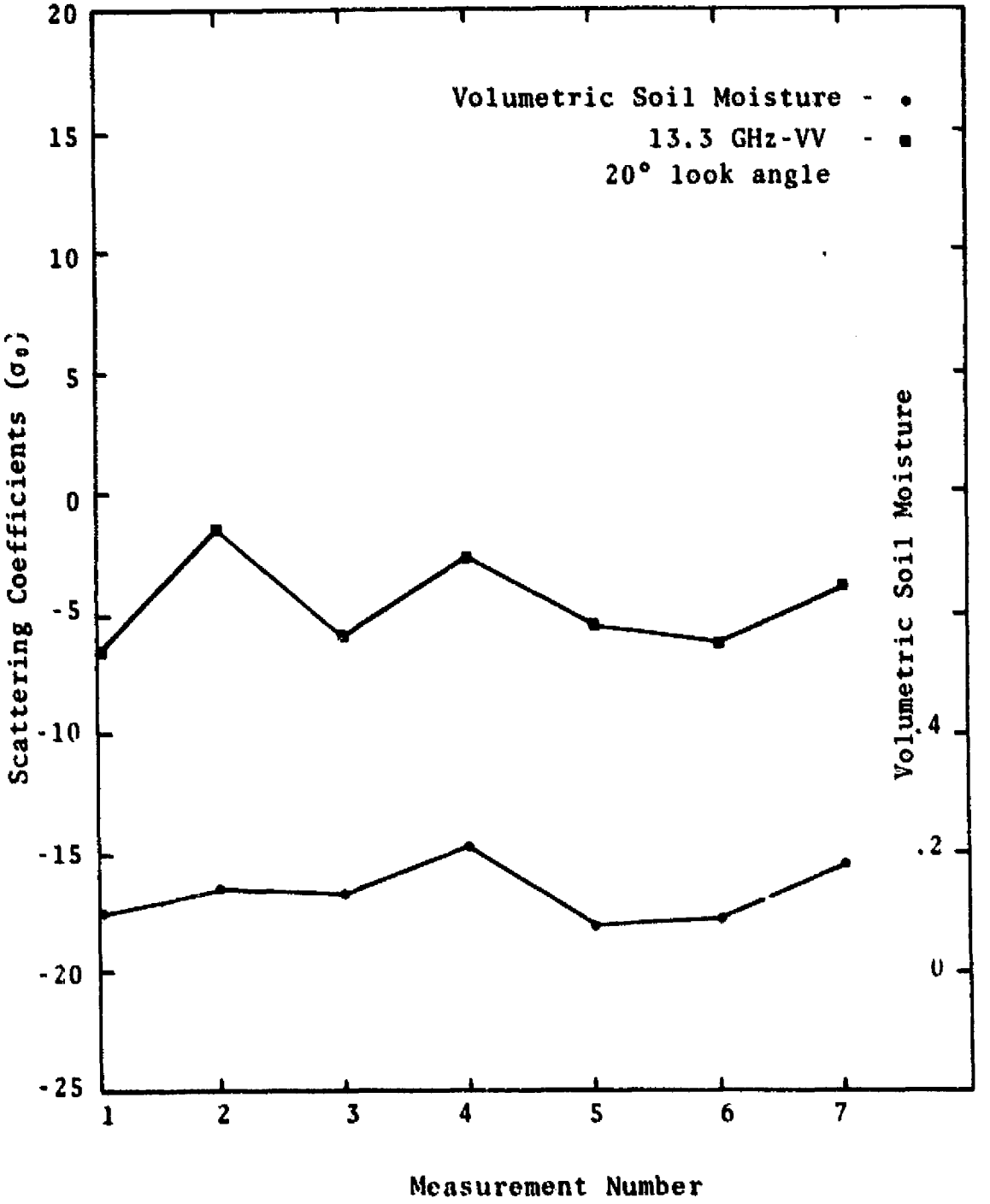

Figure A30. The Relation Between 13.3 GHz-VV Scattering Coefficient (σ_0) and Volumetric Soil Moisture for Field 6 for the Series of Seven Flights (Disked Bare Ground on the First Six Flights and Vegetated on the Final Flight).

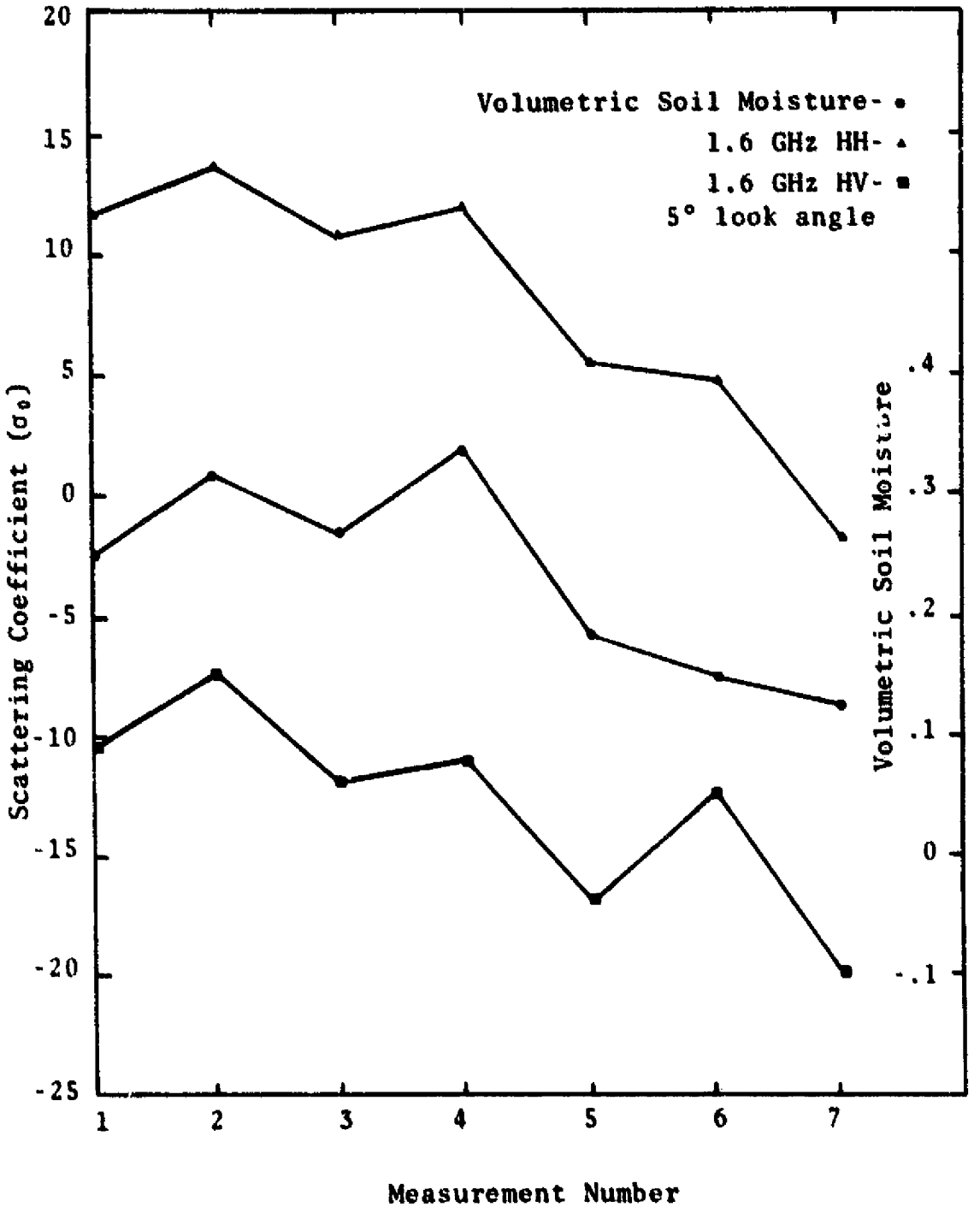

Figure A31. The Relation Between 1.6 GHz-HH and HV Scattering Coefficient (σ_0) and Volumetric Soil Moisture for Field 1 for the Series of Seven Flights (Disked Bare Ground on the First Six Flights and Vegetated on the Final Flight).

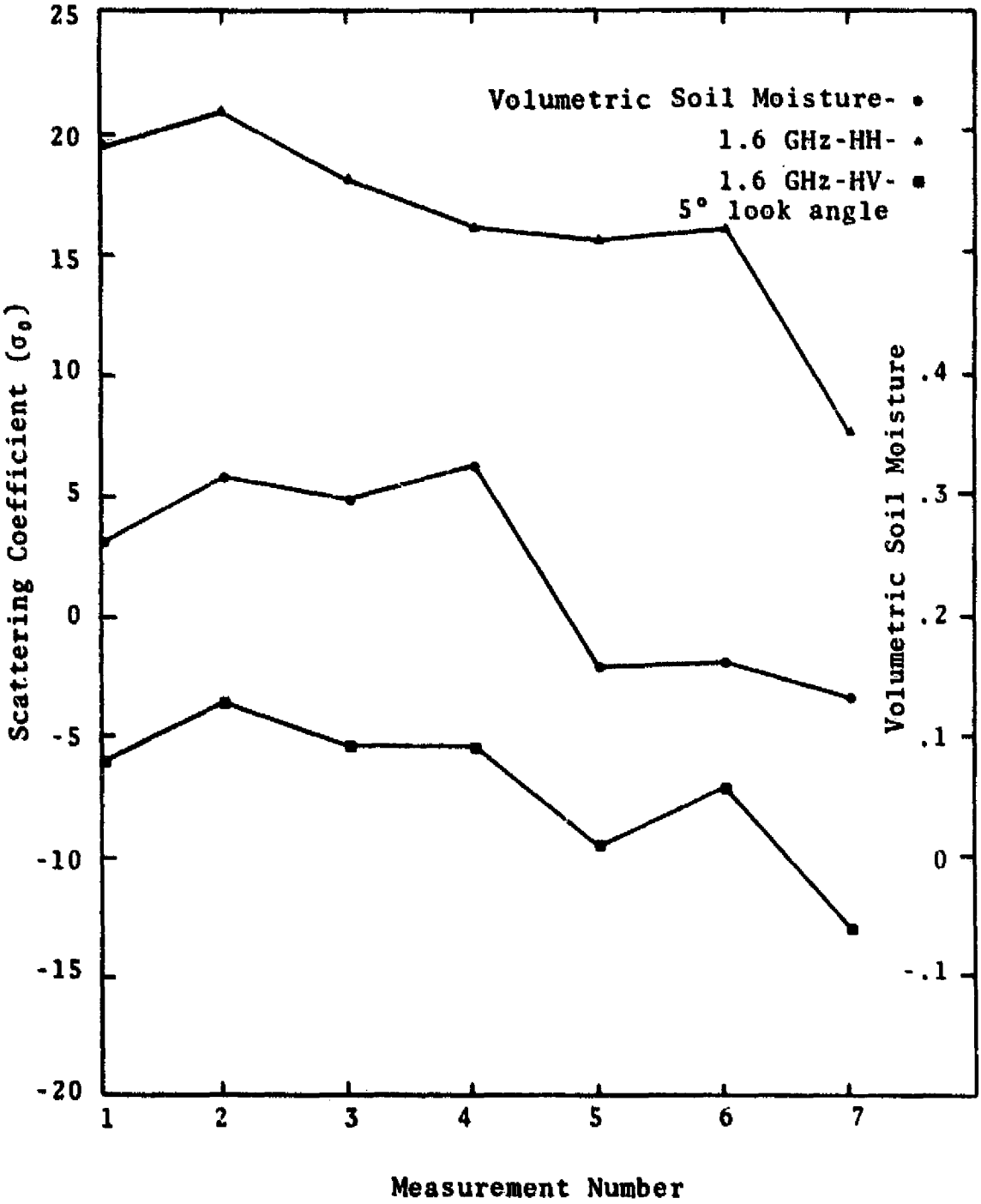

Figure A32. The Relation Between 1.6 HGz-HH and HV Scattering Coefficient (σ_0) and Volumetric Soil Moisture for Field 2 for the Series of Seven Flights (Disked Bare Ground on the First Six Flights and Vegetated on the Final Flight).

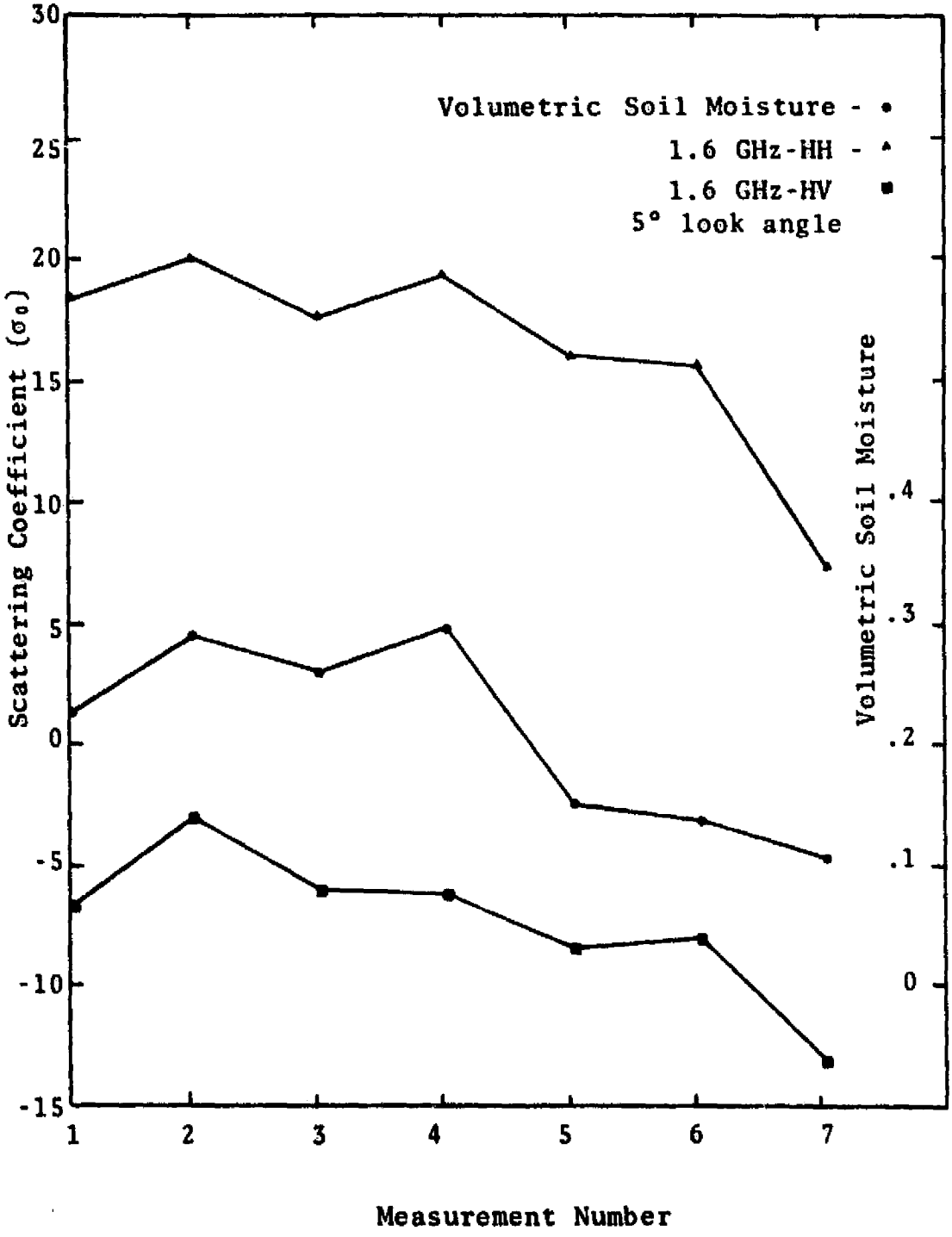

Figure A33. The Relation Between 1.6 GHz-HH and HV Scattering Coefficient (σ_0) and Volumetric Soil Moisture for Field 3 for the Series of Seven Flights (Disked Bare Ground on the First Six Flights and Vegetated on the Final Flight).

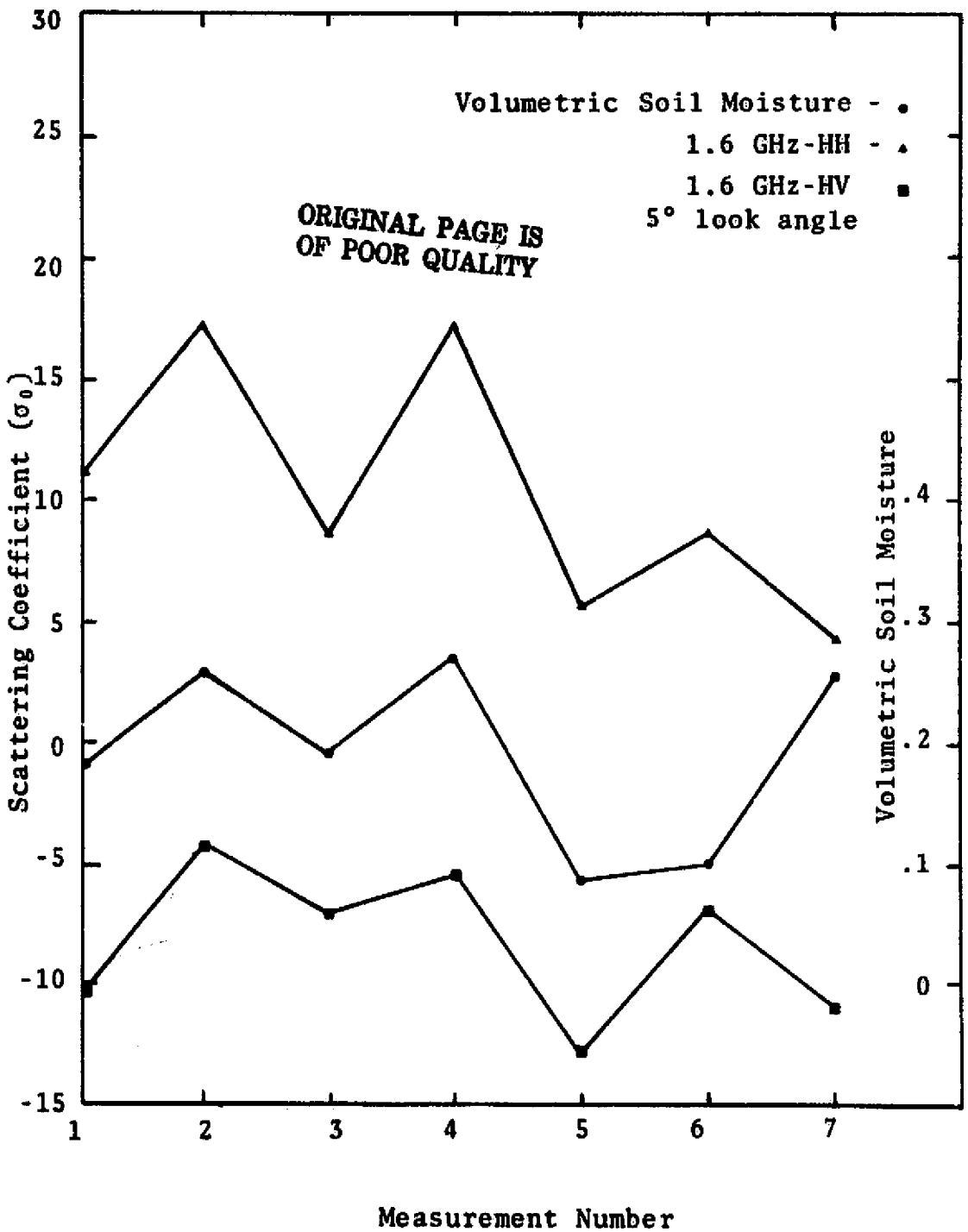

Figure A34. The Relation Between 1.6 GHz-HH and HV Scattering Coefficient (σ_0) and Volumetric Soil Moisture for Field 4 for the Series of Seven Flights (Disked Bare Ground on the First Six Flights and Vegetated on the Final Flight).

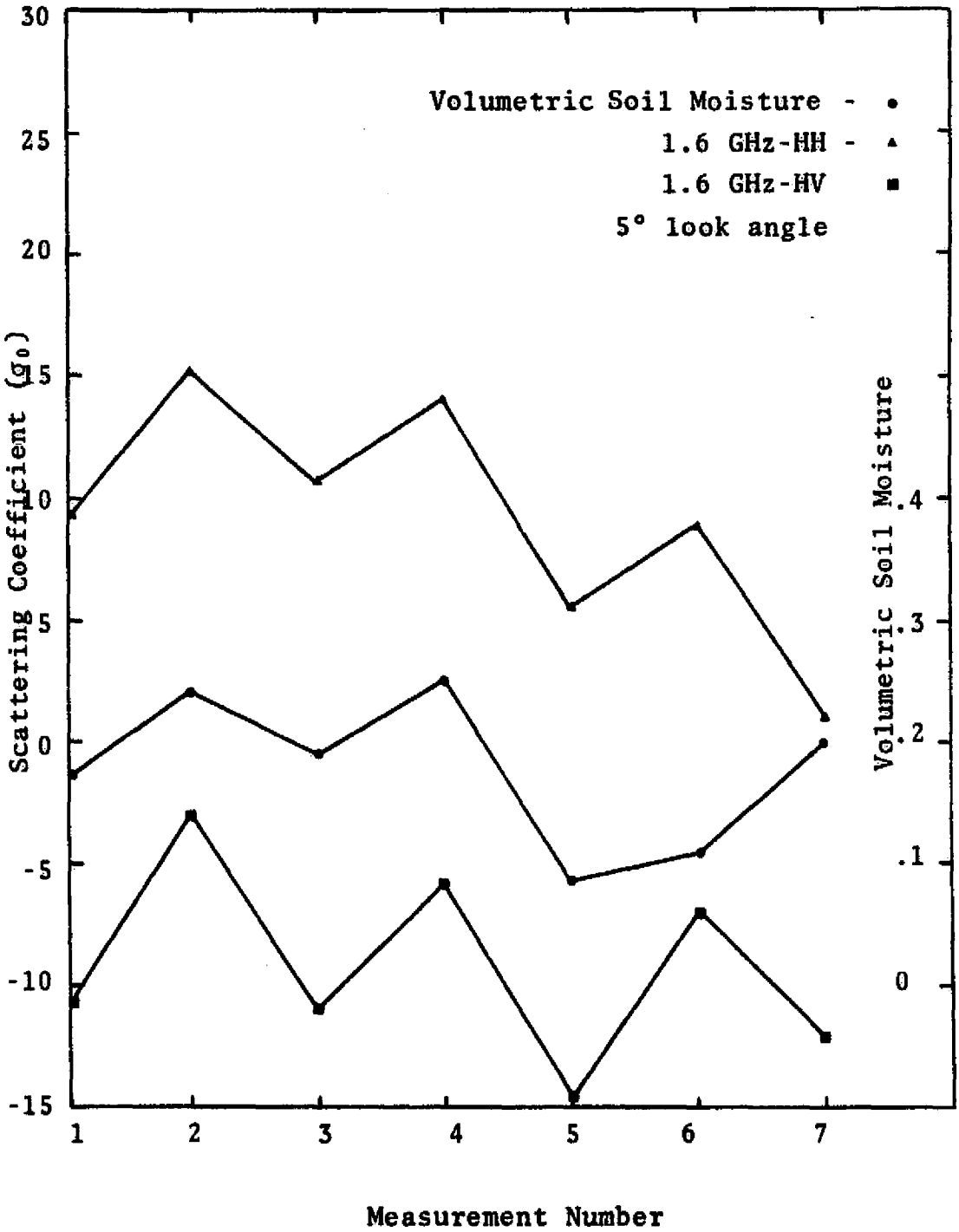

Figure A35. The Relation Between 1.6 GHz-HH and HV Scattering Coefficient (σ_0) and Volumetric Soil Moisture for Field 5 for the Series of Seven Flights (Disked Bare Ground on the First Six Flights and Vegetated on the Final Flight).

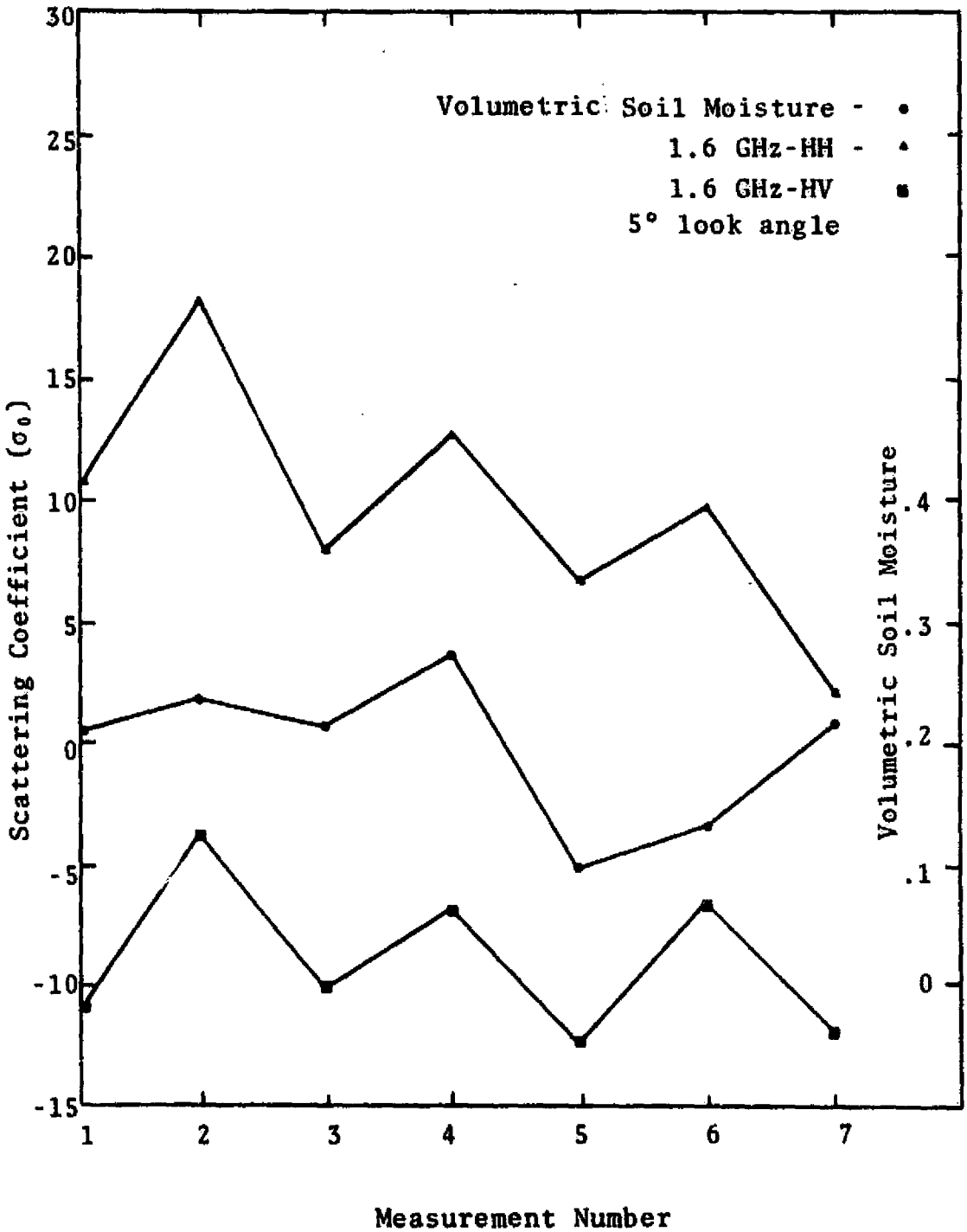

Figure A36. The Relation Between 1.6 GHz-HH and HV Scattering Coefficient (σ_0) and Volumetric Soil Moisture for Field 6 for the Series of Seven Flights (Disked Bare Ground on the First Six Flights and Vegetated on the Final Flight).

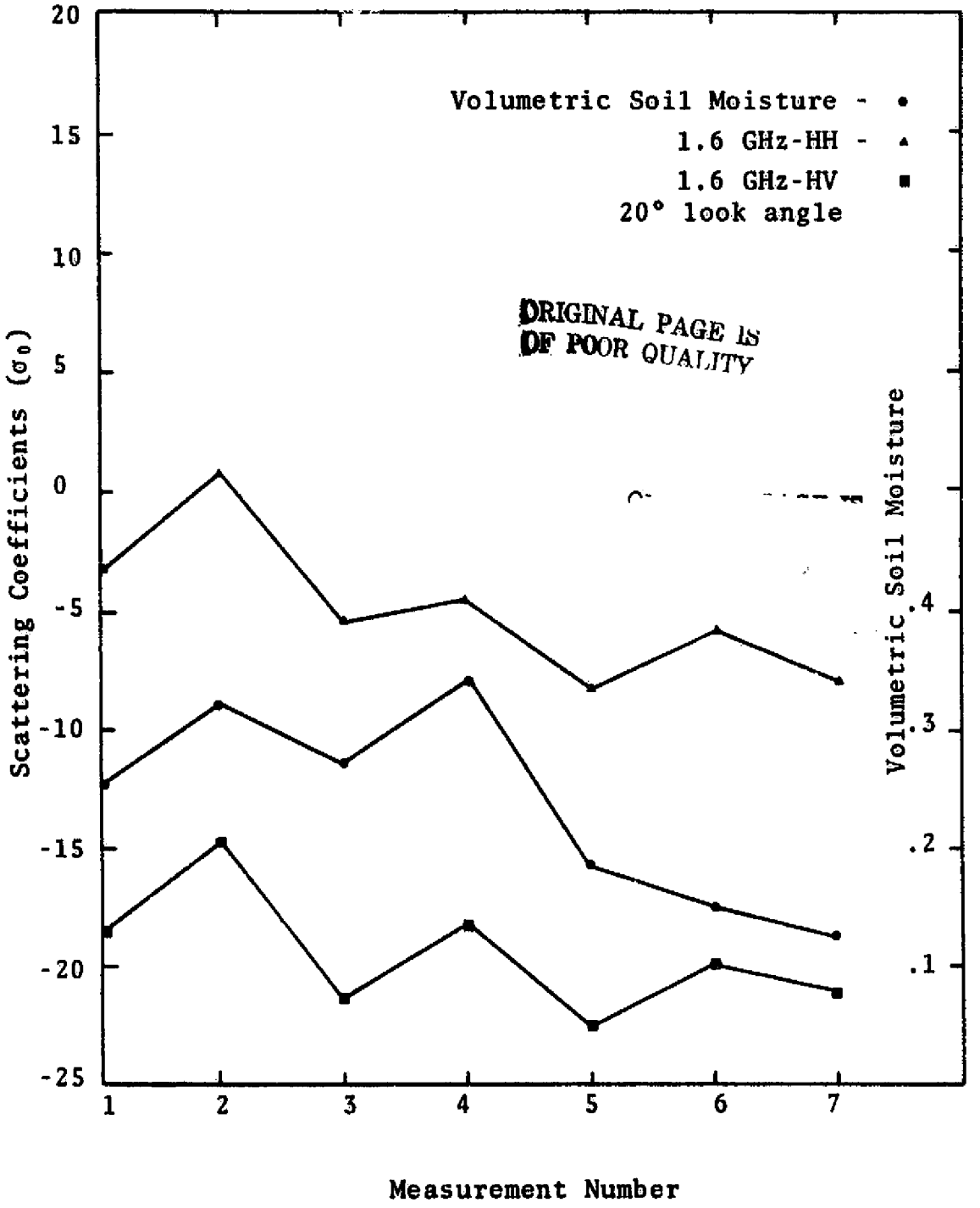

Figure A37. The Relation Between 1.6 GHz-HH and HV Scattering Coefficient (σ_0) and Volumetric Soil Moisture for Field 1 for the Series of Seven Flights (Disked Bare Ground on the First Six Flights and Vegetated on the Final Flight).

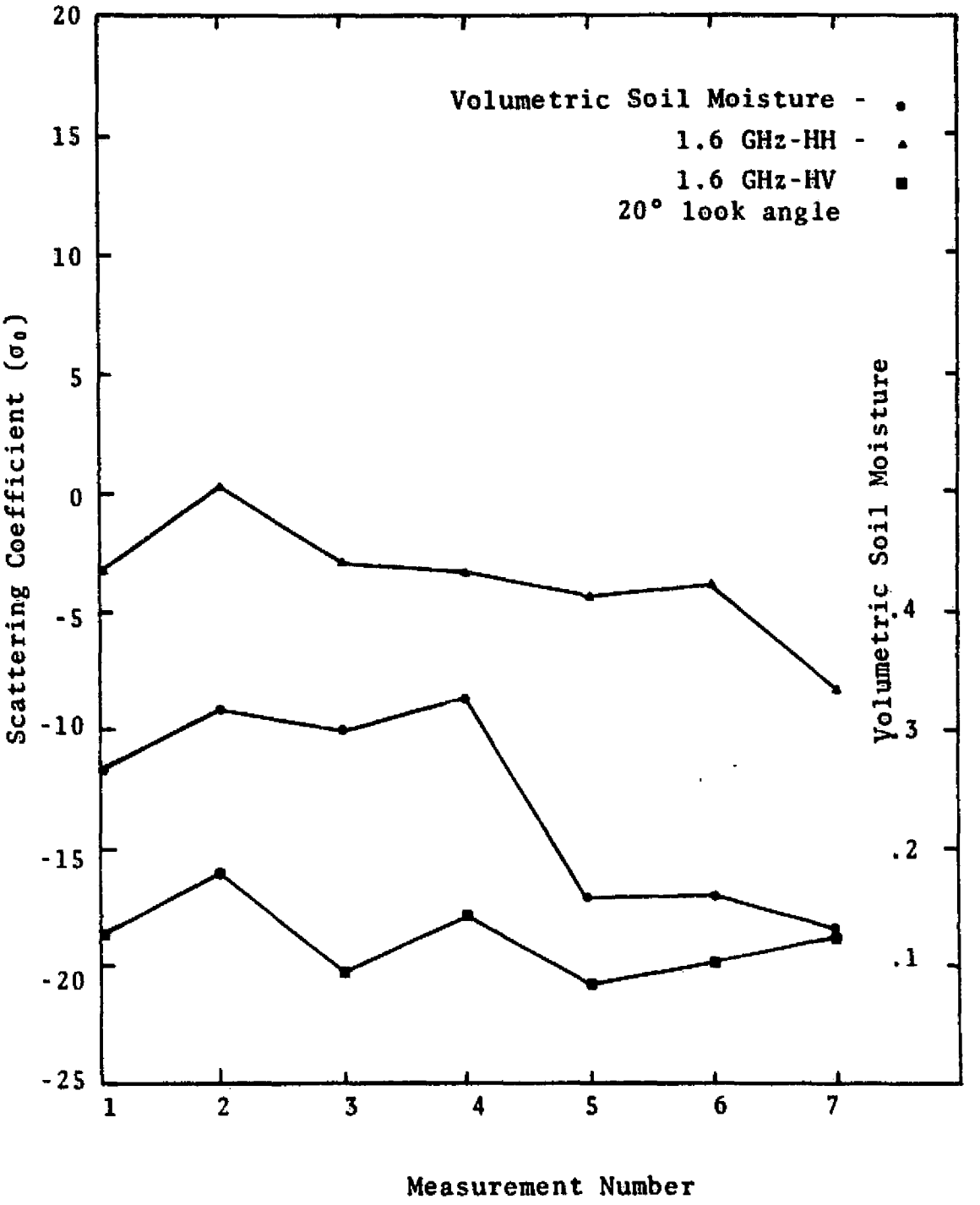

Figure A38. The Relation Between 1.6 GHz-HH and HV Scattering Coefficient (σ_0) and Volumetric Soil Moisture for Field 2 for the Series of Seven Flights (Disked Bare Ground on the First Six Flights and Vegetated on the Final Flight).

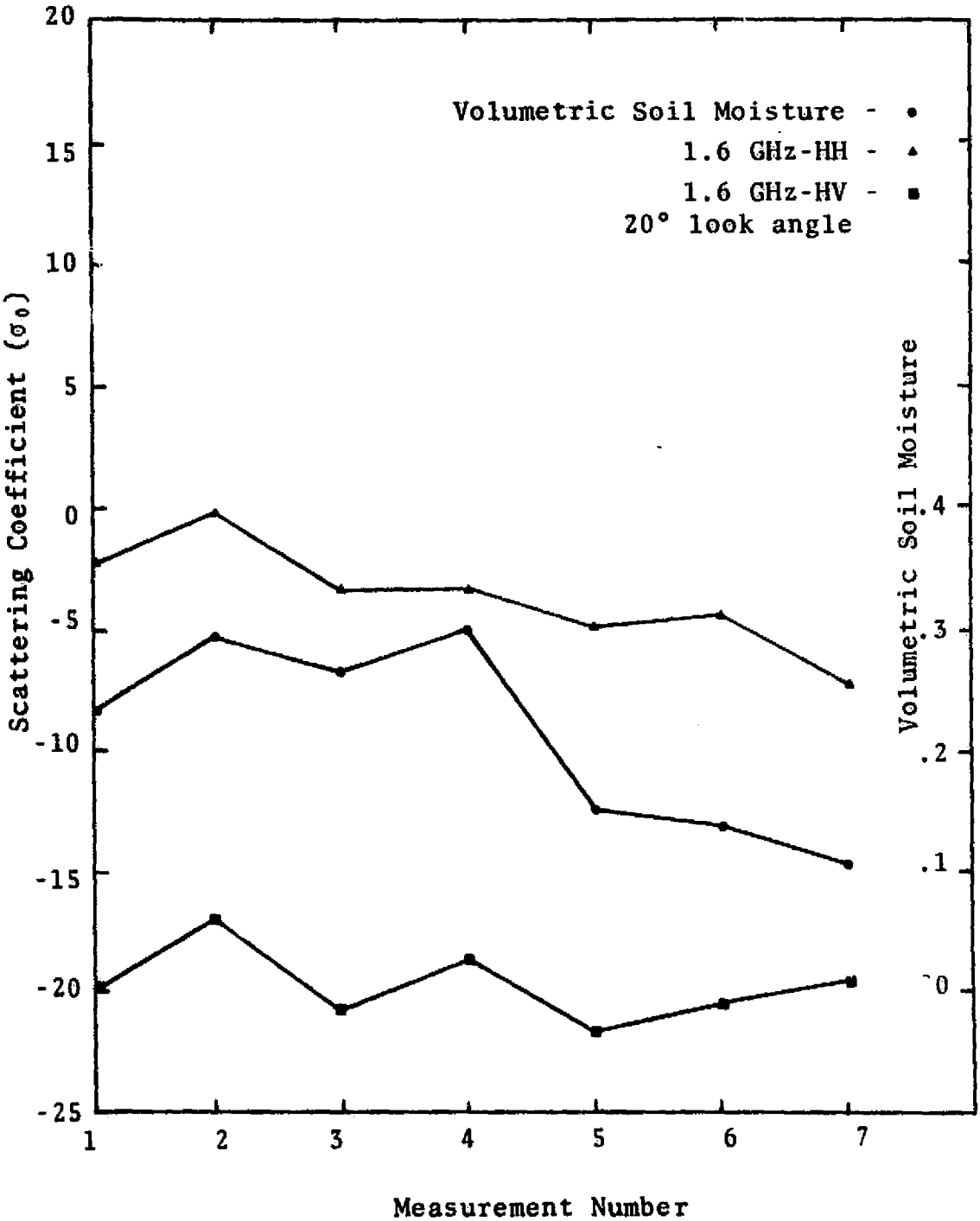

Figure A39. The Relation Between 1.6 GHz-HH and HV Scattering Coefficient (σ_0) and Volumetric Soil Moisture for Field 3 for the Series of Seven Flights (Disked Bare Ground on the First Six Flights and Vegetated on the Final Flight).

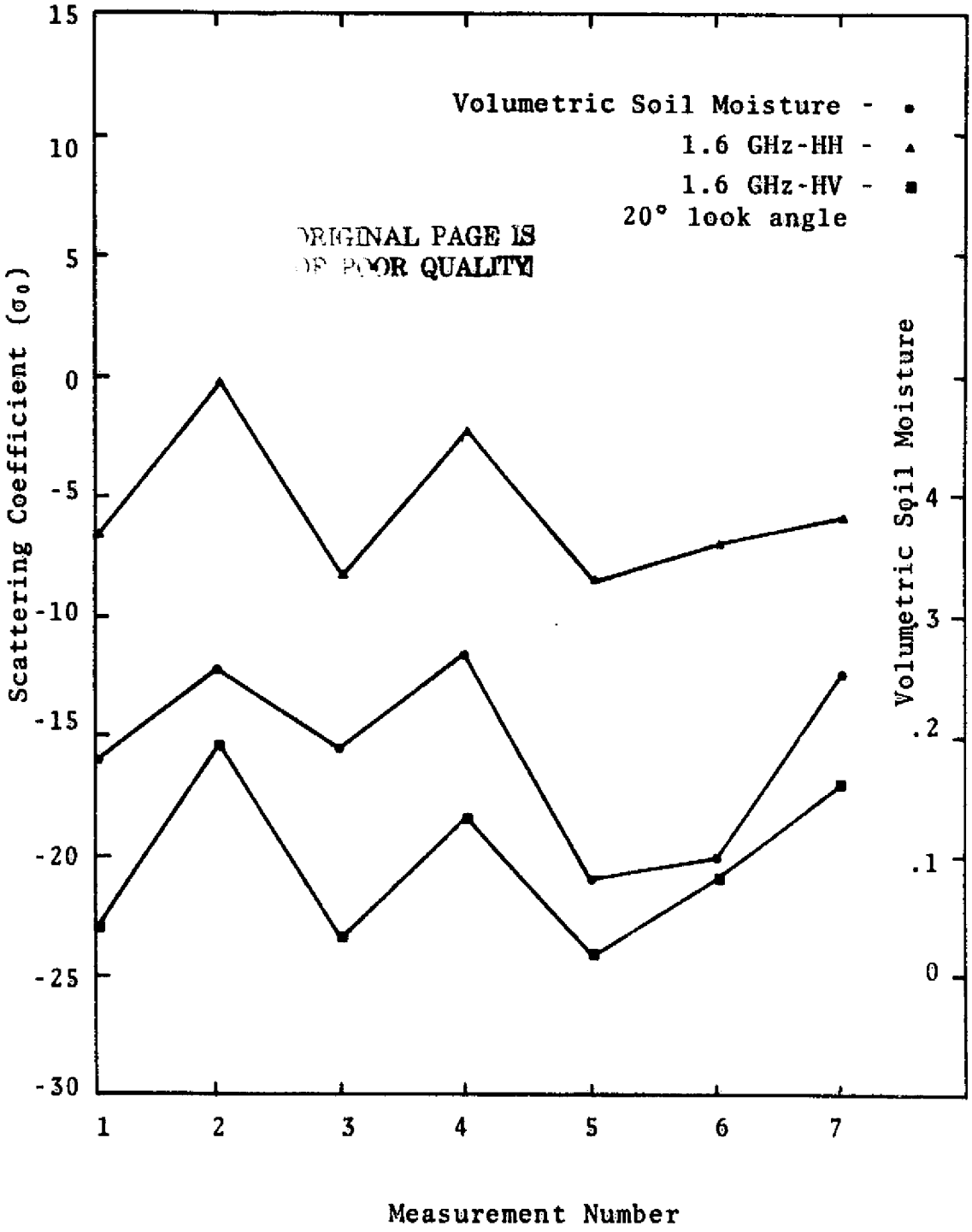

Figure A40. The Relation Between 1.6 GHz-HH and HV Scattering Coefficient (σ_0) and Volumetric Soil Moisture for Field 4 for the Series of Seven Flights (Disked Bare Ground on the First Six Flights and Vegetated on the Final Flight).

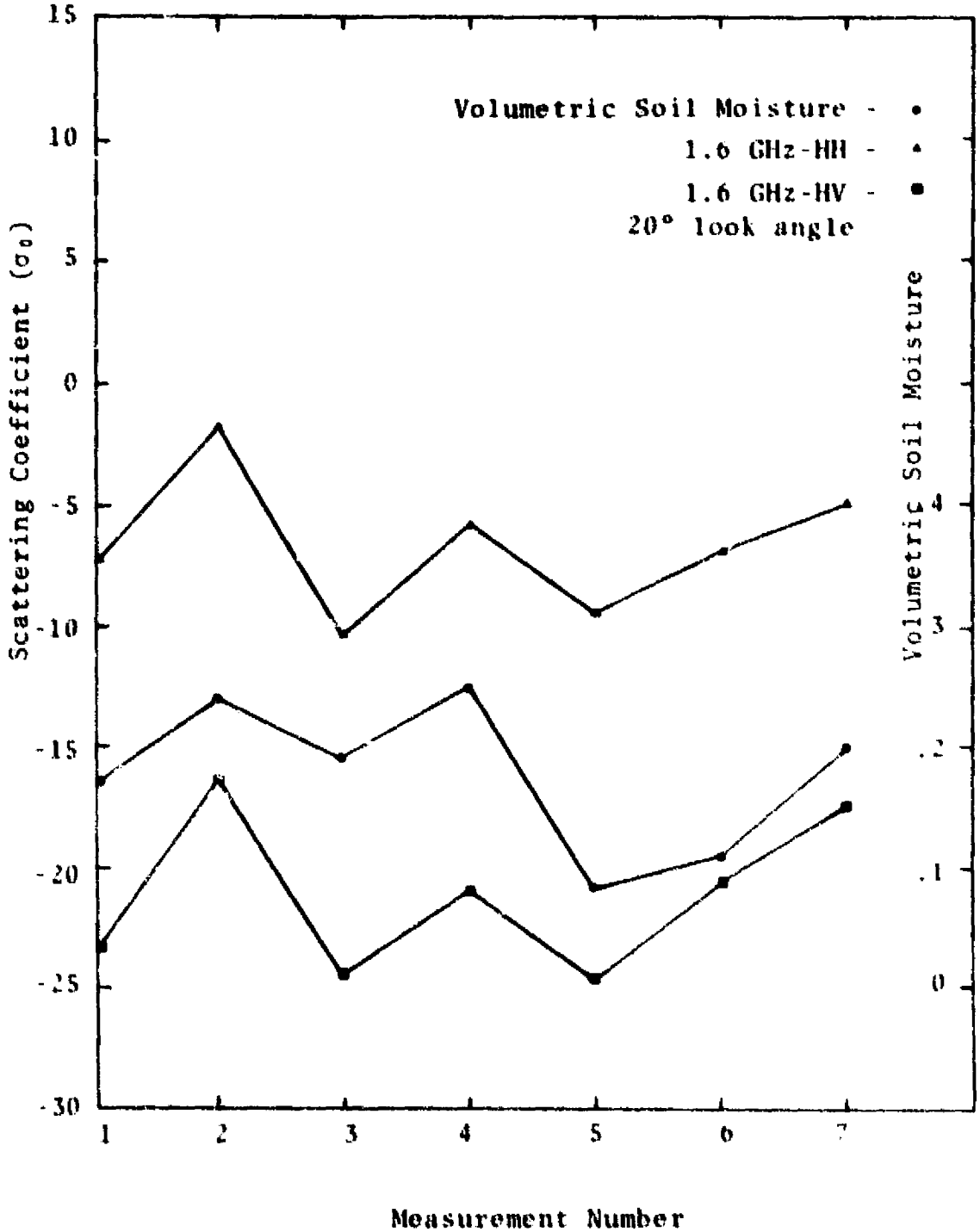

Figure A41. The Relation Between 1.6 GHz-HH and HV Scattering Coefficient (σ_0) and Volumetric Soil Moisture for Field 5 for the Series of Seven Flights (Disked Bare Ground on the First Six Flights and Vegetated on the Final Flight).

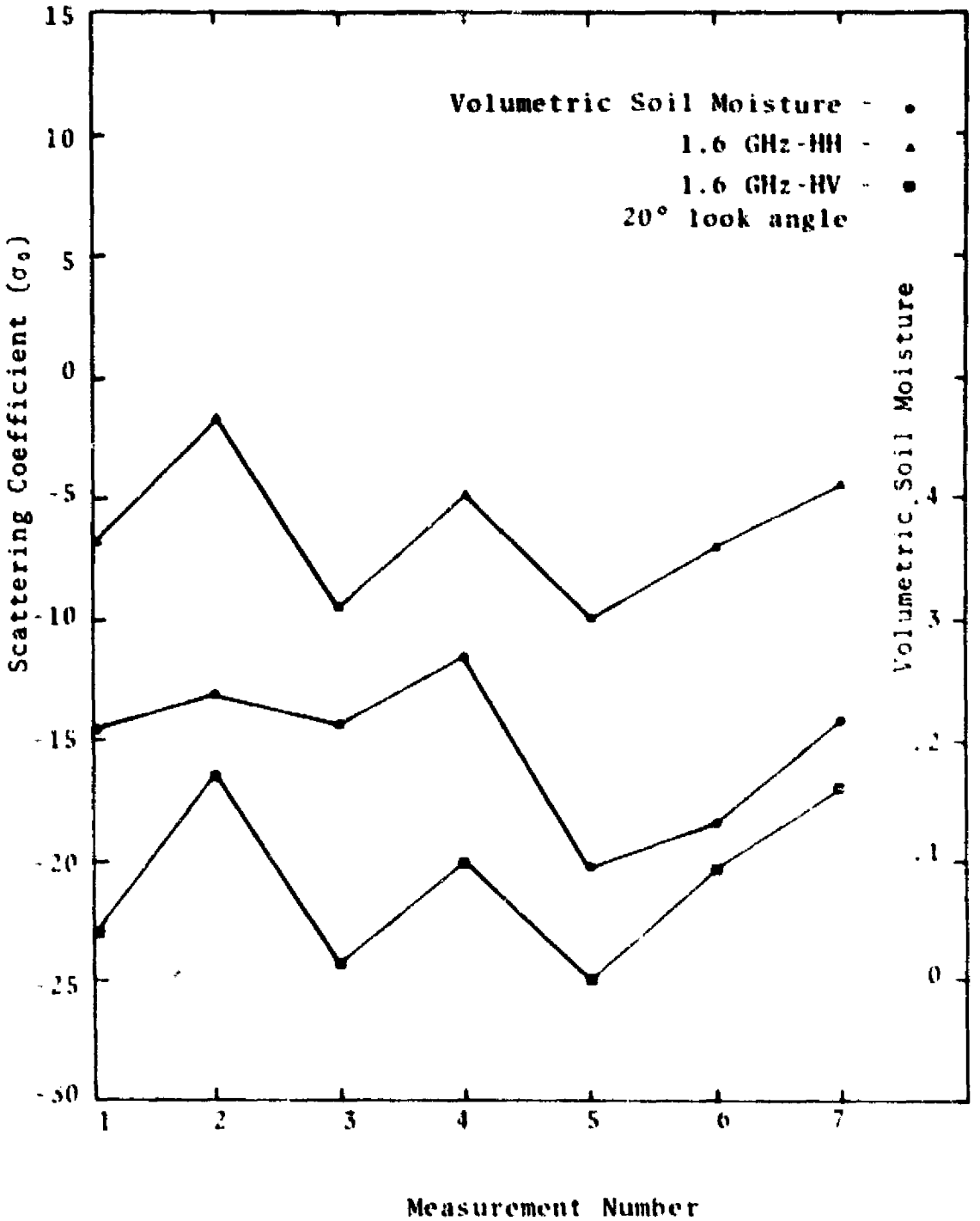

Figure A42. The Relation Between 1.6 GHz-HH and HV Scattering Coefficient (σ_0) and Volumetric Soil Moisture for Field 6 for the Series of Seven Flights (Disked Bare Ground on the First Six Flights and Vegetated on the Final Flight).

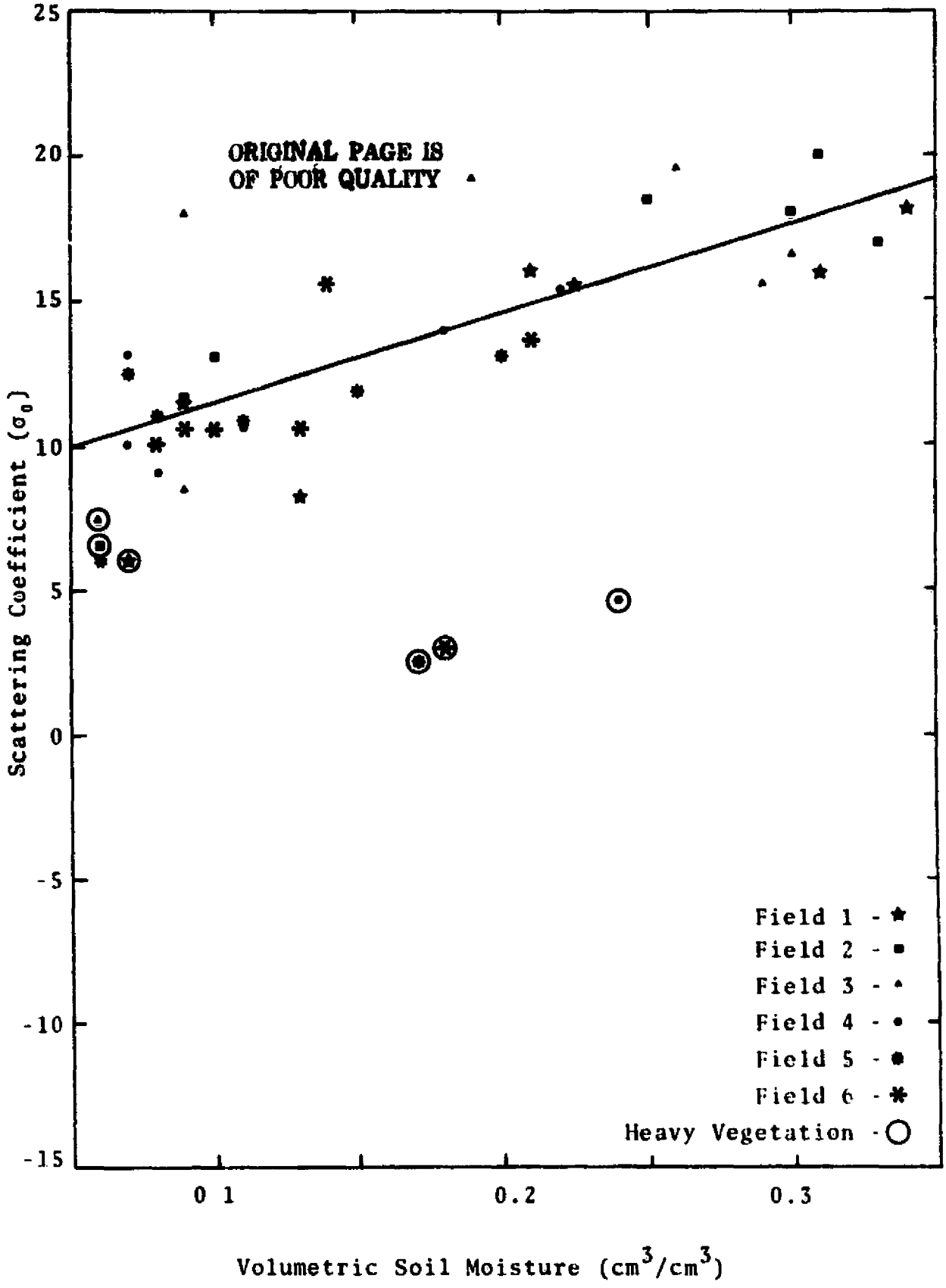

Figure A43. Relation Between 13.3GHz-VV Scattering Coefficient and Volumetric Soil Moisture at 5 Degree Look Angle

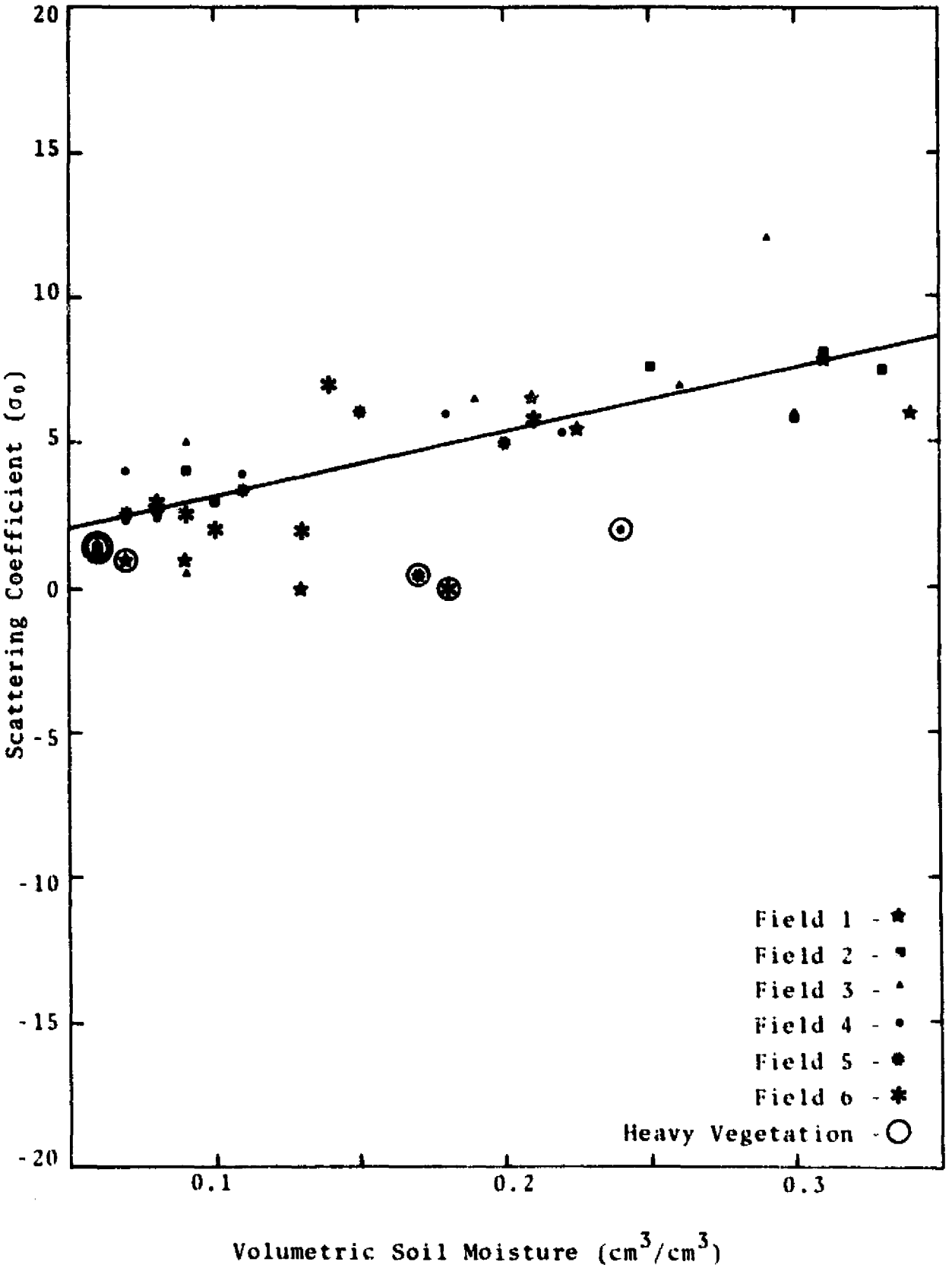

Figure A44. Relation Between 13.3 GHz-VV Scattering Coefficient and Volumetric Soil Moisture at 10 Degree Look Angle

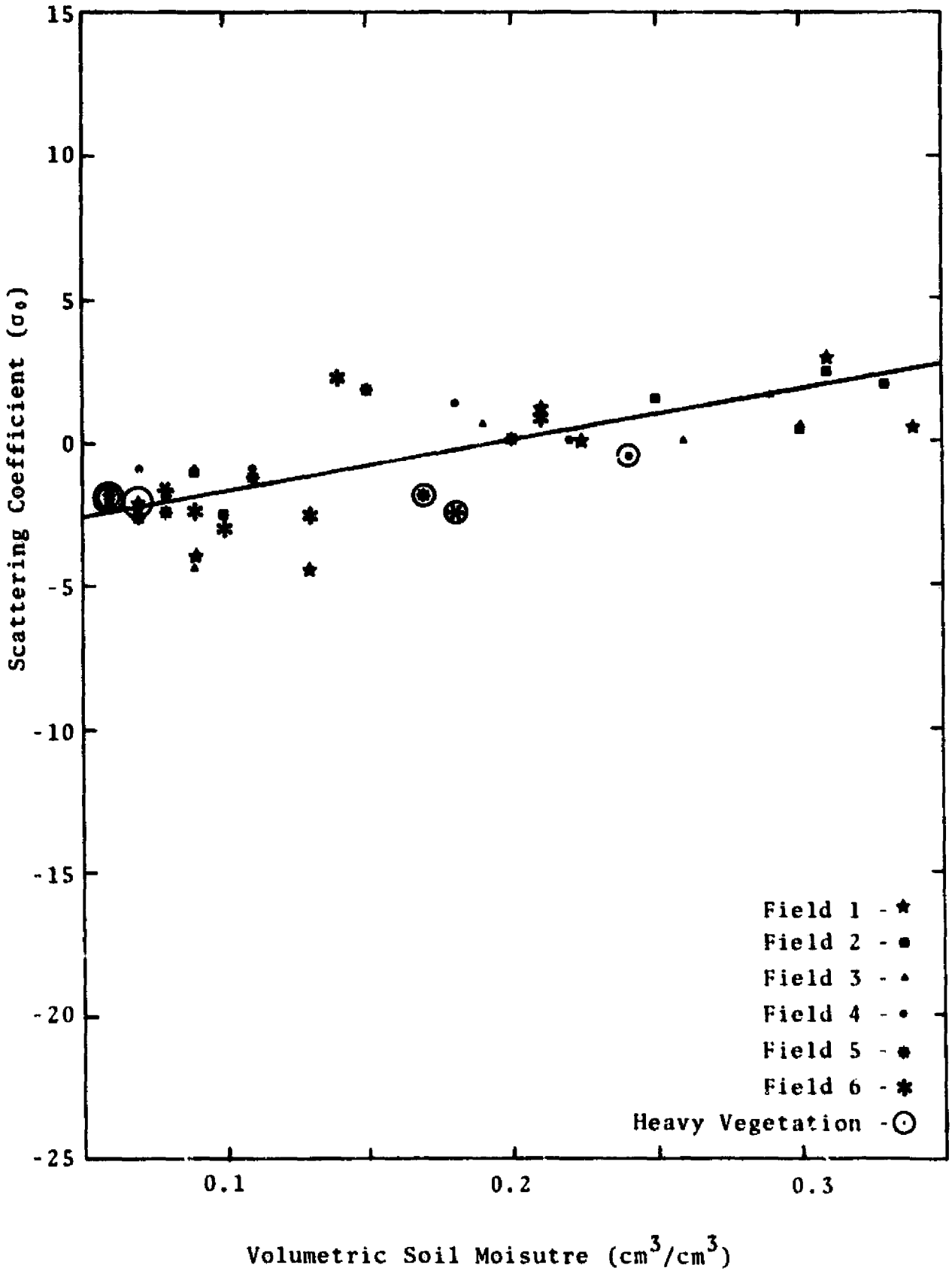

Figure A45. Relation Between 13.3 GHz-VV Scattering Coefficient and Volumetric Soil Moisture at 15 Degree Look Angle

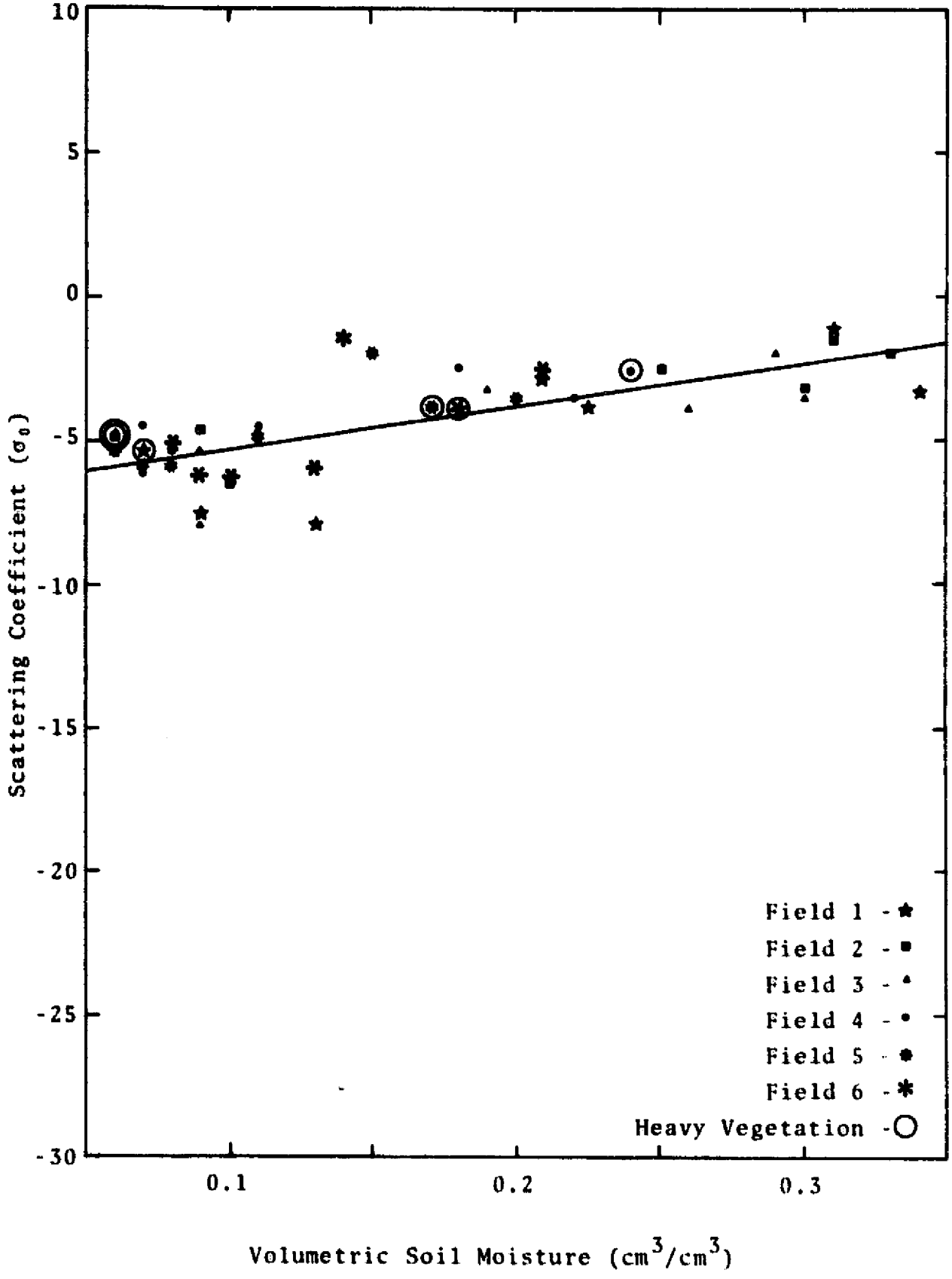

Figure A46. Relation Between 13.3 GHz-VV Scattering Coefficient and Volumetric Soil Moisture at 20 Degree Look Angle

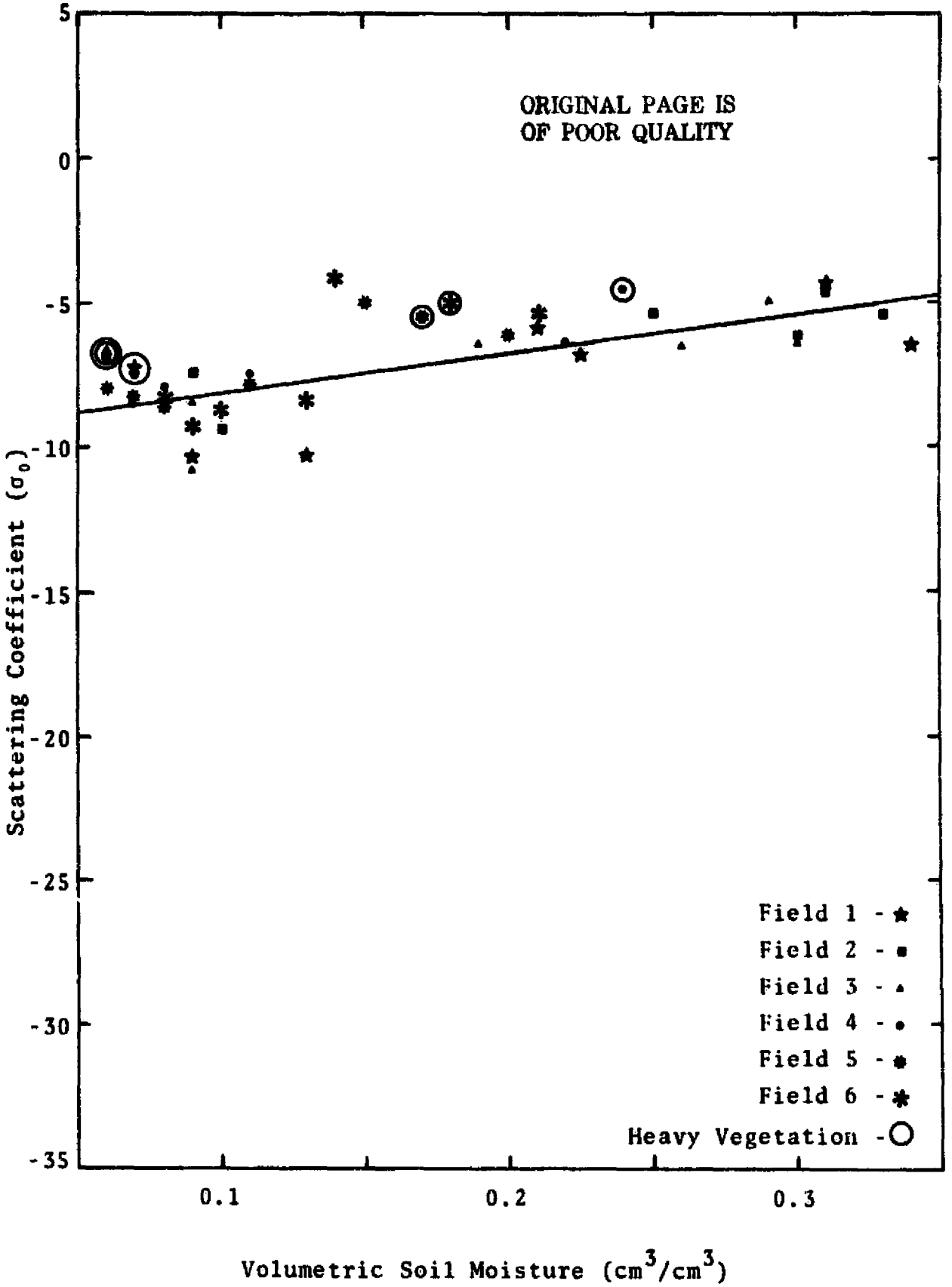

Figure A47. Relation Between 13.3 GHz-VV Scattering Coefficient and Volumetric Soil Moisture at 25 Degree Look Angle

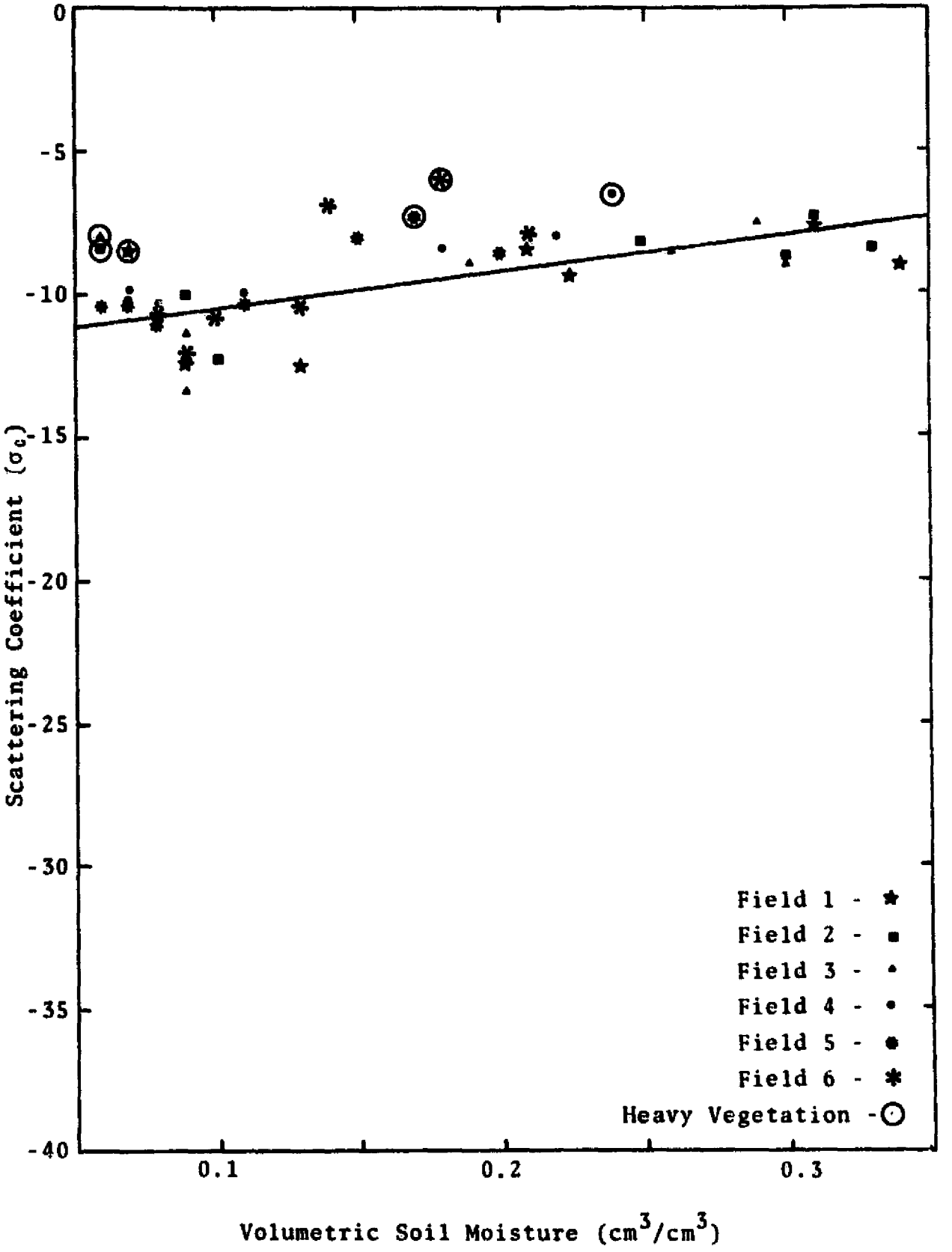

Figure A48. Relation Between 13.3 GHz-VV Scattering Coefficient and Volumetric Soil Moisture at 30 Degree Look Angle

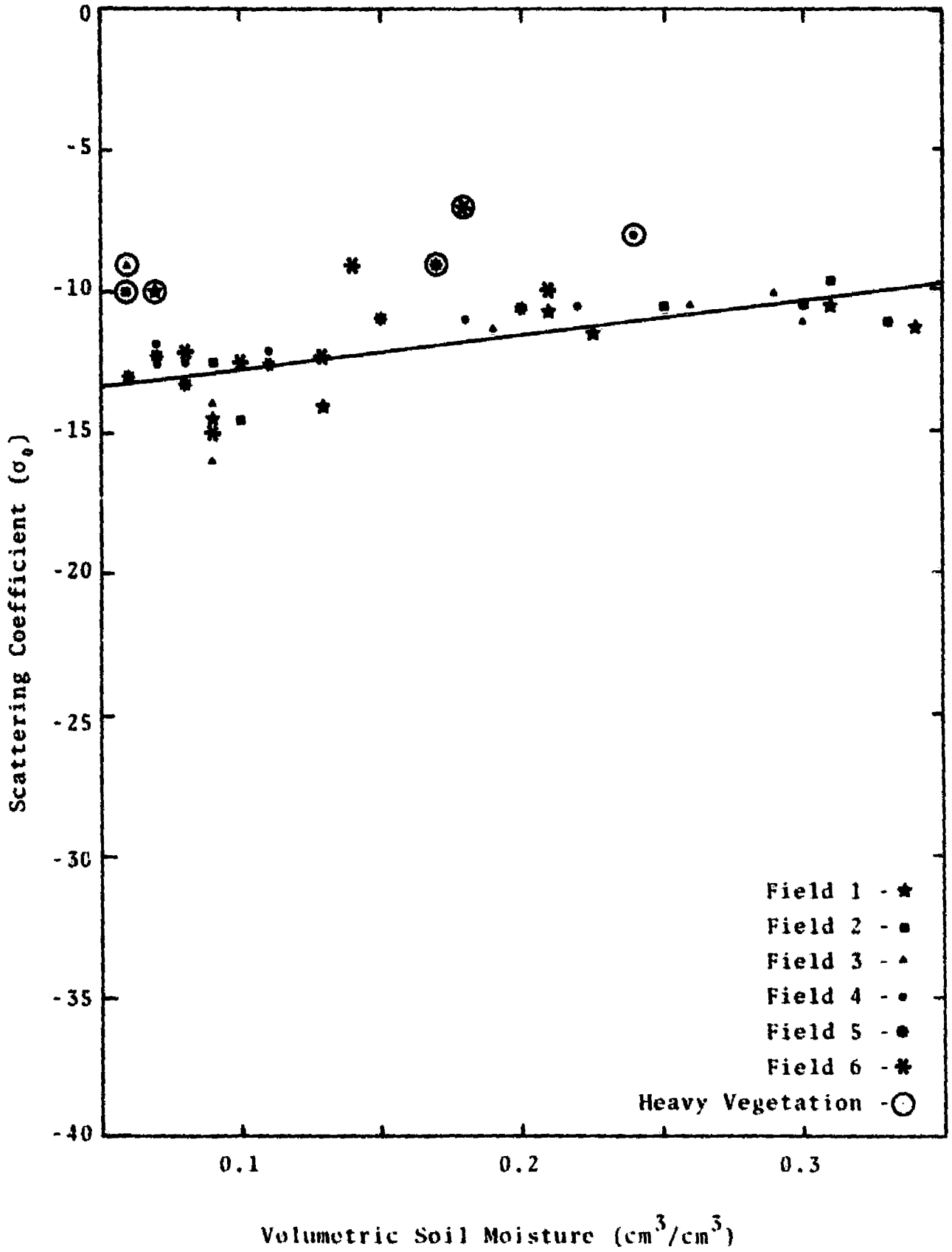

Figure A49. Relation Between 13.3 GHz-VV Scattering Coefficient and Volumetric Soil Moisture at 35 Degree Look Angle

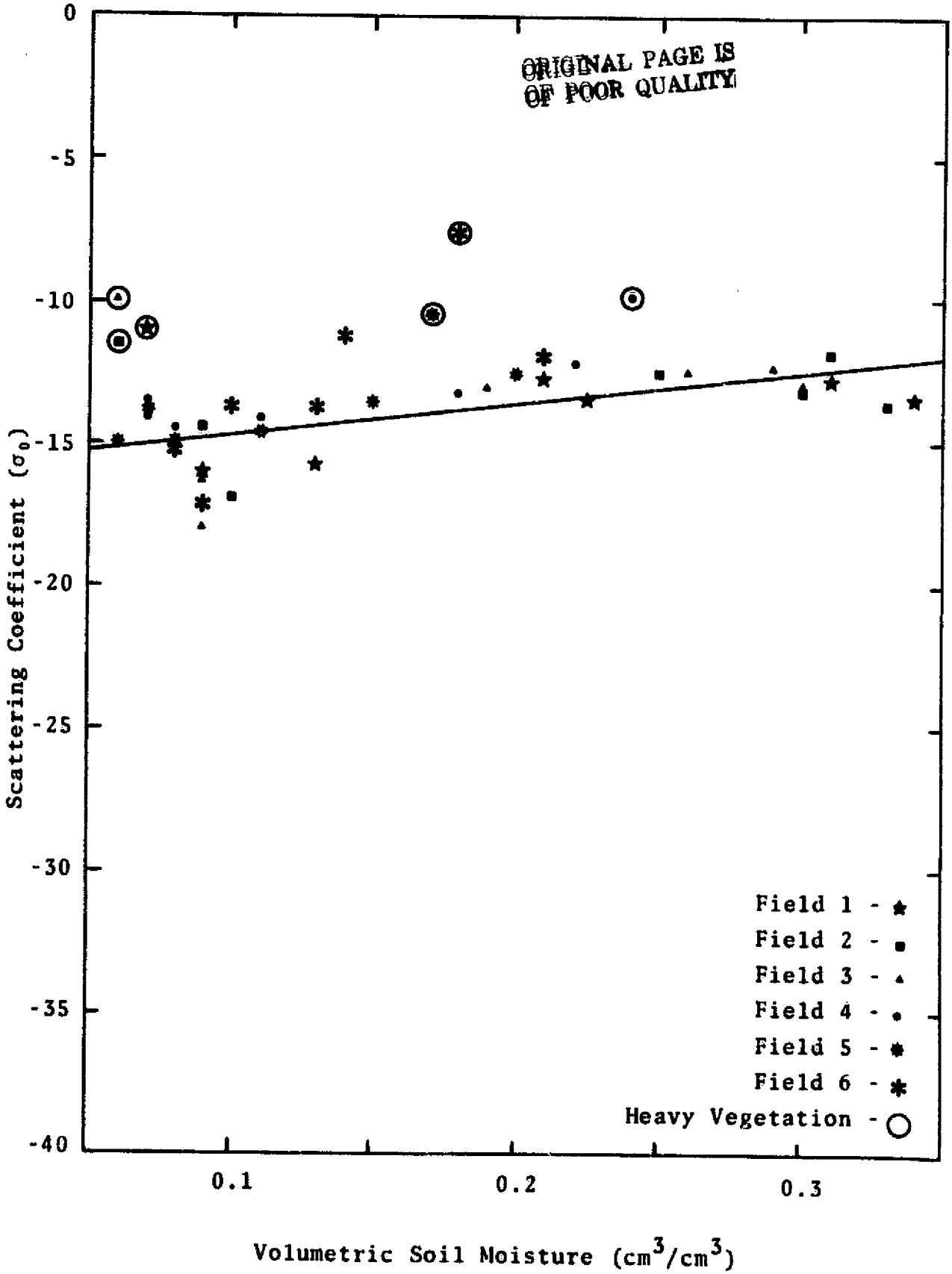

Figure A50. Relation Between 13.3 GHz-VV Scattering Coefficient and Volumetric Soil Moisture at 40 Degree Look Angle

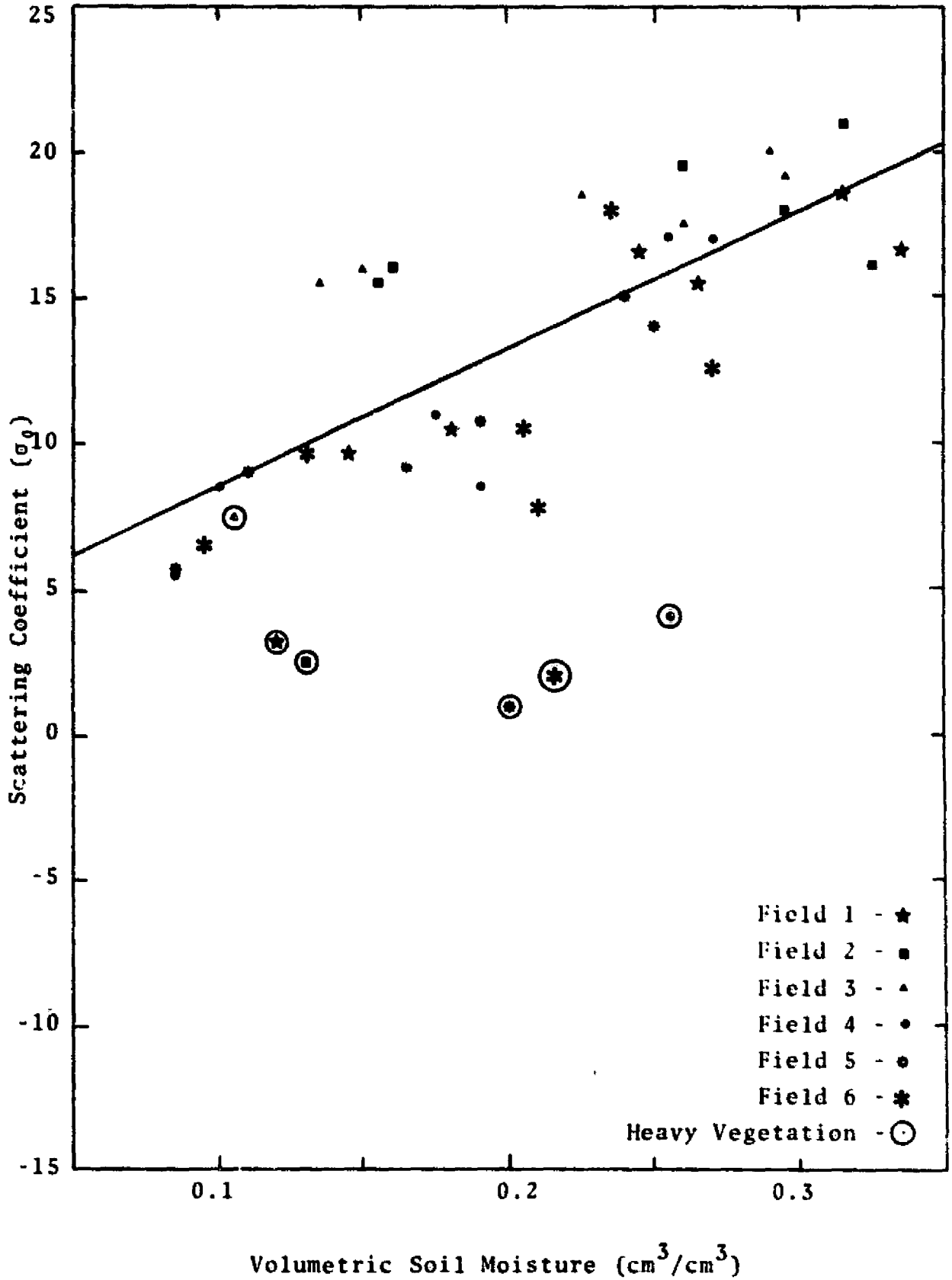

Figure A51. Relation Between 1.6 GHz-HH Scattering Coefficient and Volumetric Soil Moisture at 5 Degree Angle

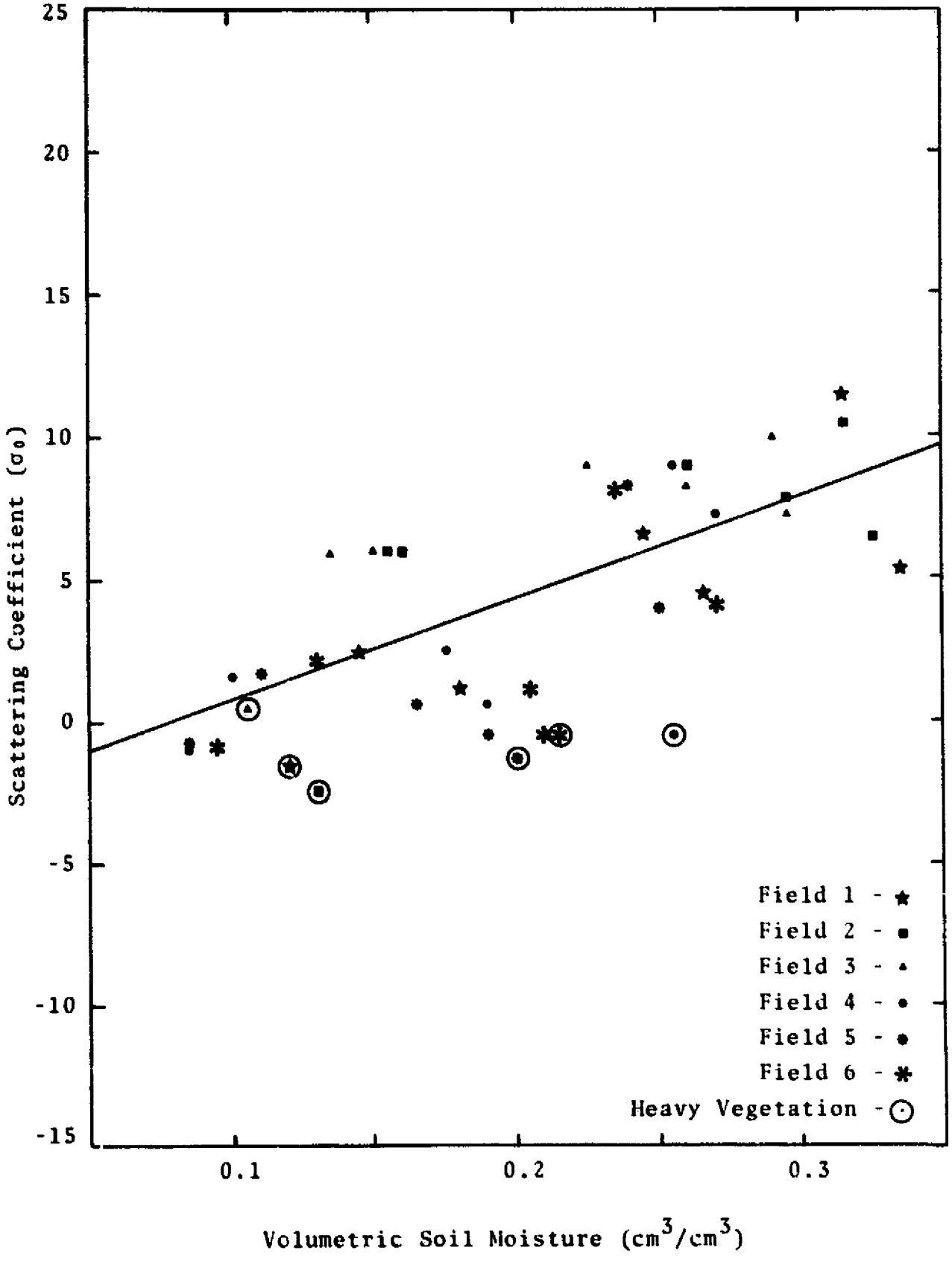

Figure A52. Relation Between 1.6 GHz-HH Scattering Coefficient and Volumetric Soil Moisture at 10 Degree Look Angle

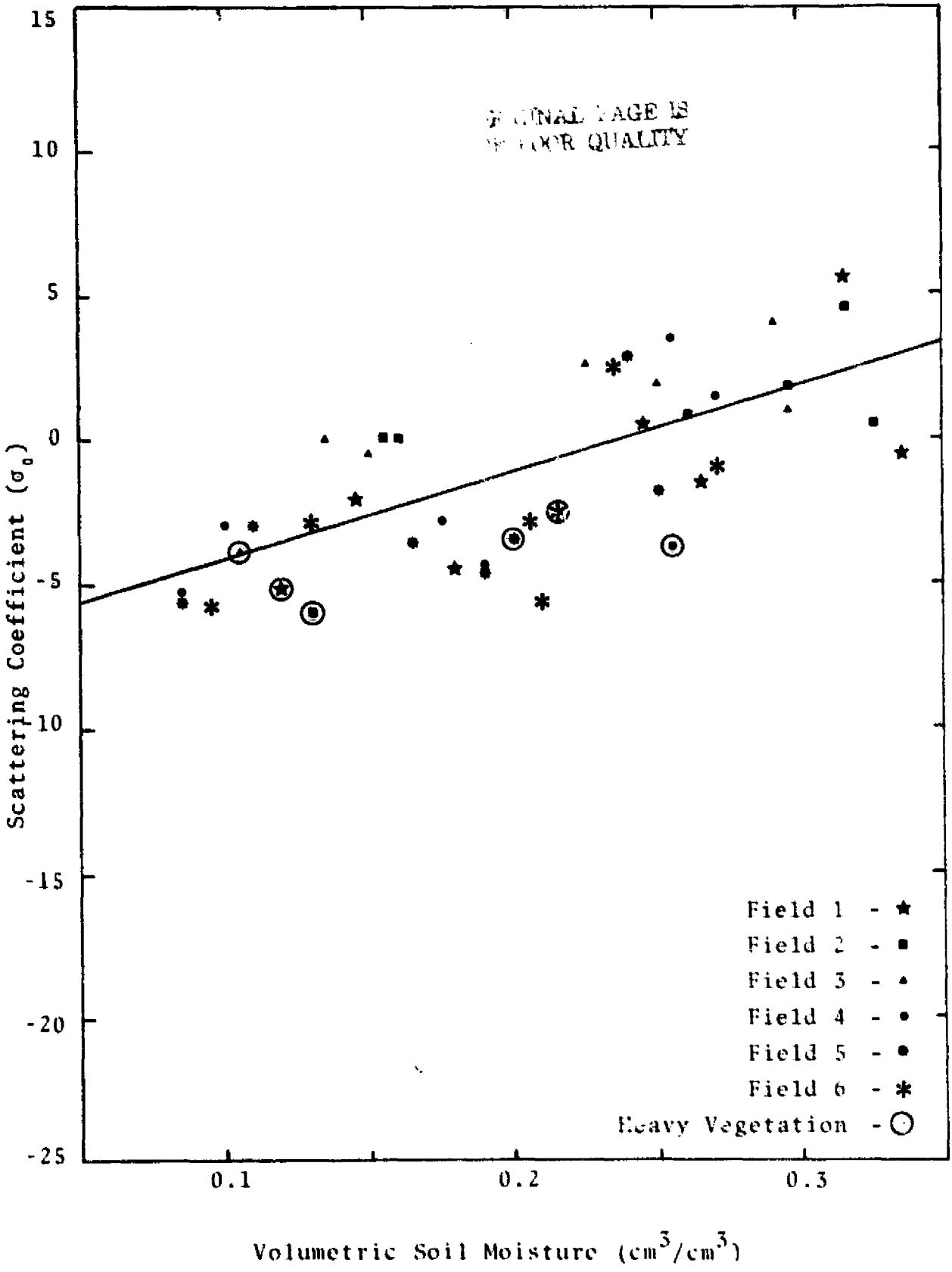

Figure A53. Relation Between 1.6 GHz-HH Scattering Coefficient and Volumetric Soil Moisture at 15 Degree Look Angle

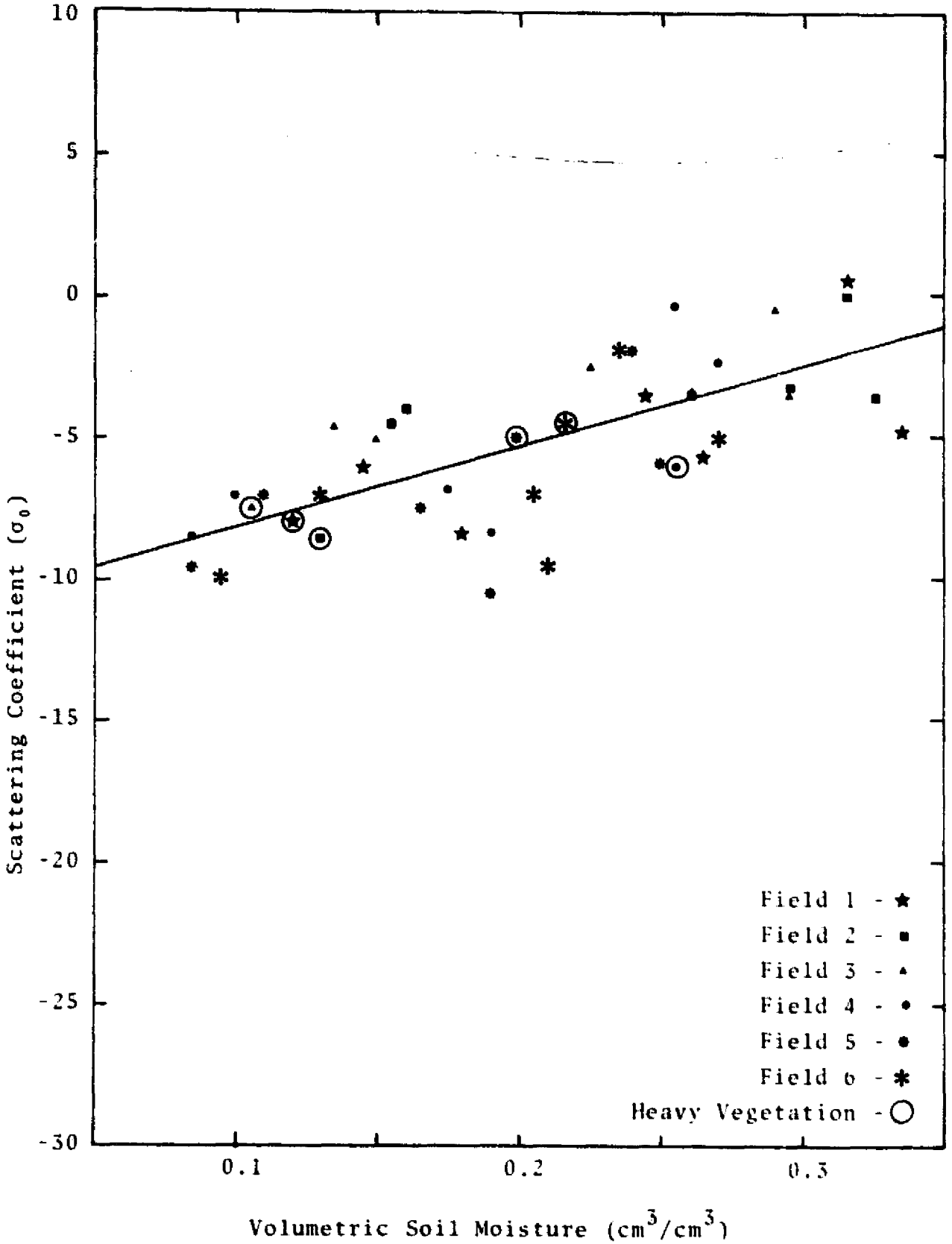

Figure A54. Relation Between 1.6 GHz-HH Scattering Coefficient and Volumetric Soil Moisture at 20 Degree Look Angle

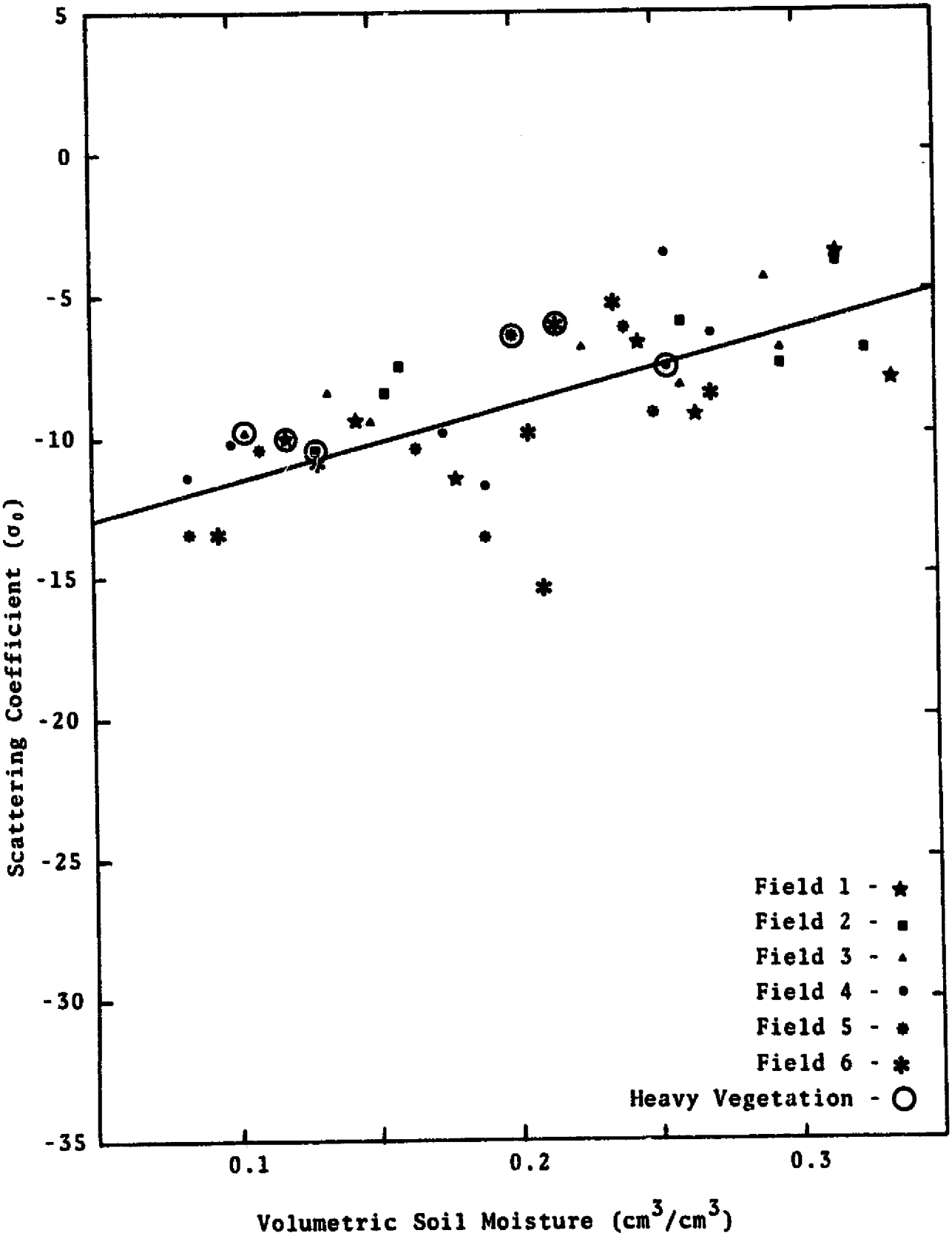

Figure A55. Relation Between 1.6 GHz-HH Scattering Coefficient and Volumetric Soil Moisture at 25 Degree Look Angle

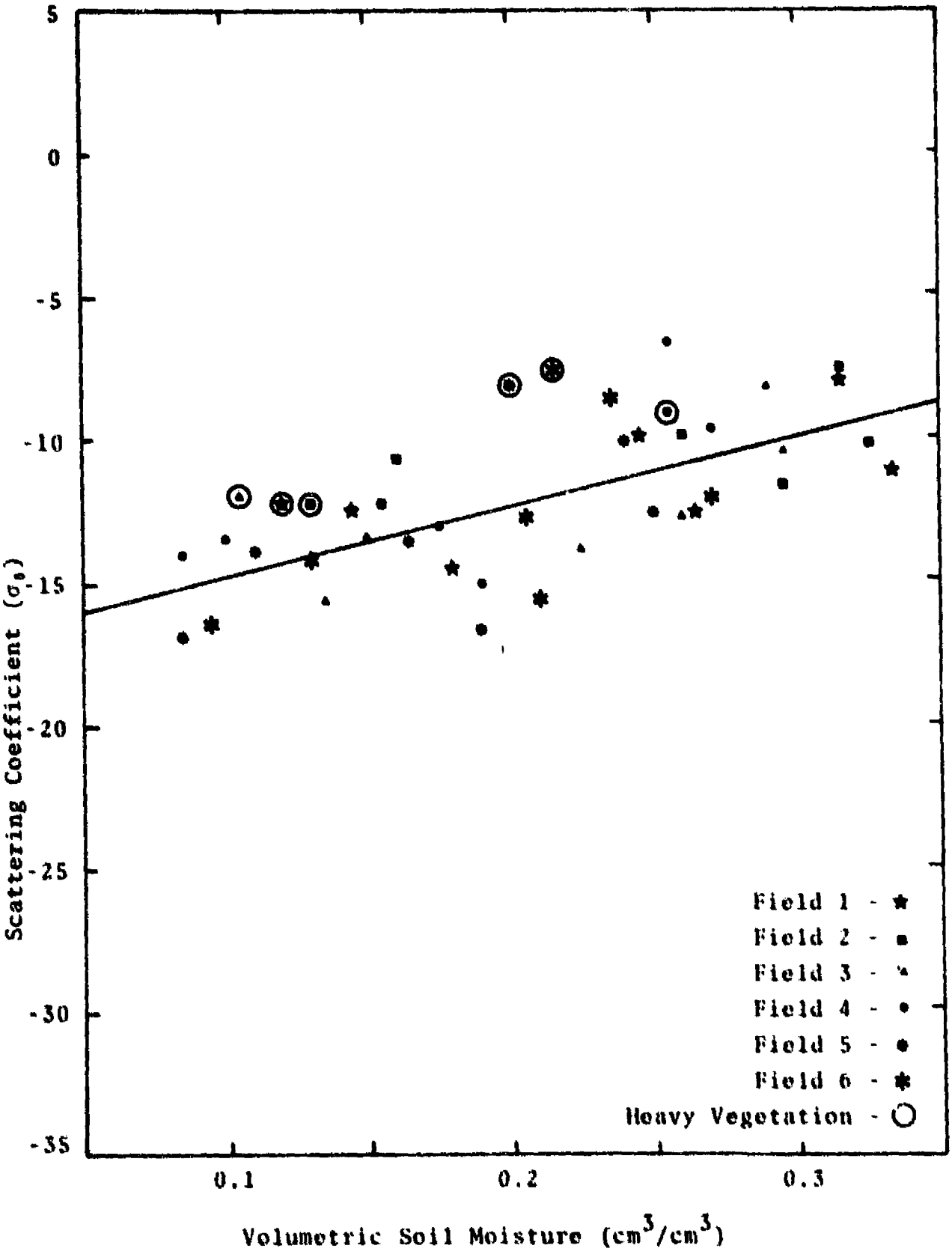

Figure A56. Relation Between 1.6 GHz-HH Scattering Coefficient and Volumetric Soil Moisture at 30 Degree Look Angle

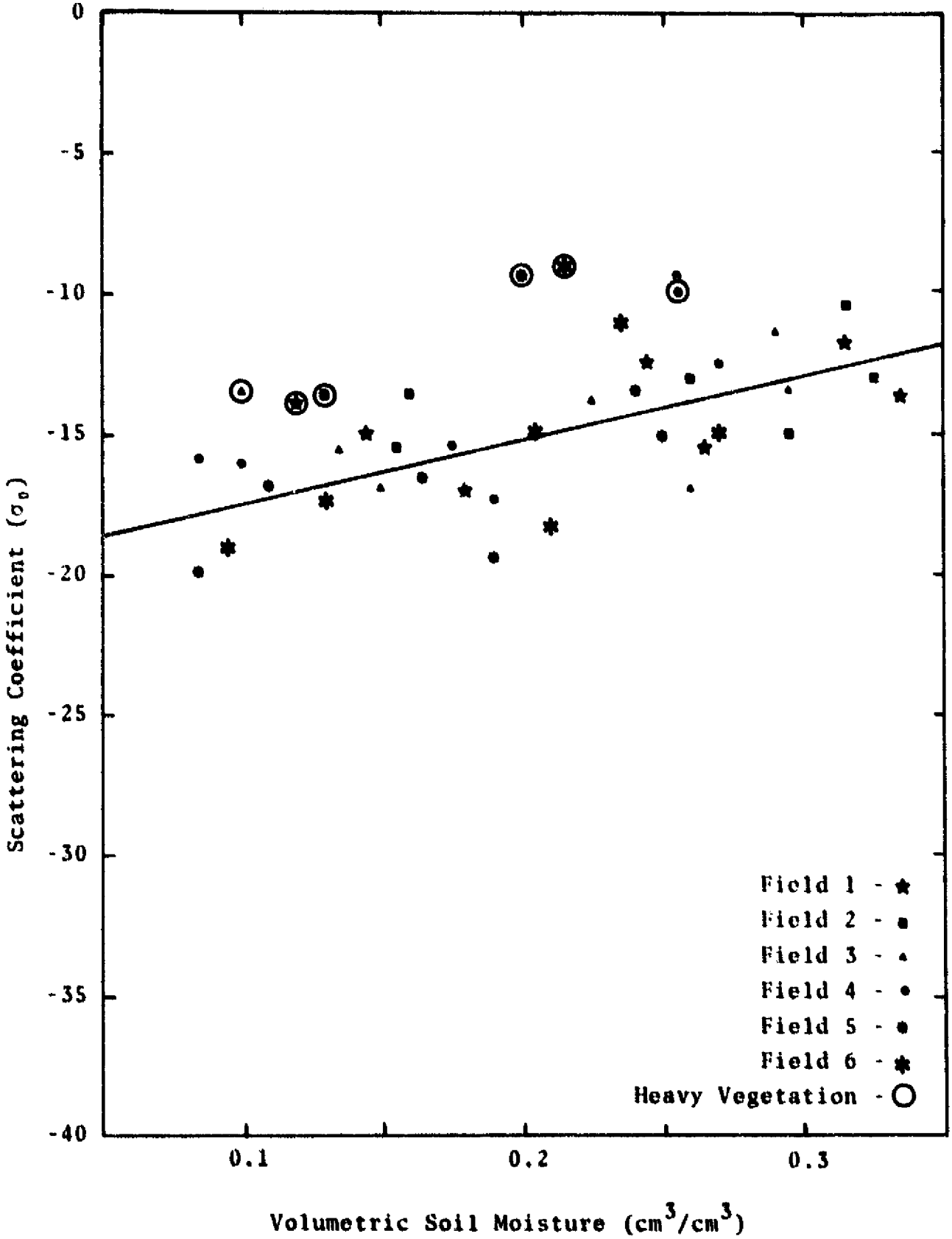

Figure A57. Relation Between 1.6 GHz-HH Scattering Coefficient and Volumetric Soil Moisture at 35 Degree Look Angle

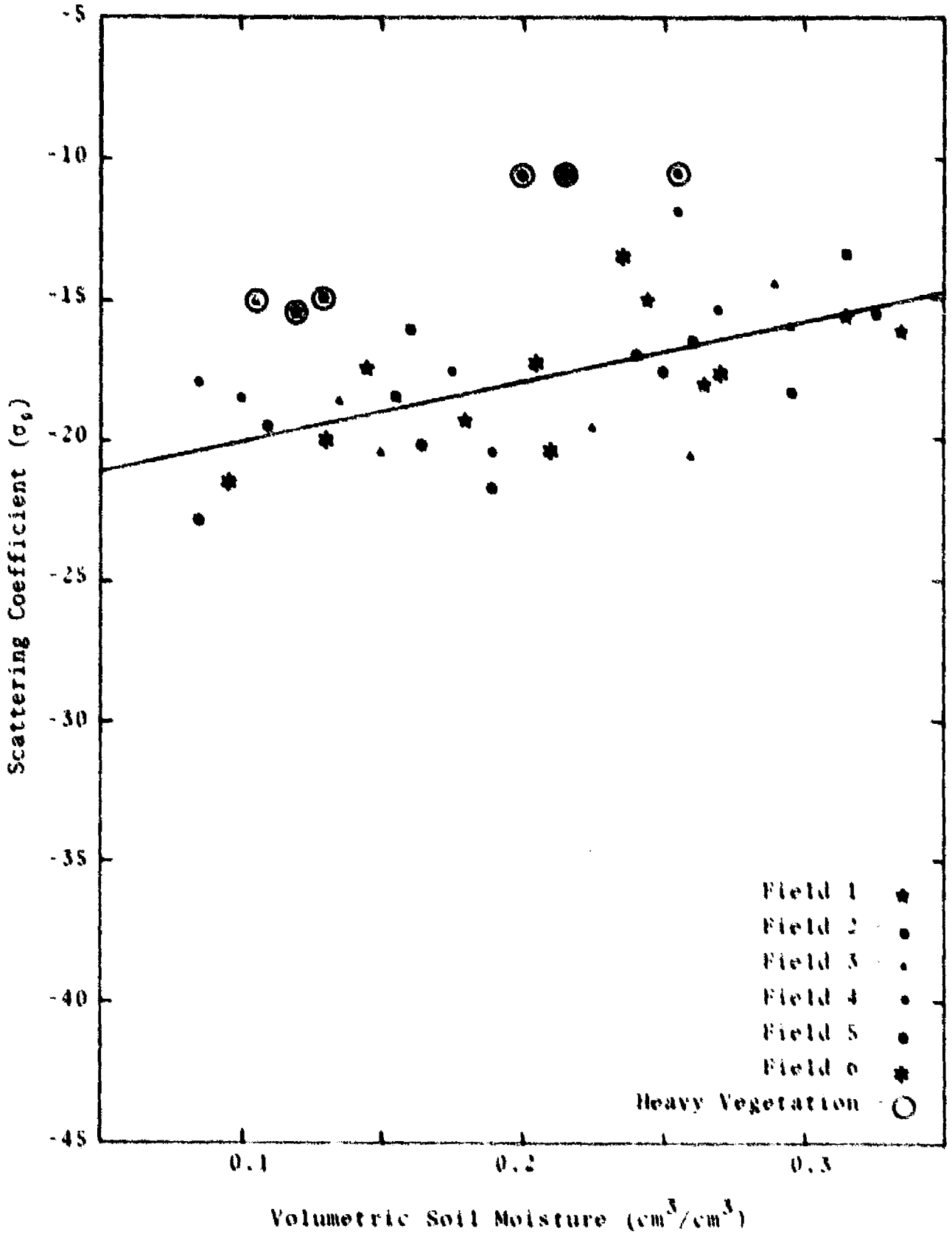

Figure A58. Relation Between 1.6 GHz-HH Scattering Coefficient and Volumetric Soil Moisture at 40 Degree Look Angle

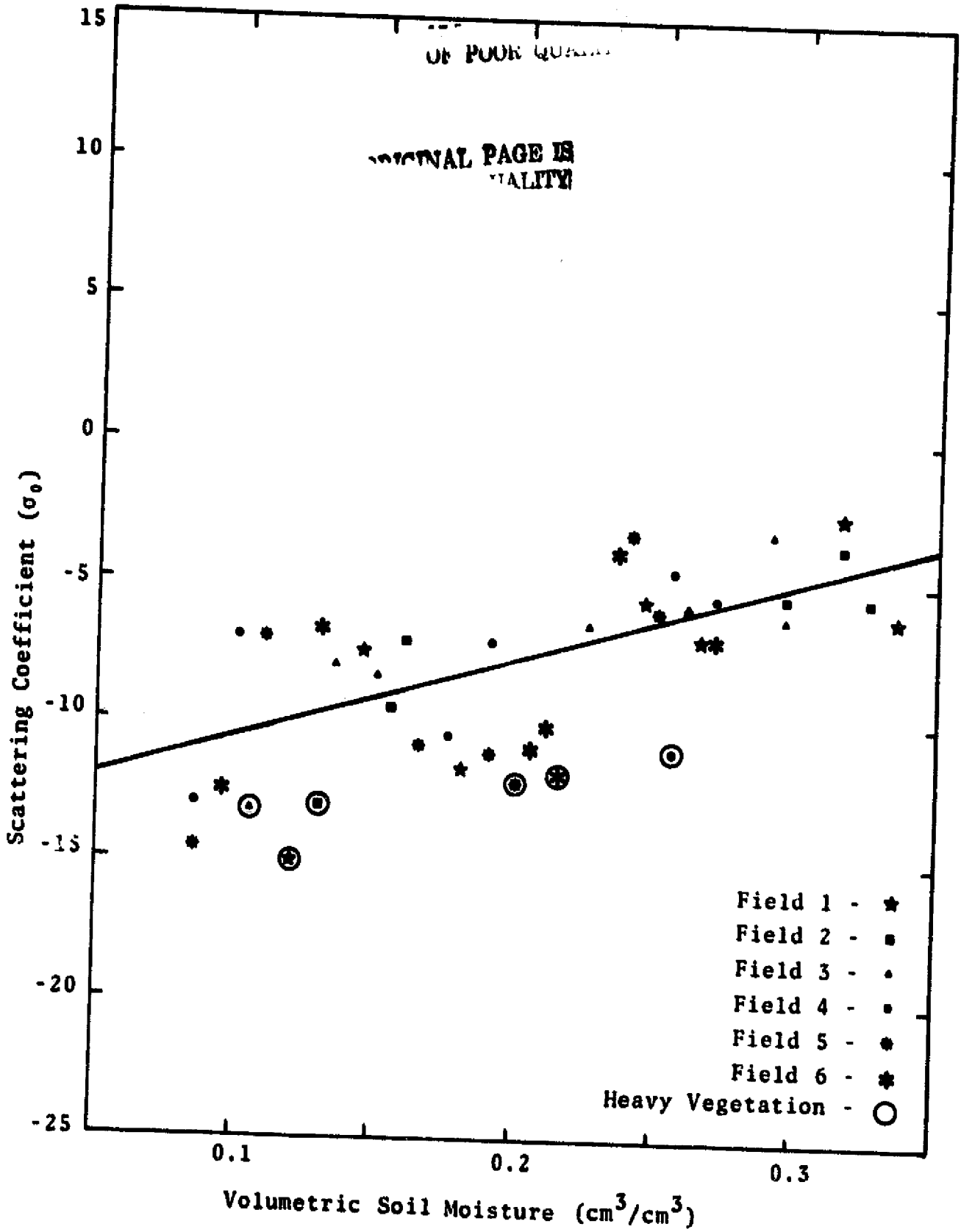

Figure A59. Relation Between 1.6 GHz-HV Scattering Coefficient and Volumetric Soil Moisture at 5 Degree Look Angle

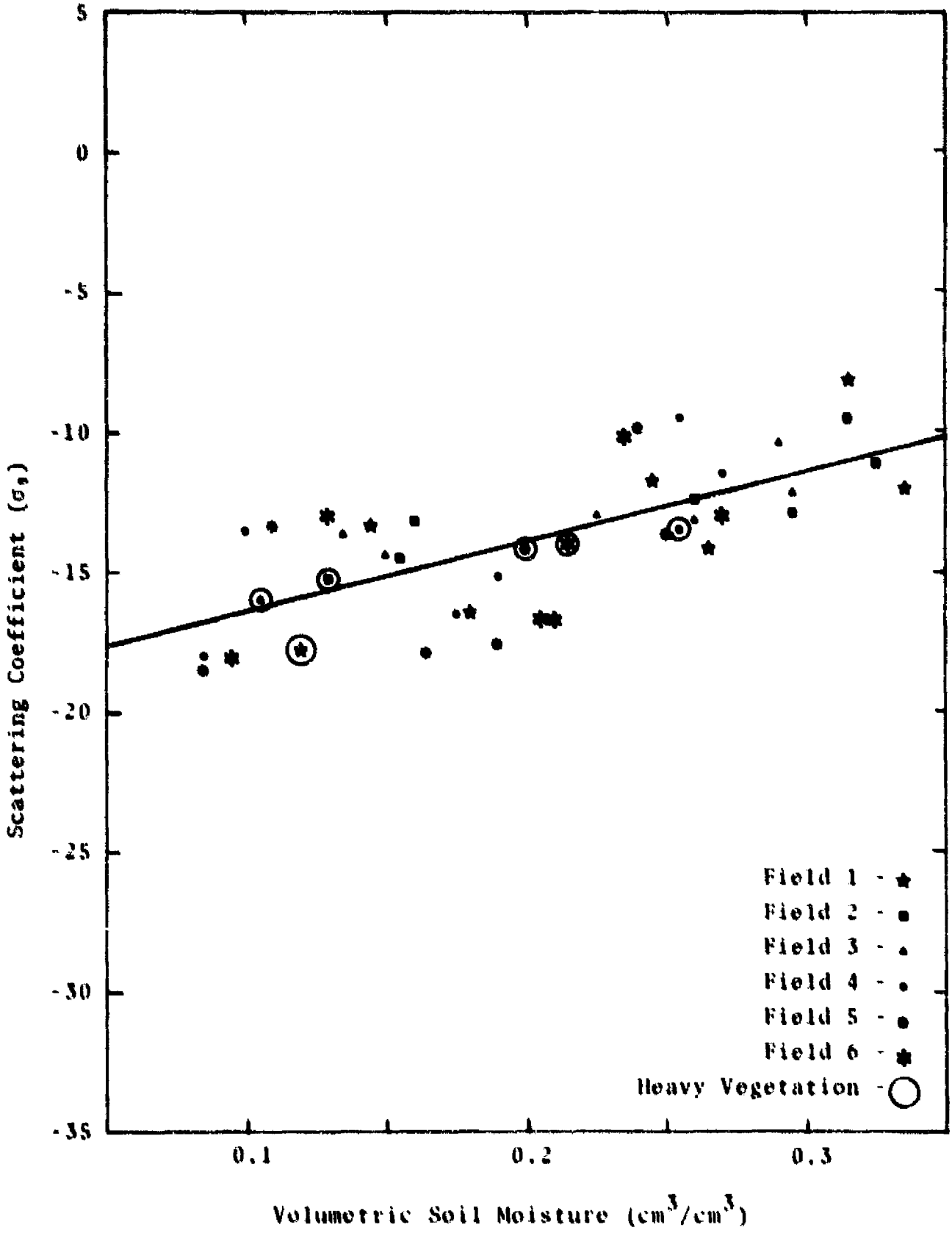

Figure A60. Relation Between 1.6 GHz-HV Scattering Coefficient and Volumetric Soil Moisture at 10 Degree Look Angle

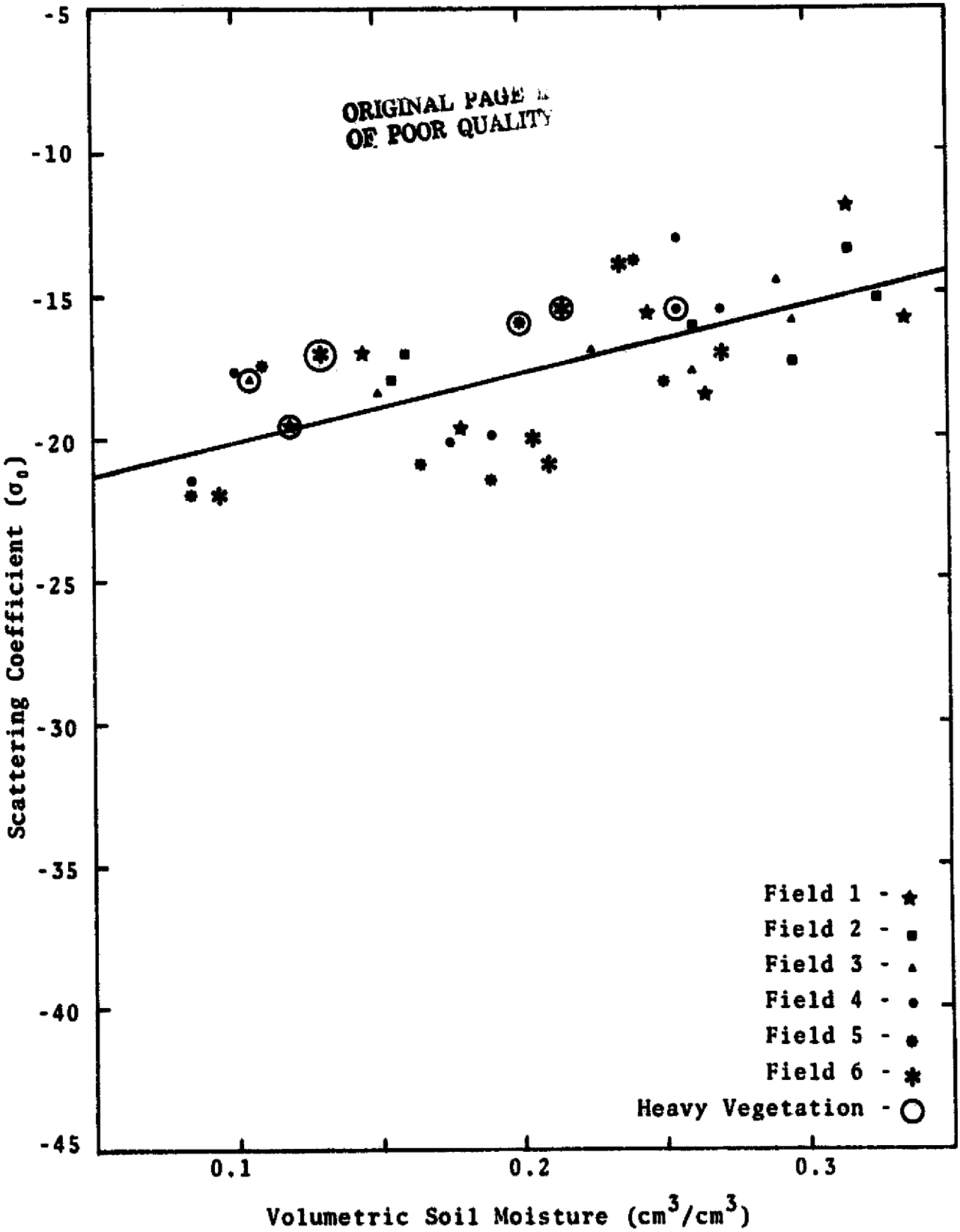

Figure A61. Relation Between 1.6 GHz-HV Scattering Coefficient and Volumetric Soil Moisture at 15 Degree Look Angle

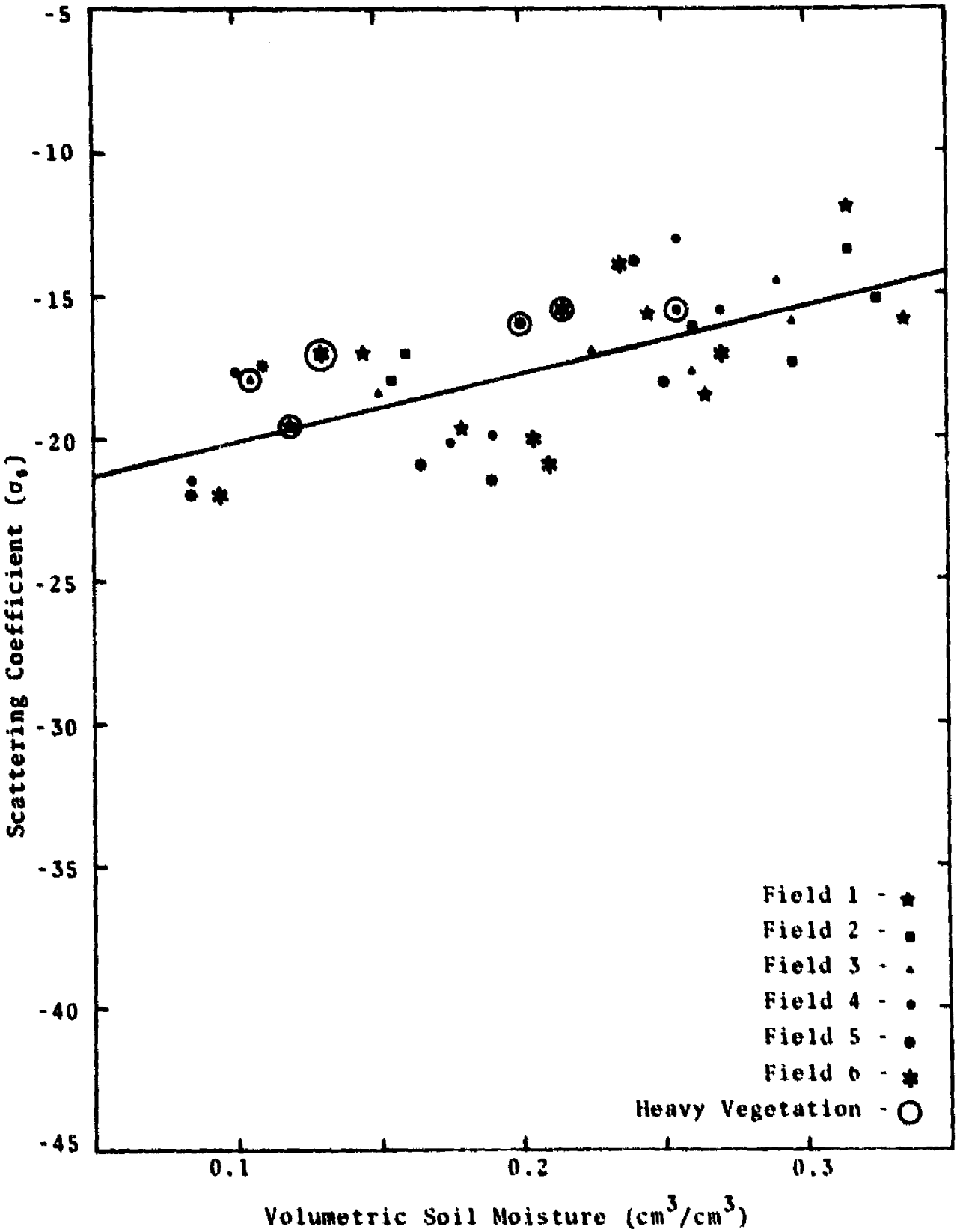

Figure A61. Relation Between 1.6 GHz-HV Scattering Coefficient and Volumetric Soil Moisture at 15 Degree Look Angle

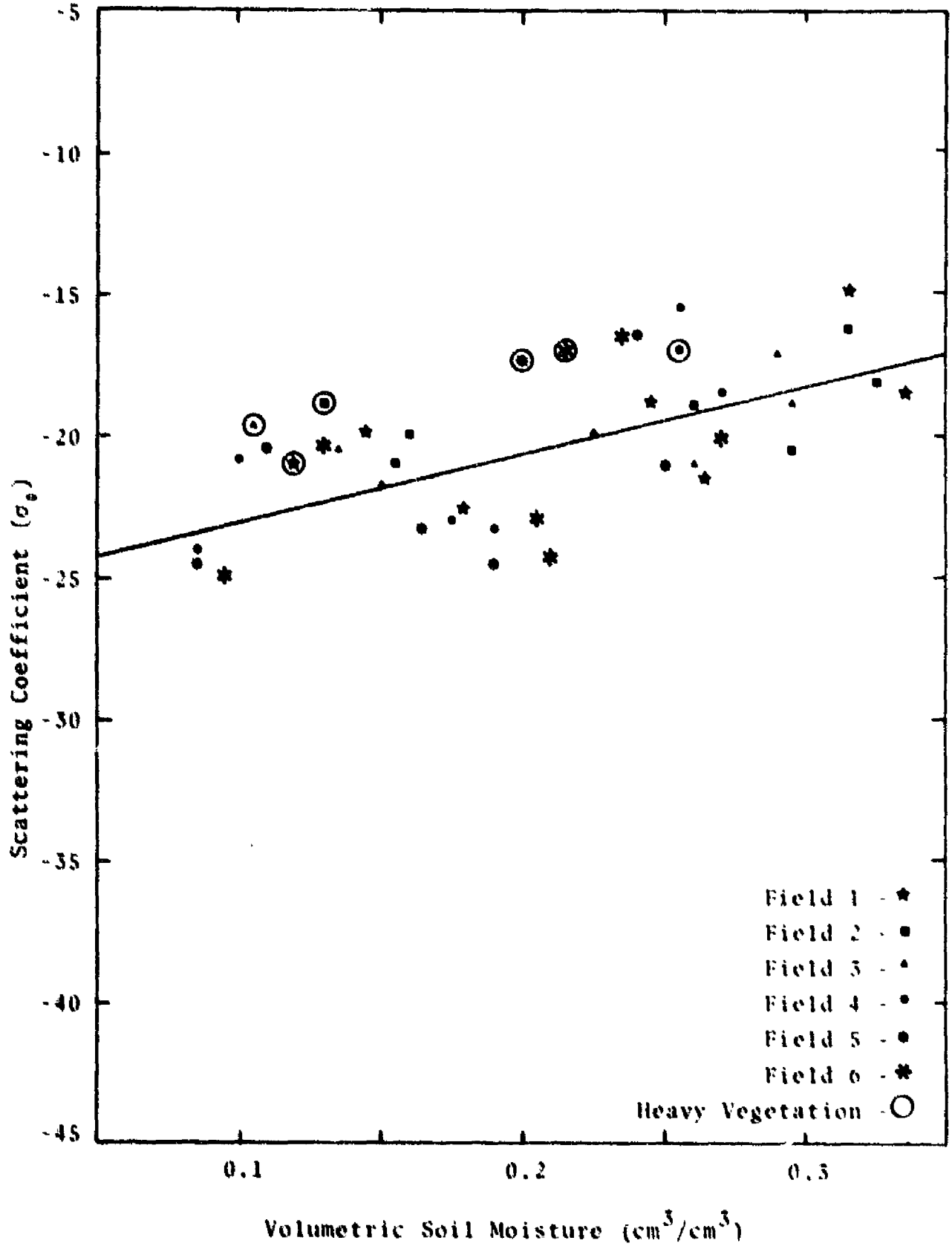

Figure A62. Relation Between 1.6 GHz-HV Scattering Coefficient and Volumetric Soil Moisture at 20 Degree Look Angle

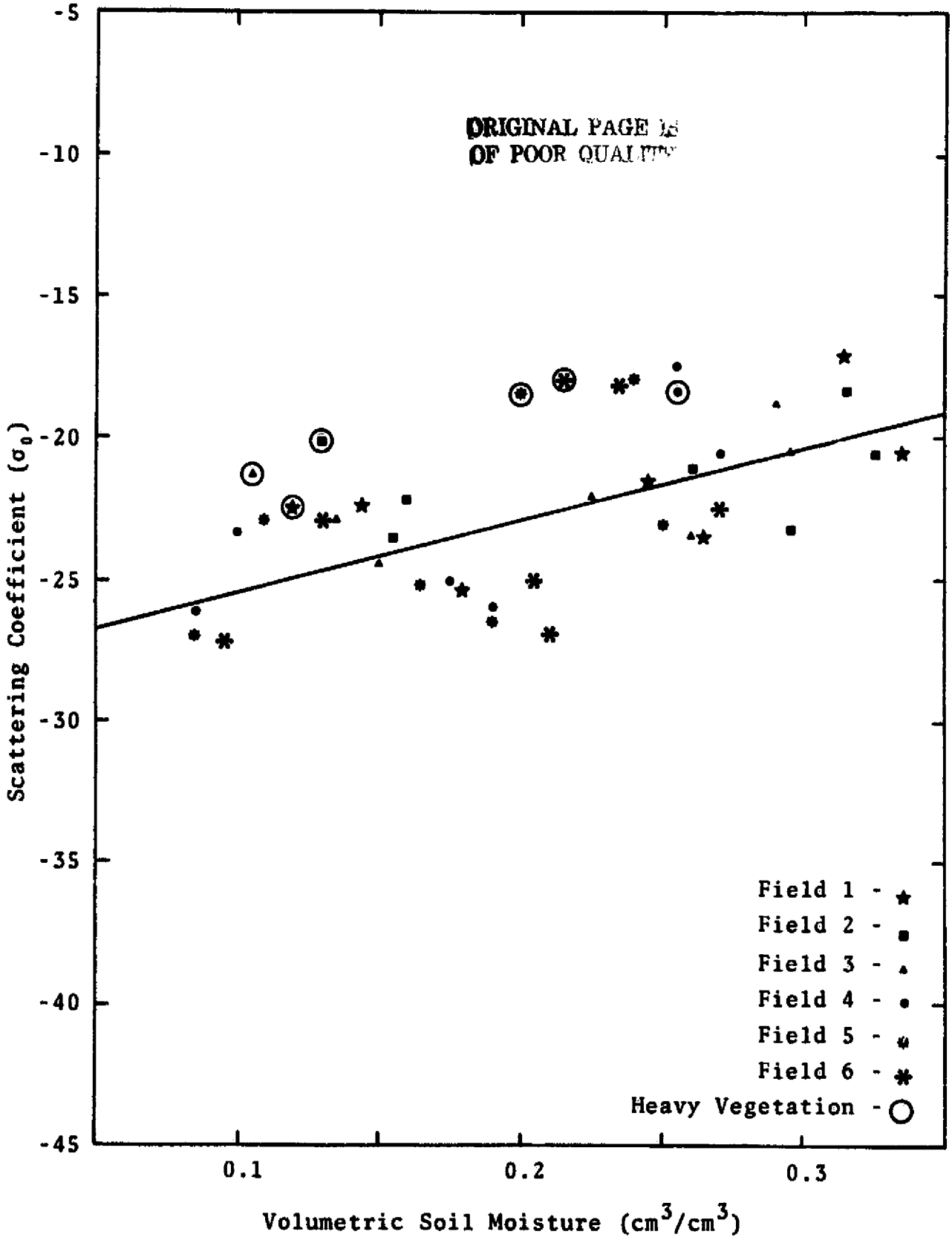

Figure A63. Relation Between 1.6 GHz-HV Scattering Coefficient and Volumetric Soil Moisture at 25 Degree Look Angle

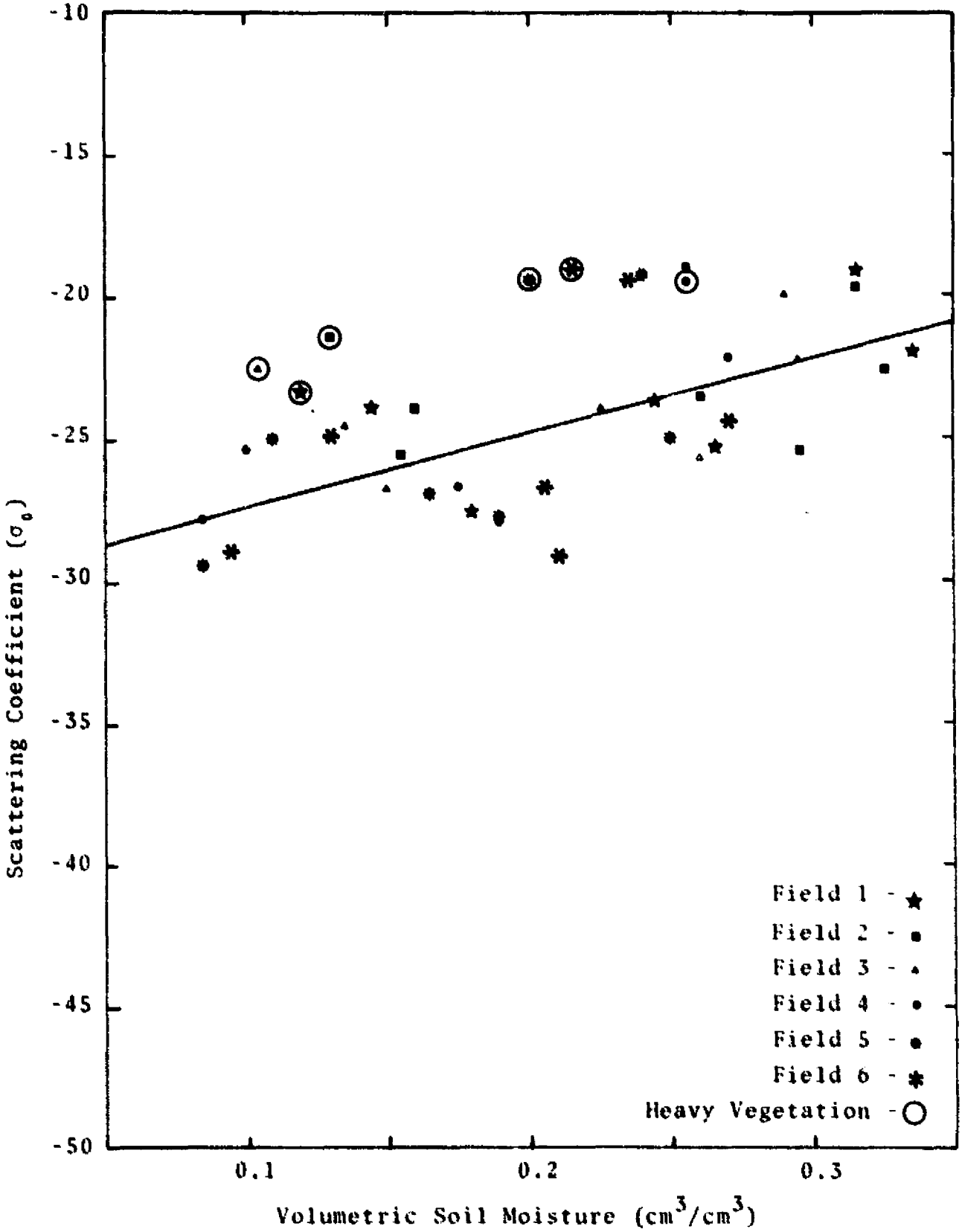

Figure A64. Relation Between 1.6 GHz-HV Scattering Coefficient and Volumetric Soil Moisture at 30 Degree Look Angle

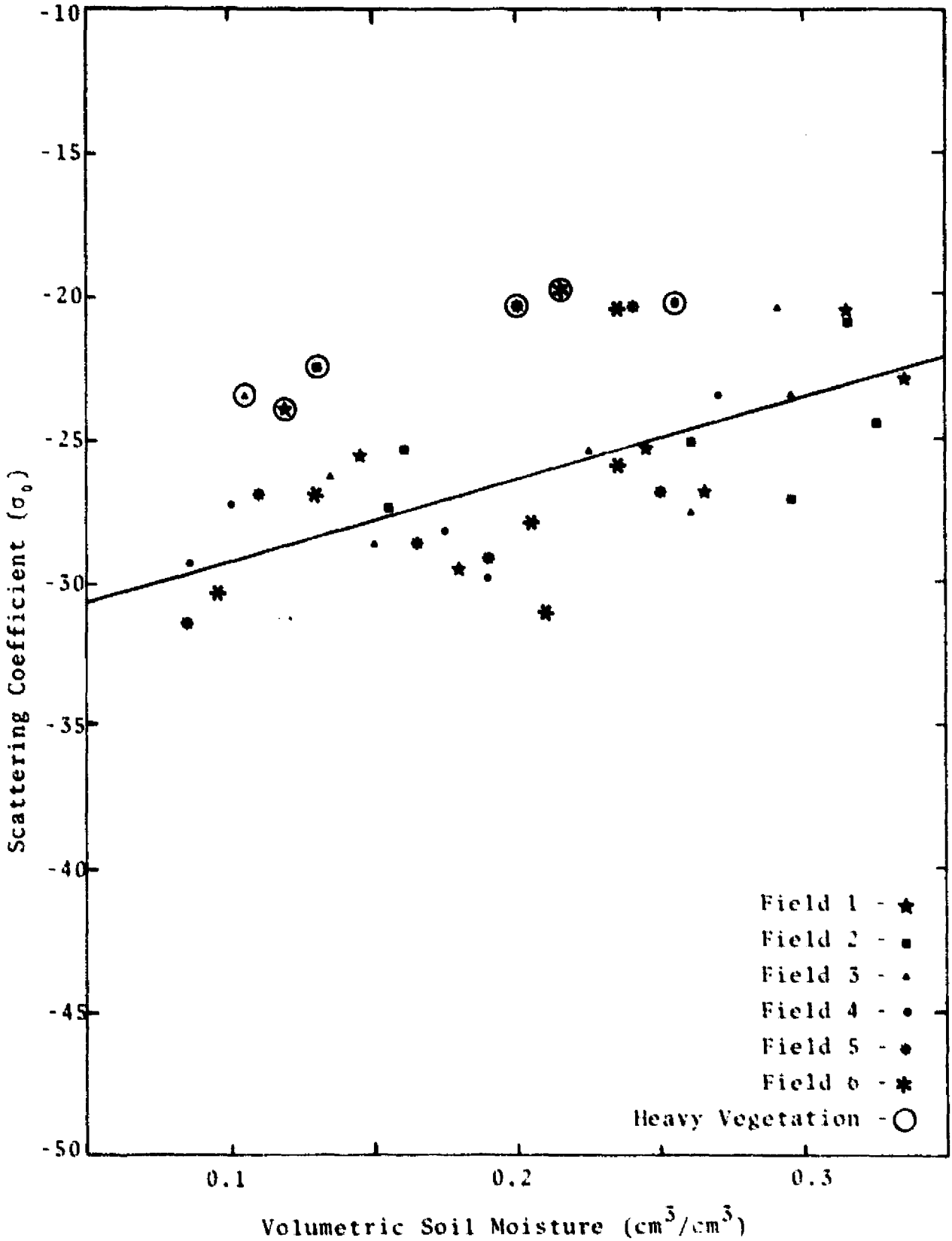

Figure A65. Relation Between 1.6 GHz-HV Scattering Coefficient and Volumetric Soil Moisture at 35 Degree Look Angle

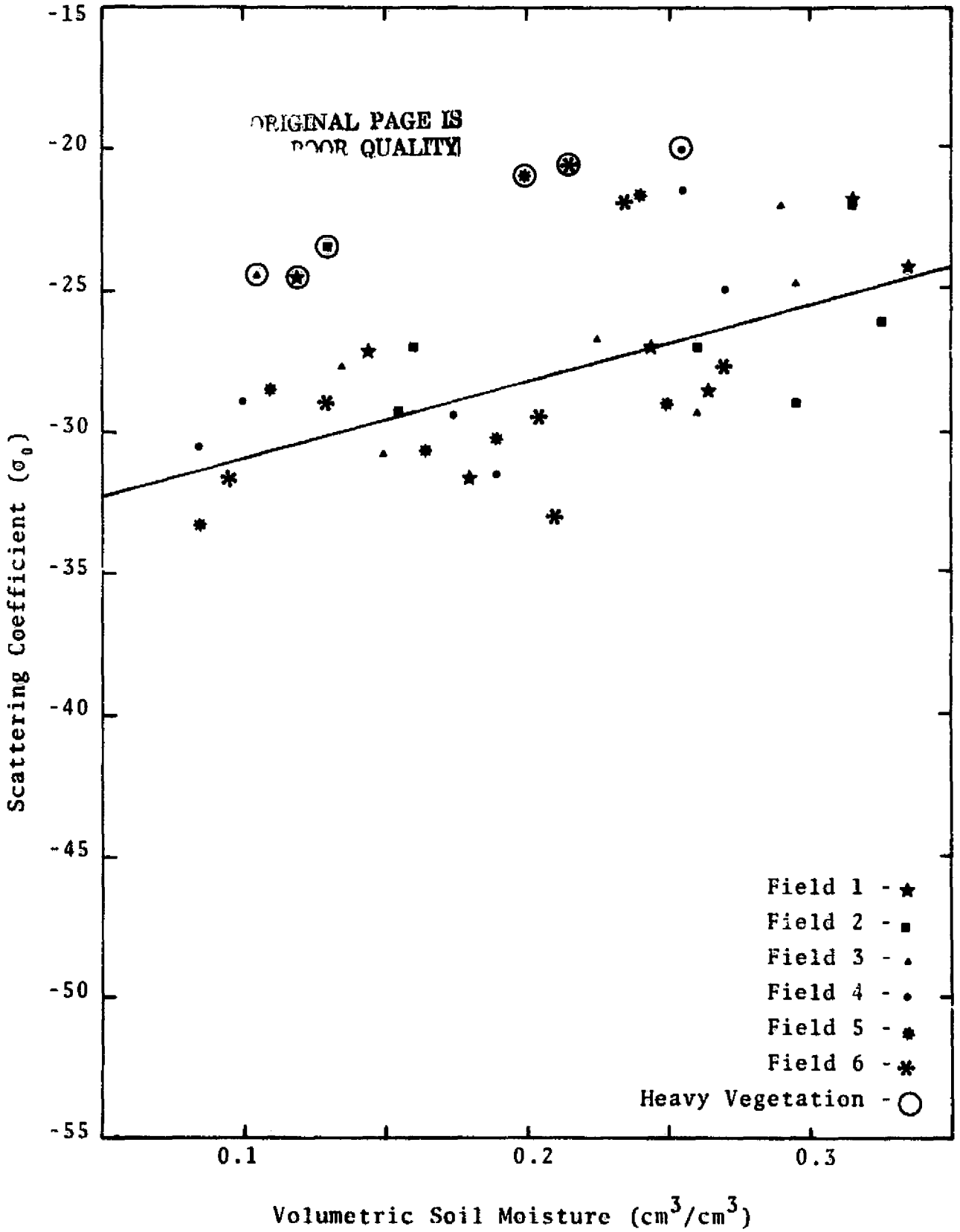

Figure A66. Relation Between 1.6 GHz-HV Scattering Coefficient and Volumetric Soil Moisture at 40 Degree Look Angle